

Development and Feasibility of an Altitude Controlled Bushfire Sensing Balloon.

DAVID REVAY

SID: 309208041



THE UNIVERSITY OF
SYDNEY

Supervisor: Dr. Xiaofeng Wu

This thesis is submitted in fulfilment of

the requirements for the degree of

Bachelor of Engineering (Mechanical (Space))

School of Aerospace, Mechanical and Mechatronic Engineering (AMME)

The University of Sydney

Australia

5th June 2014

Statement of Student Contribution

- *I, with the help of Dr. Xiaofeng Wu, came up with the idea of using an altitude controlled balloon for bushfire remote sensing.*
- *I came up with the idea of using a triangular trajectory (making use of three different atmospheric layers) to loop / station-keep in a small observation area.*
- *I carried out the literature survey in order to determine the types of remote sensing technologies currently used to fight bushfires.*
- *I determined the basic design considerations that would be required for this novel remote sensing platform.*
- *I applied a range of conventional static and dynamic engineering techniques to develop the mechanical model describing the balloon's motion.*
- *I applied knowledge of well-known wind models to the bushfire environment, in order to propose how winds are affected by the heat of a bushfire.*
- *I designed and created the Physical Balloon Model using a Runge-Kutta integration routine. This implemented a Mooney-Rivlin stress-strain relationship that was explained by a Matlab function created by M. Chapman.*
- *I designed and created the Lifting Gas Control System, Goal Estimation Routine and the Observed Wind Array Update Routine. In particular, this Goal Estimation Routine is a very innovative way to solve a computationally intensive problem that has eluded current systems.*
- *I designed and created the Initial Trajectory Estimate, the Main Model, and the Monte-Carlo Robustness Test. This Monte-Carlo Robustness Test is a novel way of determining the best position to launch a balloon from.*
- *I designed and conducted all statistical analyses, using either in-built Matlab functions or routines I designed. For example, I created codes to conduct Log Likelihood curve fitting for a large range of obscure PDFs. I also created a function that could simulate random values from a Generalised Normal Distribution (based on a technique described by Dr. Boris Choy).*
- *I carried out the writing of this thesis. The Results, Discussion and Conclusion are my own.*

The above represents an accurate summary of the student's contribution.

Signed:

5th June 2014

.....
David Revay - Student

.....
Dr. Xiaofeng Wu - Supervisor

Acknowledgements

I would like to express thanks to all who assisted me with this thesis. In particular, my supervisor Dr. Xiaofeng Wu, who offered invaluable support and guidance throughout a very hurried semester. In addition, I would like to thank Dr. Boris Choy, whose knowledge of actuarial risk analysis has found a new use within the realm of wind risk analysis.

I would also like to express my deepest gratitude to my family for their constant encouragement. I am so thankful that a little of their sense of wonder and intrigue has made its way into me.

Finally, I would like to acknowledge the incredible resources, made available, free of charge over the internet. It has never been so easy, to stand so tall, on the shoulders of the giants who came before us.

ABSTRACT

Remote sensing is a crucial component of modern rural fire-fighting procedures. Currently, data is derived from satellites and conventional aircraft. However, these fail to provide the high resolution, real-time photography required for proper bushfire tracking and analysis.

This thesis proposes filling this operational gap with a robotic, altitude controlled balloon. Such a balloon would stream back, real-time, high-resolution infrared bushfire photography. This would surpass the quality of existing systems at significantly lower cost. A novel station-keeping method is proposed wherein the balloon's altitude is adjusted to allow the balloon to catch desirable winds in a large looping trajectory, allowing it to return to where it started.

To address the feasibility of such a system, this thesis focuses on the balloon's innovative looping trajectory. Can the trajectory be accurately predicted under uncertain wind forecasts and can a trajectory loop be reliably performed?

Examples of the balloon's potential trajectory were simulated in Matlab by merging a number of theoretical dynamic models with forecast wind predictions provided by NOAA. A multi-layered iterative control algorithm was developed, requiring the simulation of GPS and inertial sensors. This control system was added to the simulation to demonstrate the real-world performance of a trajectory loop. A Monte-Carlo robustness test was then used with a classical statistical analysis to determine how likely the trajectory loop was to succeed under real wind conditions.

Simulated pre-launch calculations suggested that reliably completing a trajectory loop was impossible during 70.83% of the 36 day period examined. Launches were simulated for the 29.17% where success was deemed likely. Of these launches, the balloon successfully completed trajectory loops 92.86% of the time. An average loop consumed 62.92 grams of hydrogen gas in order to induce the required control forces. Completing three loops would allow the bushfire to be observed for 15.09 hours, consuming roughly 188.76 grams of H₂.

This low chance of success was highly dependent on the location selected. In other regions which exhibit more distinct wind layers, the chance of success would be greatly increased. Further analysis of geographic regions must be conducted to better investigate this success rate. Additional analysis should be conducted on the ability of the system to produce the required control forces (given the difficulty storing hydrogen gas). Importantly, improvements to the control system could potentially reduce the lifting gas requirement by as much as 85%.

CONTENTS

1	INTRODUCTION	1
1.1	Background.....	1
1.2	Thesis Aims.....	2
1.3	Thesis Structure.....	3
2	LITERARY REVIEW	4
2.1	Bushfires In Australia.....	4
2.2	Fire Remote Sensing	6
2.2.1	Fire Detection - The Sentinel Detection System	6
2.2.2	Strategic Imagery.....	7
2.2.3	Hot-Spot Detection.....	8
2.3	Emerging Technologies	9
2.3.1	UAV based Fire Detection	9
2.3.2	Balloon based Fire Detection.....	11
2.4	Balloon Trajectory Control Systems.....	12
2.4.1	Control Forces.....	12
2.4.2	Trajectory Calculation	13
2.4.3	Station Keeping	14
3	SYSTEM DESIGN CONSIDERATIONS	15
3.1	System Goals	15
3.2	The Triangular Looping Trajectory	15
3.3	Aerostat Design.....	17
3.3.1	Elastic Weather Balloon.....	17
3.3.2	Control Forces.....	17
3.4	Payload Design	19
3.4.1	Thermal Camera.....	19
3.4.2	Lens	20
3.4.3	Other Systems	21

4 GOVERNING PHYSICS AND MODEL	22
4.1 Internal Balloon Physics.....	22
4.1.1 Pressure Summation.....	22
4.1.2 Elastic Force.....	23
4.1.3 Governing Equation.....	23
4.2 External Balloon Physics.....	24
4.2.1 Force Summation.....	24
4.2.2 Drag Force	25
4.2.3 Lift Force	25
4.2.4 Governing Equation.....	26
4.2.5 Lift Force Control.....	26
4.3 Atmospheric Model	27
4.4 Wind Model.....	27
4.4.1 Turbulent momentum flux	28
4.4.2 Neutral logarithmic wind-shear profile	29
4.4.3 Thermal Stratification.....	30
4.4.4 Wind Data	32
5 SIMULATION METHODOLOGY	33
5.1 Area Of Interest.....	33
5.2 Data Acquisition.....	35
5.3 Data Remapping and Interpolation	36
5.4 System Algorithms.....	37
5.4.1 Physical balloon Model (PBM)	37
5.4.2 Lifting Gas Control System (LGCS)	38
5.4.3 Goal Estimation Routine (GER).....	39
5.4.4 Observed Wind Array Update Routine (OWAUR).....	42
5.5 Simulation Algorithm	42
5.5.1 Initial Trajectory Estimate (ITE).....	43
5.5.2 Monte-Carlo Robustness Test (MCRT)	44
5.5.3 Main Model.....	45

6 RESULTS AND DISCUSSION.....	47
6.1 Winds Analysis	47
6.1.1 Layer Consistency.....	47
6.1.2 Changes with Altitude.....	48
6.1.3 Changes with Time.....	50
6.1.4 Forecast Variation	52
6.1.5 Forecast Precision	54
6.2 Looping Example.....	59
6.2.1 Forecast Trajectory with Forecast Winds	59
6.2.2 Forecast Trajectory with Real Winds.....	60
6.2.3 Real Trajectory with Real Winds.....	61
6.3 Looping Viability	65
6.3.1 Chance of Success	66
6.3.2 Further Examples	67
6.3.3 Average Moles Required For a Loop.....	69
6.3.4 Average Time Required For a Loop	71
7 FUTURE CONSIDERATION AND CONCLUSIONS.....	72
7.1 Conclusions.....	72
7.2 Future Considerations.....	74
7.2.1 Improvements to simulation accuracy	74
7.2.2 Other Considerations	75
8 WORKS CITED	76
8.1 Open Source Matlab Functions.....	80
9 APPENDIX	81
9.1 Matlab Code.....	81
9.2 Initial Parameters	81

NOMENCLATURE

P_{out}	Atmospheric Pressure
P_{in}	Pressure inside the balloon
P_{el}	Pressure due to elasticity of balloon
n	Number of Moles of lifting gas
R	Universal Gas Constant
T	Atmospheric Temperature
V	Volume of the balloon
μ	Shear Modulus
r	Radius of balloon
α	Elastic Coefficient
t	Thickness of balloon
F	Force
m	Mass
a	Acceleration
C_D	Coefficient of Drag
ρ	Density
π	Pi
A	Cross sectional area of balloon
v	Velocity
g	Gravity
M	Molar Mass
θ	Camera Angle
h_{gnd}	Height above ground
r_{gnd}	Ground radius / width of photo
A_{gnd}	Ground area of photo
CCD_x	Number of pixels in camera's x direction
\vec{u}	Wind velocity
δ_t	Delta Time
∇	Del / Nabla operator
∇p	Pressure Gradient
$\bar{\Omega}$	Angular Velocity (Coriolis force)
η	Viscosity
f_g	Body force due to gravity
$\nabla \tau_t$	Turbulent Momentum Flux
z_0	Roughness length (due to surface terrain)
$U(z)$	Logarithmic Wind Shear Profile (at height z)
H	Heat Flux
$\Gamma(z)$	Dry Adiabatic Temperature Gradient
L	Monin-Obukhov length
ϕ	Thermal Modification Function

ACRONYMS

ACT	Australian Capital Territory
AIC	Akaike Information Criterion
ASICS	Application Specific Integrated Circuits
AVG	Average
BOM	Bureau of Meteorology (Australia)
CCD	Charge Coupled Device
CDF	Cumulative Distribution Function
CFS	County Fire Service
CONUS	Continental United States
CSIRO	Commonwealth Scientific and Industrial Research Organisation
CV	Coefficient of Variation
ERDDAP	Environmental Research Division's Data Access Program
EXP	Exponential
FOV	Field Of View
GA	Geoscience Australia
GER	Goal Estimation Routine
GFS	Global Forecast System
GIS	Geographic information system
GND	Generalised Normal Distribution
GPS	Global Positioning System
IR	Infrared
ITE	Initial Trajectory Estimate
LEO	Low Earth Orbit
LGCS	Lifting Gas Control System
LTAP	Lighter Than Air Platform
MCRT	Monte Carlo Robustness Test
NAM	North American Model
NASA	National Aeronautics and Space Administration (USA)
NCEP	National Centers for Environmental Prediction (USA)
NOAA	National Oceanic and Atmospheric Administration (USA)
NOMADS	NOAA Operational Model Archive and Distribution System
NSW	New South Wales
OWAUR	Observed Wind Array Update Routine
PBM	Physical Balloon Model
PDF	Probability Density Function
RF	Radio Frequency
SA	South Australia
SD	Standard Deviation
SIMBAD	Set of Identifications, Measurements, and Bibliography for Astronomical Data
UAV	Unmanned Aerial Vehicle

1 INTRODUCTION

1.1 BACKGROUND

Remote sensing is a crucial component of modern fire-fighting procedures. Firefighters need accurate information on the location, size and movement of bushfires in order to predict ground path, inform residents, position fire-fighting assets and allocate resources.

This information is typically obtained from visible light and infrared photography. There are three different categories of imagery, each obtained from a different remote sensing platform:

- **Fire Detection** – Low resolution infrared satellite imagery is used for initial detection of fires in remote areas (1km per pixel).
- **Strategic Imagery** – High resolution infrared and visible light satellite imagery is required for strategic information such as fire size and movement (1-10m per pixel).
- **Hotspot Detection** – Super high resolution infrared imagery is taken from conventional aircraft. This is used to detect embers (that are prone to re-ignition) left in the wake of a bushfire (10cm per pixel).

Geoscience Australia manages the ‘Sentinel Satellite Network’ which provides information for both initial Fire Detection and Strategic Imagery. Only a few satellites in this network are capable of the high resolution required for effective Strategic Imagery, resulting typically, in an unacceptable delay of around 6-12 hours between image request and retrieval. As changes in wind direction alter the speed and movement of fires, it is important to obtain this imagery at a shorter time intervals.

A remote sensing, high altitude balloon platform could provide very high resolution, real-time imagery with a flexibility and low cost that is unmatched by satellite or fixed-wing system. A balloon should be capable of staying aloft in a high altitude trajectory that allows for detailed images to be taken over the course of a day or more.

To achieve this objective, a new form of station keeping method is proposed, the ‘triangular looping trajectory’. Different layers of the atmosphere are under the effects of different winds. Often these winds blow in opposite directions. The balloon will modify its altitude in order to allow it to catch desirable winds back to where it started (the looping trajectory).

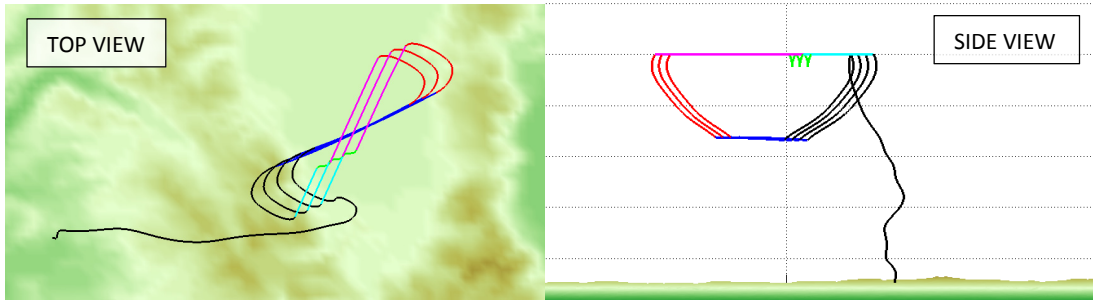


*Figure 1-1: One of the simulated balloon trajectories from later in this thesis.
This shows the balloon performing 3 trajectory loops.*

The idea of using a lighter-than-air platform for bushfire detection and observation is new and unstudied. The use of a looping, altitude controlled trajectory is also novel. Such altitude controlled robotic balloons could be used in many remote sensing applications, such as aerial photography, weather, communication relay or niche markets such as monitoring wildlife parks to reduce poaching.

1.2 THESIS AIMS

The feasibility of any lighter-than-air fire sensing system lies with the ability to reliably control and predict the trajectory. This is required in order to ensure that the goal area is successfully imaged. Questions examined include:

1. *Can the balloon be positioned in a wind-blown trajectory which takes it over a substantial portion of the fire front?*
2. *Can this trajectory be manipulated by means of multiple altitude control steps, so as to utilise favourable winds that allow the trajectory to loop back on itself?*
3. *Is forecast wind data reliable enough to calculate such a trajectory with reasonable certainty, accuracy and predictability?*

1.3 THESIS STRUCTURE

In order to answer these questions the thesis attempts to:

1. Design a trajectory control system that will allow the balloon to perform a loop.
2. Model the balloon's dynamics.
3. Model the external environment, incorporating real wind data.
4. Simulate the full system mechanics.
5. Run a classical statistical analysis to determine the accuracy of forecast wind data.
6. Run a Monte-Carlo analysis to determine how likely the trajectory loop is to succeed.

This thesis outlines a basic system architecture, sufficient to further the trajectory simulation process. If the trajectory is deemed feasible, it will become apparent that a balloon platform offers significant benefits over existing systems. A practical balloon platform will then require further development.

Chapter 2 provides a review of existing literature. This includes a basic description of Australian bushfires and the remote sensing technologies which are currently used by rural firefighters. This section also describes existing literature that mentions any form of UAV platform in the field of bushfire remote sensing and a brief summary of existing theory related to balloon trajectory simulation.

Chapter 3 explains the basic system architecture required for such a balloon. This section includes basic descriptions of the hardware and sub-systems that would be required.

Chapter 4 gives a basic explanation of the physical models and equations which govern the dynamic simulation of the balloon's trajectory. This section also includes information on wind data.

Chapter 5 outlines the simulation methodology, how the simulation was conducted and how the various algorithms work.

Chapter 6 presents and interprets the simulation results. These results include a statistical analysis of the wind fields as well as statistical analysis of the looping trajectory. Several example of simulated trajectories are also included.

Chapter 7 concludes the thesis and suggests elements which could be refined or further analysed. Given the early stages of this analysis, additional research will be required to confirm the feasibility before a prototype can be constructed.

2 LITERARY REVIEW

2.1 BUSHFIRES IN AUSTRALIA

"Bushfires are a natural part of ecosystem processes in Australia. However, as human settlements expand into or adjacent to bushland areas, the risk to lives and property increases." (Bushnell & Cottrell, 2007)

Bushfires are a natural part of the Australian environment with a history pre-dating human settlement. Some Australian animals and plants have developed ways to coexist with fire activity, while others such as eucalypt forests rely on bushfires as part of their natural regeneration cycle. Aboriginal arrival saw an increase in bushfire frequency as many fires were intentionally lit for forest regeneration, pasture management and hunting purposes. Since European settlement there has been a drastic increase in both accidental and intentional human induced bushfires. (Romsey Australia, 2012).

Because of Australia's dry climate and high temperatures, thousands of fires occur each summer, posing a significant threat to life, property and the economy. As these fires will continue to occur, it is appropriate to adopt technologies that result in a reduction in loss of life and damage to physical assets and the environment.

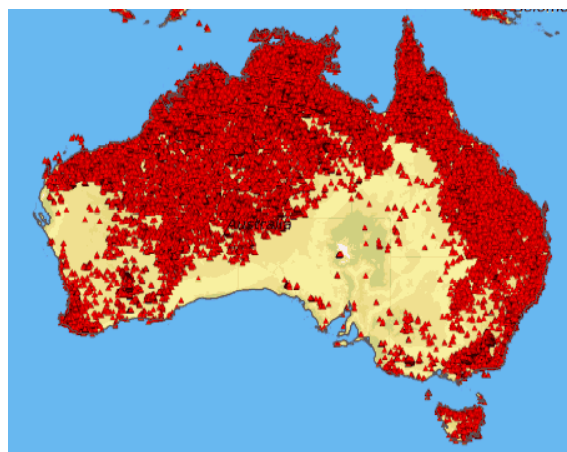


Figure 2-1 - Australian major bushfires, 1997 to 2008 (Romsey Australia, 2012)

Figure 2-1 above shows the distribution of bushfires across an 11 year period – this data was derived from satellite remote sensing data. For example, the 1998 and 1999 fire season saw 115,000 and 230,000 fires per year.

The South-Eastern corner of Australia, below the line drawn between Adelaide and Sydney is best known for bushfire activity and risk owing to its weather and population density. This area sees an annual bushfires as a result of hot and dry weather combined with strong winds. In addition, Tasmania and the South Western corner of Western Australia are home to significant forest areas with large fuel loads. These typically wet forests can also facilitate particularly devastating and intense fires when they dry out (Australian Bureau of Statistics, 2006).

It should be noted that a low rate of fires leads to an increase in fire danger due to a build-up of fuel, increasing fire intensity. For this reason, an increase in climate volatility (such as climate change) will lead to an increase in intensity and a decrease in predictability.

State	Attended Bushfires	Area Burnt ('000 ha)	Human fatalities	Houses destroyed	Livestock fatalities
NSW	459	1,465	3	86	3,400
VIC	843	1,346	-	41-43	10,000-11,000
QLD	2,618	1,056	-	6	n.a
SA	1,419	50	-	4	27
WA	656	2,112	-	n.a	n.a
TAS	n.a	52	-	6	n.a
NT	n.a	15,000	-	n.a	n.a
ACT	n.a	160	4	501	n.a
SUM	5,999	21,241	7	644 - 646	13,427-14,427

Table 2-1-1 - Key Bushfire statistics for the 2002-2003 bushfire season (Australian Bureau of Statistics, 2006)

The figures in the above table give some indication of the enormous loss of assets and life that result from poorly managed fires. Technology has and will continue to provide fire-fighters and evacuators with the information they require to work effectively and efficiently.

Experience shows that small investments in technology and the provision of appropriate information about the location, extent and movement of fires can result in a significant increase in the effectiveness of fire fighters. This means less destruction, fewer wasted resources and fewer deaths, (Flynn, 2009).

2.2 FIRE REMOTE SENSING

A variety of useful data can be derived from bushfire remote sensing, much of which has become a staple of modern fire-fighting. The three most common types of remote sensing information are:

1. Fire Detection – typically using 1km resolution IR satellite imagery.
2. Strategic Imagery – higher resolution IR satellite imagery of active fires.
3. Hot Spot Detection – super high resolution IR imagery taken conventional aircraft.

2.2.1 Fire Detection - The Sentinel Detection System

The Sentinel Detection System was developed by Australia's CSIRO as a result of devastating bushfires through NSW and the ACT in 2002. The system is now operated by Geoscience Australia, a Federal initiative. It provides national bushfire monitoring through a web-portal (Geoscience Australia, 2014).

The system itself uses infrared data from 7 different sun synchronous satellites; American, Japanese and Korean owned. These are all equipped with infrared cameras which are used to determine potential bushfires.

Satellite, Sensor	Type	Scenes Acquired	Resolution	Acquired By
ALOS, AVNIR-2	Optical	18	10 m	GA
ALOS, PALSAR	RADAR	16	10-30 m	Sentinel Asia
Terra, MODIS	Optical/Thermal	24	250 m	GA
Aqua, MODIS	Optical/Thermal	21	250 m	GA
LANDSAT 5, TM	Optical	11	30 m	GA
LANDSAT 7, ETM	Optical	10	30 m	GA
KOMPSAT-2, MS	Optical	3	4 m	KARI
TOTAL		103		

Table 2-2: Satellites currently used by Geoscience Australia's Sentinel Network (Geoscience Australia, 2014)

The Sentinel System receives a stream of image data as satellites pass over Australia. Data is automatically analysed to determine fire location and produce detailed multispectral maps. Significant difficulty lies with thick cloud emanating from the fire regions, making visible light sensing impossible. Nevertheless useful data can be obtained from infrared sensing.

Wavelengths of band 3 (3.55 to 3.93 micro meters) enable the indication of the hot fire-front as infrared can easily pass through smoke relatively unaffected (Tupper et al 2011). Remote sensing from above a cloud layer is ineffective because infrared radiation cannot penetrate clouds due to absorption by water molecules. Nevertheless, on cloudless days, infrared data is easily digitised using GIS polygons. Changes can be monitored over a 4 hour period to determine fire progression. In addition, smoke clouds can be analysed using visible light cameras. Changes in smoke cloud magnitude and direction help predict wind and subsequently fire path (Forghani, et al., 2007).

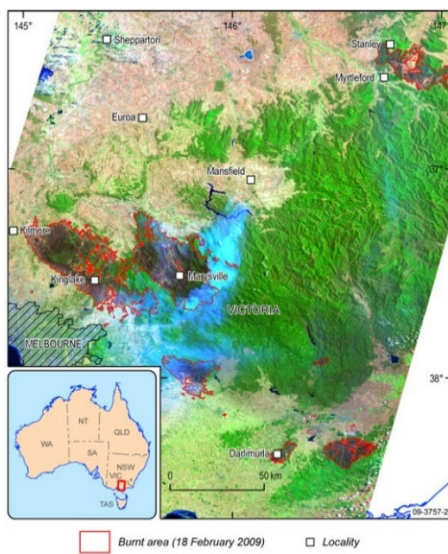


Figure 2-2: GIS polygon fire digitisation of satellite data using conventional recognition algorithms.

2.2.2 Strategic Imagery

Real-time imagery of bushfire areas forms the backbone of firefighting strategy. It facilitates the prediction of bushfire path, calculation of danger zones and the formulation of evacuation plans. Currently strategic imagery comes from newer, high resolution satellites in the Sentinel network.

LandSat 7 is one of the more recent American satellites used for data collection. It is a large 2 tonne satellite in a 700km polar sun-synchronous orbit fitted with a 15m resolution panchromatic and 30m resolution multispectral visible light camera. It is these multispectral images which make up the majority of Google Earth's mapping. In addition this multispectral camera is capable of imaging with a thermal infrared channel, providing 60m resolution in this final band. One of the limitations of early LandSat variations were their inadequate temporal resolution; the data acquisition and transmission process took in the order of 16 days. This

newer variant can transmit its data in the same orbital period, under 1 hour (Lin et al 2011). Nonetheless, the long period sun-synchronous orbits of these new satellites mean significant delays are still apparent as it can take a long time until the satellite is above the target position.

The disadvantage of any satellite fire monitoring system is that it cannot obtain infrared images through cloud. While monitoring of large fires is easily achieved, the detection of smaller fires is not possible due to poor resolution, bandwidth and temporal periods often in excess of 6 hours.

2.2.3 Hot-Spot Detection

A 'hot-spot' is the colloquial term for the smouldering embers that are left in the wake of a passing or quenched bushfire. Hot-spots can remain active across extinguished bushfires. These are of particular concern as they are liable to reignite and cause a resurgence of a once contained fire. This effect caused the tragic loss of 9 lives, 110 injuries and damages exceeding \$27 million during the 2005 Eyre Peninsula bushfire (Emergency Management Australia, 2006).

According to the South Australian County Fire Service (CFS), one of the most important aspects of modern firefighting is searching for and eliminating hot-spots (Tupper et al 2011). Traditionally, fire-fighters have had to visually search for hot-spots from the ground. More recently observation has been done by conventional fixed-wing fly-bys.

This aerial observation is costly and has significant time lag due difficulty mobilizing the aircraft and crew. It is also dangerous because flights are often over hazardous terrain and affected by smoke obstruction, unpredictable hot air pockets and winds.

This conventional method of using pilots and spotters introduces human error and time delays, while data is transmitted back to base and converted to the required formats. Presently the data obtained from such methods is qualitative as it is difficult to accurately pinpoint location when human observation is used. Computerised hot-spot sensors to be used with conventional aircraft have seen little development with focus shifting towards UAV technology.

2.3 EMERGING TECHNOLOGIES

Developments with powerful microcontrollers and control systems have led to an explosion of opportunities within the realm of remote sensing. Highly functional, low-cost platforms can now be designed to fulfil niche roles that have previously been completed by expensive satellites or manned systems. For example, a fixed wing UAV based systems would be safer and more versatile than manned missions – providing faster, high resolution imagery of fire fronts and potential hot-spot areas (Merino, et al., 2005).

The idea of using fixed-wing UAVs for hotspot detection has been in development for the last half decade and is finally seeing real-world deployment. The idea of using high altitude robotic balloons for high resolution, real-time strategic imagery is new and has seen little to no development.

Existing research in these areas will be explained in the following sections:

2.3.1 UAV based Fire Detection

Low flying fixed-wing and rotary aircraft have proven benefits when it comes to hotspot detection (Merino, et al., 2005). Piloted aircraft have been used for many years, in particular by state fire-fighting services in Australia and America. Safety concerns and high costs of piloted systems have led to research in comparable un-manned vehicles. There is consensus that manned flying missions should be limited to fire suppression rather than data acquisition.

Functions performed by a pilot can be performed using modern automated UAV flight computers. Such fire detecting drones require little more than a specified flight path to be inputted with new mission data uploaded remotely. Importantly, this form of UAV could easily communicate in real-time to ground stations or satellites, quickly relaying back image and position data for processing.

For the purpose of a low cost versatile remote fire sensing, a UAV platform with roughly 3m wingspan is adequate. These small UAVs have similar functionality to large UAVs but at significantly reduced purchase and operating costs. In addition they are lightweight and portable which make launch and operation much more manageable (Graml et al 2008).

Although these smaller UAVs have many benefits, they do suffer when it comes to payload capability as both power and capacity are limited. Although payload mass is limited to roughly 5kg it is considered adequate for image sensors and controllers. Field programming techniques are implemented due to low processor power requirements. In addition, Reconfigurable Computing (RC) allows similar benefits, combining efficiency with easy-to-modify programming with Application Specific Integrated Circuits (ASICs) (Graml et al 2008).

Vision sensor processing and transmission consume a significant component of processor time and power. If processing power permits; image processing can be done on board the UAV in order to build up a spatial map and suggest areas which may require further imaging.

A CCD with a resolution of roughly 4096 x 4096 pixels capable of infrared and visible light imaging can be purchased off-the-shelf. Rayleigh limits are not problematic at the low operation altitudes of a few hundred meters. To give a rough illustration of imaging block size a resolution which is adequate for hot-spot detection, say 10cm is selected.

$$4096 \times 10\text{cm} = 0.4096\text{km square block}$$

The lens can be adjusted to achieve this field of view at operating altitude. The UAV would be flying at roughly 150 km an hour. This means $150\text{km} \times 0.4096\text{km} = 61.44\text{ km}^2$ could be imaged in one hour by just one small UAV. If the resolution requirement is increased to 20cm pixels this rate would be double. Thus, a fleet of these vehicles could quickly image a large forest area with great accuracy.

It is anticipated that UAVs will soon replace piloted missions for hot-spot detection. These can provide real-time information with resolution significantly superior to that of satellites. However, due to their limited spatial coverage they cannot replace satellite systems used for fire detection and strategic imaging.

2.3.2 Balloon based Fire Detection

Unlike conventional UAVs, lighter-than-air UAVs have had little attention within the field of bushfire remote sensing. Using a weather balloon to remotely image a bushfire from a high altitude appears to be a novel concept with no mention of feasibility studies within existing literature. The only mention of balloons in existing literature refers to their use as a potential tethered communication relay in remote areas for fixed wing UAV systems (Barrado, et al., 2010).

Interestingly, the 2005 paper ‘Cooperative Fire Detection using Unmanned Aerial Vehicles’ outlines a co-operative algorithm to link information and goals within a fleet of heavier-than-air UAVs. This paper briefly mentions the potential benefits of integrating airships into the system:

“Helicopters are suited to agile target tracking and inspection and monitoring tasks. On the other hand, airships, having much less manoeuvrability, can be used to provide global views or to act as communications relay.” (Merino, et al., 2005)

Balloons or airships cannot compete with a fixed wing UAV’s speed or super high resolution, nor can they match a satellite’s overall ground coverage. Nevertheless, balloons could fill the critical capability bracket between these extremes, by offering larger overall area coverage than a fixed wing UAV as well as a large increase in overall flight time. They could also offer image resolution superior to those of satellites with data available in real-time, instead of the 6 hour delay associated with satellites.

The combination of these three systems would see a significant improvement to the usefulness of data available for fire analysis and fighting purposes. For example, continual satellite monitoring would be used for initial fire detection, followed by rapid deployment of both unmanned balloons and fixed wing craft for high resolution strategic imaging and hot-spot detection respectively.

2.4 BALLOON TRAJECTORY CONTROL SYSTEMS

Since the earliest days of ballooning, people have sought to master the skies – take back control from the whim of the winds. The earliest ideas of balloons are of sky-ships, well equipped with sails and oars to take their masters where they please. Inventors soon realised that balloons travel at the same speed as the winds around them as there is no relative wind to fill a sail or generate lift. The balloons of today continue to float passively with the winds.

The idea of modifying a balloons' trajectory by means of an altitude change is not new. It has been in development since the early days of hot-air ballooning. These early balloonists discovered that favourable winds could be reached by modifying their altitude. To this day, competitions still exist wherein balloonist compete to reach goals through this method – largely relying on their own assumptions of the various wind layers. Clearly, if mastered, this could become an efficient form of travel. Effectively integrating this mechanism into a computerised control systems may be the key.

2.4.1 Control Forces

Any altitude change requires some form of control force. In the case of a traditional balloonist, this force is a result of burning fuel to adjust the temperature (and density) of the balloon. Similarly, the altitude of a helium or hydrogen balloon can be controlled by venting gas or releasing ballast masses. Such systems are not sustainable as they require the use of a finite on-board resource.

Importantly, control forces can also be achieved by means of potentially inexhaustible electrical and atmospheric resources. Most obviously, propeller driven airships could control X, Y and Z position by means of electrical motors. Likewise, more conventional weather balloons can be given similar propeller systems. These have been studied quite extensively (Beemer, 1975) (Perry, 1998) (Carten, 1974). These studies all conclude that the power required to overcome the large stratospheric winds mean only very large systems are practical.

Another method involves the use of a fluid with a phase-change point within the range of the atmospheric temperatures. The fluid can be heated or cooled artificially in order to make it condense or boil, resulting in a very large change in density. (Aaron, et al., 2001). On the other hand, 'Sky anchor' balloons are equipped with a fixed volume air container in addition to their standard helium/hydrogen envelope. The air-container allows for a mass increase or decrease

by pumping in or releasing air from the ambient atmosphere. This method can also be achieved by adding an additional air balloonet inside the main helium envelope (Blamont, et al., 1974). However, the low atmospheric pressures at high altitude makes it difficult to pump air into the high pressure container, demanding surprisingly large power reserves.

Some proposed systems use long tethers with suspended aerofoils (Aaron, et al., 2001) or drag chutes (Bourke, 1969). The tether length can be adjusted in order to position the active surface in the desired wind-field. Such a system could implement a complicated air foil design to provide control forces in any of the 3 axes.

2.4.2 Trajectory Calculation

Balloon trajectory calculations have historically served to guide manned balloon missions, including the round-the-world and cross-ocean attempts that attract public interest. Trajectory calculation is also used in meteorology for long duration flights that aim to capture data (such as atmospheric particulate sensing) across a continent or ocean. As these scientific exploits do not have taxing trajectory parameters they do not require a complicated control system.

Such trajectories are typically hundreds or thousands of kilometres long with a reasonably simply goal. The trajectory is selected by studying wind-field maps and selecting the altitude that corresponds to the wind direction required (Wetzel, et al., 1995). Calculating the trajectory of a weather balloon experiment is easier, requiring entry of a few balloon and geographic parameters into a web tool (University of Wyoming, 2014) (Sowman, et al., 2010). These tools are based on a very simple wind model (the low resolution GFS model) with no ability to account for any control forces.

The availability of these simple online tools supports the popularity of free-floating balloons. Calculating and optimising the trajectory of an actively controlled balloon has been considered too complicated. In fact, the idea of using computation procedures to model the trajectory of a variable altitude balloon is in relative infancy (Draxler, 1995). Draxler demonstrated that it is possible to simulate a balloon at a constant altitude and then adjust the altitude to one of several levels after some period of time. By combining the trajectories at various altitudes, Draxler created a matrix of optimal trajectories. Notably, Draxler's analysis still revolved around long distance trajectories where the balloon is under the effect of simple-to-model constant-level wind vectors rather than complex dynamics associated with smaller trajectories.

Arora (2005) presents another computational method that could be used as part of a balloon system for planetary exploration. Arora suggests the use of an altitude controlled hot-air balloon for navigating the wind currents of Saturn's moon, Titan. Arora presents an earth-based model where certain goal position are reached whilst minimising fuel usage. This optimisation routine is based on discrete mechanical model combined with built-in Matlab minimisation functions such as 'fmincon'. This method has problems finding true optimal solutions as it depends on an initial guess, easily converging to local minima.

The random and unpredictable nature of wind fields make typical control algorithms and trajectory calculation difficult to implement for multi-altitude controlled paths. Fuzzy-based Kalman filters have been proposed with some success but there is much work to be done (Yadaiah, 2011). The ability to feed in new wind-vector measurements and estimates largely eludes current control systems. Instead, balloons typical rely on forecast wind data which has been used with varying degrees of success (Wetzel, et al., 1995).

2.4.3 Station Keeping

Station keeping in the ballooning world refers to the static positioning of very large stratospheric airships – often used for remote sensing, disaster monitoring and communications relay applications (Onda, et al., 1999). In terms of conventional weather balloons; station keeping is a very foreign concept due to both the dynamic and computational difficulties it presents.

Conventionally, weather balloons are used for free floating applications with no control forces other than potentially expelling gas to reach neutral buoyancy at a goal altitude. This thesis proposes the use of altitude changes to catch desirable winds to produce one large looping trajectory. This method can allow for a more passive, wider area station keeping – particularly suitable for imaging applications. No research into this technique is evident in existing literature. This will be a major point of examination throughout this thesis.

3 SYSTEM DESIGN CONSIDERATIONS

3.1 SYSTEM GOALS

Remote sensing is a challenging field that benefits from a wide variety of acquisition methods, each with its own cost, temporal or spatial advantages. The benefits of an aerostat system over other technologies lies with good spatial coverage, low cost and low upkeep.

The system must be designed so that it does not duplicate functions best performed by conventional aircraft, fixed wing UAVs or satellites. This means it should be designed specifically for high quality, real-time strategic imaging of fires. It is expected that a balloon is the best platform for such data acquisition.

Summarising, the system should:

- Provide high quality infrared images (sub 1m pixels) of the bushfire front.
- Be capable of imaging the same fire for a useful period of time (many hours or a day).
- Provide close to real-time access to image data.
- Be quick to deploy and quick to reach goal position.
- Be low cost and simple to operate.
- Complete several trajectory loops above the fire zone, maximising imaging time.
- Be easily recoverable by using the control system to select landing zone.

3.2 THE TRIANGULAR LOOPING TRAJECTORY

Satellites can produce wind forecasts that describe wind directions between altitudes of 100m to 25km. There is typically a large amount of variation between these extremes, in particular, stratospheric winds (jet stream) often blow in a very different direction to tropospheric winds.

If two layers had winds in exactly opposite directions, a balloon could travel along one and then change altitude to the other layer when it was required to loop back. Reality it is not so simple; it is very rare for two layers to exist with winds 180 degrees from one another. Instead, there are often many layers which vary by less than 180 degrees from one another.

The triangular looping trajectory is a very simple concept. It suggests that performing a loop does not require two layers opposite two one another. Instead it merely requires three layers with winds directions that can added to create a triangle, i.e. three layers with relative angles that add up to 180 degrees.

For example, if there are three layers which are each 60 degrees from one another, a loop can still be formed by following a triangular trajectory. An example is demonstrated below:

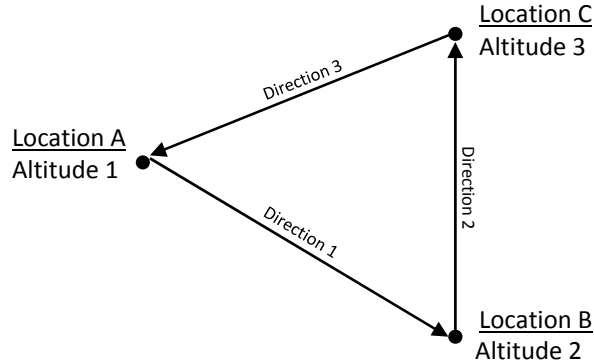


Figure 3-1: A simplified triangular trajectory (viewed from above) made from three layers, 60 degrees from one another.

This simplified trajectory assumes the balloon can move perfectly vertically from one altitude layer to another. In reality, when a balloon changes layer it must do so slowly. Whilst changing layer the balloon is under the effect of a variety of different winds, giving a curved path. If the transfer between two layers is slow, the size of these curved sections will increase.

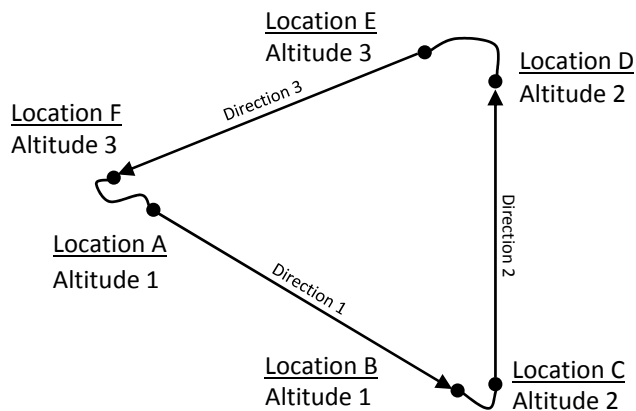


Figure 3-2: An example of a more realistic triangular trajectory made from three layers 60 degrees from one another.

Although these curved sections add complexity, they actually make creating loops a much more flexible process. It becomes possible to create figure-8 style loop with just two wind layers.

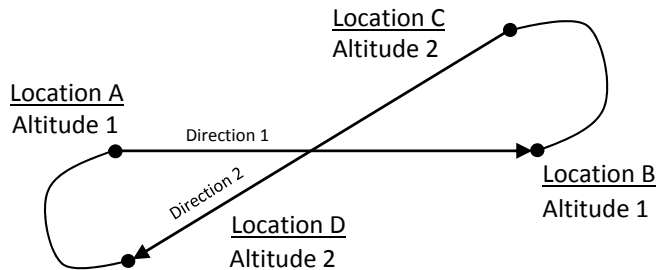


Figure 3-3: An example of a figure-8 style loop using just two different wind layers. Curved sections are the areas where the balloon is changing altitude

3.3 AEROSTAT DESIGN

A large variety of balloon designs could suit a fire sensing aerostat, ranging from weather balloons to transosondes. More complicated lighter-than-air vehicles such as blimps and zeppelins provide great manoeuvrability and control at the expense of launch time and cost. Elastic weather balloons sacrifice control for low cost and simplicity.

The simplest practical system, from the point of view of availability and manoeuvrability is the standard elastic weather balloon. It has been adopted it to simulate the feasibility of the proposed looping trajectory. The simulation model can easily be modified to suit larger balloons (for more lift) or adapted for similar craft such as zero-pressure or super-pressure balloons.

3.3.1 Elastic Weather Balloon

Elastic weather balloons have been used by meteorologists for over hundred years. Recently, they have been used in a variety of remote sensing and ‘near space’ applications. Their low cost and simplicity means they are suitable for the rapid deployment required in an emergency fire situation. They also have an altitude ceiling of around 30km, perfect for the requirements.

This simulation used a hydrogen filled Novalynx 400-8242 sounding balloon. This is a well-studied balloon with easily available specifications allowing for accurate modelling of elastic properties (NovaLynx, 2014).

Weight	Material	Neck Diameter	Un-inflated Diameter	Std Inflated Diameter	Burst Diameter
800 g	Natural Rubber	32 mm	108 cm	1.85 m	6.8 m
Free Lift	Gross Lift	Payload Mass	Inflation Volume	Ascent Rate	Altitude at Burst
2,000 g	3,950 g	1,150 g	3.6 m ³	400m/min	28 km

Table 3-1: Key Statistics for the 400-8242 Balloon (NovaLynx, 2014)

3.3.2 Control Forces

To complete a trajectory loop, some form of z-axis control force method must be selected. Some of these have been outlined in section 2.4.1.

This simulation assumes that the balloon carries a small bottle of hydrogen gas with an electronically controlled solenoid valve. This allows the balloon to be remotely filled or purged of additional lifting gas as required.

Hydrogen containers have been studied extensively by the automobile industry (as an efficient hydrogen storage method is key to a successful hydrogen automobile). It is important to find a technology which allows for high volume storage with a low container mass. Developments within this field will be key to a successful altitude controlled balloon as compressed gas bottles are far too heavy.

It is considered that Existing products, such as the BL-220 metal hydride container, are unlikely to be suitable because they are too heavy. The Bl-220 product has a mass of 2kg and a capacity of 242 L of hydrogen gas.



Figure 3-4: BL-220 Metal Hydride Bottle (HYDROGEN "COMPONENTS", INC, 2014)

The number of moles of hydrogen gas (given 242 L under 1 atm) is calculated as follows:

$$n = PV/RT$$

$$n = (1 \text{ atm} \times 242)/(0.0826 \frac{L \cdot atm}{K \cdot mol} \times 298)$$

$$n = 9.83 \text{ mol}$$

$$m = n \times 2 \times 1.008$$

$$m = 19.82 \text{ grams}$$

This represents roughly a 1:100 gas to bottle mass ratio. This is expected, given that the best metal hydrides have approximately a 2% absorption ratio (Appleby, et al., 2003). Newer technologies based on lithium, boron and aluminium have mass absorption ratios of up to 10%.

Off-the-shelf products using this technology cannot yet be purchased given their infancy. The details of this system will need further investigation.

If possible, this on-board gas bottle would be replaced by a more sustainable method in a future design iteration. A further development of the system, stabilised by the “Sky Anchor” would allow a balloon stay aloft within for weeks at a time. Sky Anchoring comprises the pumping air into of fixed volume container to increase or decrease system mass. Power is provided by electricity obtained from solar cells.

3.4 PAYLOAD DESIGN

The basic mission requirements suggest the following payload details:

- An Infrared camera will be attached as the primary payload.
- On board sensors will be used to determine flight path and position if required (GPS and/or Inertial).
- Images will be captured continually or at locations suggested by flight prediction software.
- Images will be transmitted to a ground station for analysis in real-time.

3.4.1 Thermal Camera

The primary sensor should be a commercially available thermal camera. This should have an un-cooled infrared sensor to avoid any costly, complicated and heavy cooling system. Unfortunately, many of the higher resolution and frame rate infrared cameras are restricted by the United States International Traffic in Arms Regulations (ITAR).

Technology which provides suitable performance and resolution is currently available, although it is considered too heavy. L3’s ‘16-Megapixel Infrared Sensor Engine’s 4k x 4k infrared sensor is designed specifically for fixed-wing observational UAVs (L3, 2013). This camera’s power and mass requirements (50W and 6kg) exceed the allowable limits for a weather balloon. Further development and simplification would be required to render it suitable for use on a simple balloon platform.

3.4.2 Lens

Calculation of ground coverage is dependent on the choice of image sensor and required resolution. L3's high resolution camera offers a 4096 x 4096 px sensor within the 3.5 and 5.1 micrometre band. Assuming a required ground resolution of 1m at 25km altitude, the angle of the camera lens is calculated as follows:

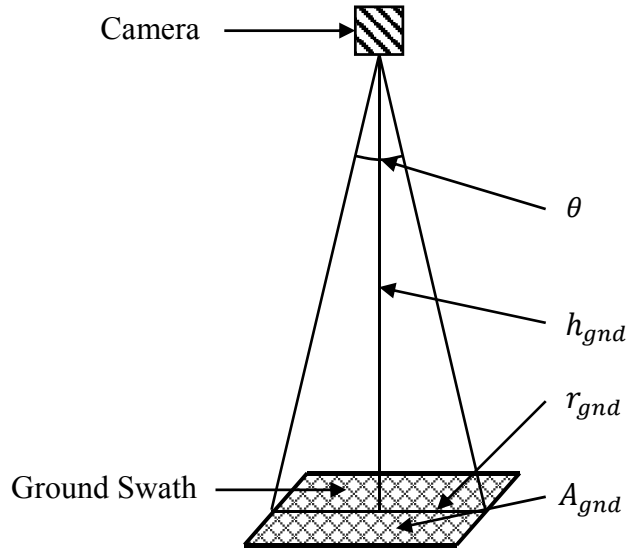


Figure 3-5: Calculation of required camera angle, θ . This figure demonstrates the simple geometry of the camera as it faces Nadir.

$$\tan\left(\frac{\theta}{2}\right) = \frac{h_{gnd}}{r_{gnd}} \quad \text{rearranging: } \theta = 2\tan^{-1}\left(\frac{h_{gnd}}{r_{gnd}}\right)$$

$$r_{gnd} = Res_{gnd} \frac{CCD_x}{2} \quad \text{substituting: } \theta = 2\tan^{-1}\left(\frac{h_{gnd}}{Res_{gnd} \frac{CCD_x}{2}}\right)$$

With $CCD_x = 4096$ px, $h_{gnd} = 25000$ m and $Res_{gnd} = 1$ m/px calculations show $\theta = 9.366$ degrees. Using this camera angle gives the following swath widths and resolutions at lower altitudes:

Height (m)	8,000	10,000	12,000	14,000	16,000	18,000	20,000	22,000	24,000
Swath Width (m)	1320	1649	1979	2309	2639	2969	3299	3629	3959
Ground Res (m/px)	0.32	0.40	0.48	0.56	0.64	0.72	0.81	0.89	0.97

Table 3-6: Image swath width and resolution for 8,000 to 24,000 m above ground assuming 9.37 degree lens.

3.4.3 Other Systems

3.4.3.1 *Communications:*

The communications system should allow real-time transmission back to a ground station. If a conventional RF signal is used, this ground station may be a mobile unit attached to the balloon's launch vehicle. There is also the possibility of using internet protocol as several Australian 3G networks extend high into the atmosphere (Brand, 2014). Both options should be explored. It is considered that cost effective solutions to communications are available and a suitable system can be developed.

3.4.3.2 *Chassis and Attachment*

The chassis must provide a strong and durable mounting point for the other components – in particular the IR sensor. If required; pan and tilting servos may be added to the chassis to give pointing control instead of passive nadir pointing. The balloon attachment rig should provide a stable payload mount as the balloon fluctuates from 1.8m to 6.8m diameter. The details of the chassis and attachment are of little importance at this stage of development.

3.4.3.3 *Software Design*

A wide variety of image processing techniques and algorithms have been developed specifically for the analysis of bushfires (Graml & Wigley, 2007). Of particular interest are algorithms governing the detection of both 'Hotspots' and the 'Transient Fire-front'. Minor modifications would be needed to apply such techniques to the requirements of a balloon platform. Such calculations could occur on the balloon itself or at a control centre or ground station.

3.4.3.4 *Guidance, Navigation and Control (GNC)*

The balloon's GNC system should implement the data collection and control commands required by the trajectory control system outlined in the following chapters. Again, at this stage it is unclear whether the trajectory simulation and control system calculations can be run on-board the balloon or must be calculated at the ground station. Considerations such as processor budget will be ignored in this simulation given the early stage of analysis.

4 GOVERNING PHYSICS AND MODEL

4.1 INTERNAL BALLOON PHYSICS

This section will describe the basic forces and principles that effect pressure (and density) inside a standard elastic weather balloon.

4.1.1 Pressure Summation

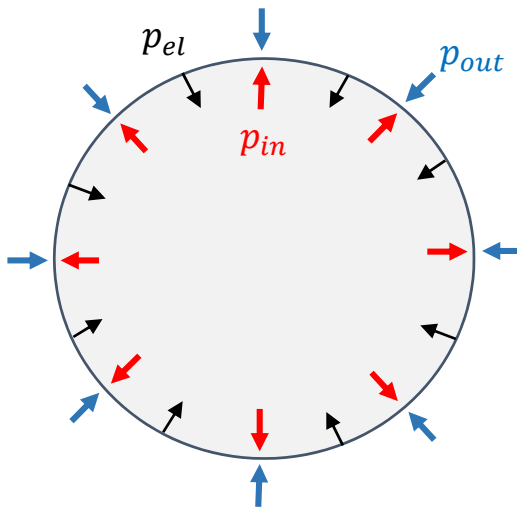


Figure 4-1: Pressure Summation on an elastic balloon.

For any elastic balloon, internal pressure must be greater than external pressure due to the force the rubber exerts inwards. In order to maximise lift, the density of the gas inside the balloon should be minimised. Minimising density requires minimal internal pressure, therefore elastic force should be minimised. The above diagram illustrates:

$$P_{out} = P_{in} - P_{el} \quad (4-2)$$

P_{out} is the atmospheric pressure outside the balloon. This pressure is a function of altitude and is typically approximated using a standard atmospheric model. This will be discussed further in subsequent sections.

P_{in} is the pressure inside the balloon. This is determined with the ideal gas law, a function of number of molecules, temperature and volume (Clapeyron, 1834):

$$P_{in} = \frac{nRT}{V} \quad (4-1)$$

The parameters R and T are the universal gas constant and Temperature at altitude – determined from the standard atmospheric model. The parameter, V (volume), is not so simple to estimate in a transient system as balloon radius changes with altitude. In order to calculate this, it is important to understand the elastic forces.

4.1.2 Elastic Force

The p_{el} refers to the pressure due to the elasticity of the balloon. This is determined from a stress-strain model. There are two well known hyperelasticity models: the Gent model and the Mooney-Rivlin model (Müller & Strehlow, 2004):

$$P_{el} = 2\mu \frac{t_0}{r_0} \left(\left(\frac{r_0}{r} \right) - \left(\frac{r_0}{r} \right)^7 \right) \left(1 + \frac{1-\alpha}{\alpha} \left(\frac{r}{r_0} \right)^2 \right) \quad (4-3)$$

The Gent model is very similar to the Mooney-Rivlin model and includes an additional J_m parameter to account for the stiffening of the rubber as it approaches breaking point.

Müller & Strehlow (2004) outline typical values for shear modulus $\mu = 300kPa$ and the parameter $\alpha = 10/11$. r_0 is the un-stretched radius of the balloon as given by the manufacturer. Similarly, t_0 , is the balloon's un-stretched thickness, this can be measured or calculated based on weight, density and diameter. A typical weather balloon has an initial thickness of 0.2 mm and bursting thickness of 5 μm .

4.1.3 Governing Equation

This governing equation is determined by substituting the Internal and Elastic pressure equations (eq 4-2 and eq 4-3) into the pressure summation, $P_{out} - P_{in} + P_{el} = 0$. In transient terms, this equation is a function of altitude (h).

$$P_{out}(h) - \frac{nRT(h)}{\frac{4}{3}\pi r(h)^3} + 2\mu \frac{t_0}{r_0} \left(\left(\frac{r_0}{r(h)} \right) - \left(\frac{r_0}{r(h)} \right)^7 \right) \left(1 + \frac{1-\alpha}{\alpha} \left(\frac{r(h)}{r_0} \right)^2 \right) = 0 \quad (4-4)$$

By setting r to the initial balloon radius at height = 0, eq 4-4 is solved to obtain the number of moles, n . Once an altitude control system is introduced, the number of moles, n , will also change as a function of time. Additionally, n will change due to gas diffusion through the balloon's walls.

This internal pressure summation reveals both the number of gas molecules and the radius of the balloon. These two parameters are critical to the calculation of the balloon's external dynamics, particularly lift and drag.

4.2 EXTERNAL BALLOON PHYSICS

4.2.1 Force Summation

A conventional force summation suggests:

$$\sum F_z = ma_z \quad (4-5)$$

Pictorially, this force summation is simple:

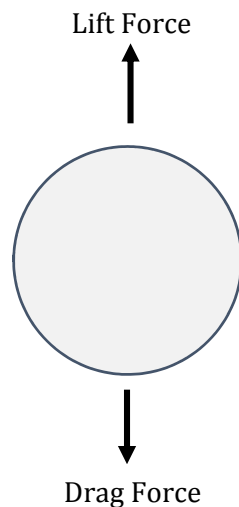


Figure 4-2: Summation of Forces in the vertical axis

In the case of a balloon, apart from the initial burst of acceleration from rest, acceleration is typically zero, changing only slightly as altitude increases. The simulation can therefore be simplified to assume the balloon is perpetually at terminal velocity. This simple relationship is:

$$F_L = F_D \quad (4-6)$$

4.2.2 Drag Force

The drag force is calculated with the standard drag equation:

$$F_D = \frac{1}{2} \rho v^2 C_D A \quad (4-7)$$

Expanding in transient terms:

$$F_D = \frac{1}{2} \rho_{(h)} v^2 C_D \pi (r_{(h)})^2 \quad (4-8)$$

Some parameters, such as r and ρ (radius and air density), are dependent on altitude. If the balloon's cross-section is a perfect circle and the shape is a perfect sphere, drag coefficient, C_D , is 0.47. The way in which drag changes as altitude increases is complicated. As altitude increases, air density decreases (lowering drag) but radius increases (increasing drag).

4.2.3 Lift Force

Archimedes' principle explains that the lift, or buoyancy is calculated by subtracting the craft's mass from the mass of fluid it displaces. This is easily converted into lift force when multiplied by gravity.

$$m_{lift} = m_{displaced} - m_{system} \quad (4-9)$$

$$m_L = \rho_{air} V_{displaced} - (n_{moles} M_{mole} + m_{total \ exl \ gas}) \quad (4-10)$$

$$F_L = \left(\rho_{air} \frac{4}{3} \pi r^3 - (n_{moles} M_{mole} + m_{Balloon} + m_{payload}) \right) g \quad (4-11)$$

Given that the peak altitude of the balloon will be around 20km, it is reasonable to assume constant gravity as at maximum altitude gravity would be 99.4% of sea-level gravity.

4.2.4 Governing Equation

By substituting the equations for Drag (eq 4-8) and Lift force (eq 4-11) into the initial force summation equation (4-6), terminal velocity in the Z direction is determined:

$$gm_L = \frac{1}{2}\rho v^2 C_D A \quad (4-12)$$

Rearranging for velocity:

$$v = \sqrt{\frac{2gm_L}{\rho C_D \pi r^2}} \quad (4-13)$$

Substituting the equation for M_L (eq 4-10):

$$v = \sqrt{\frac{2g \left(\rho_{(h)} \frac{4}{3} \pi (r_{(h)})^3 - (n_{moles} M_{mole} + m_{Balloon} + m_{payload}) \right)}{\rho_{(h)} C_D \pi (r_{(h)})^2}} \quad (4-14)$$

This equation gives the terminal velocity as a function of the number of moles at any altitude.

4.2.5 Lift Force Control

Velocity can be controlled by reducing the number of moles. For example, upon reaching a desired altitude, lift can be reduced to zero (becoming neutrally buoyant) by expelling gas. The number of moles of gas required for this is calculated as follows:

$$n_{moles} = \frac{\rho_{(h)} \frac{4}{3} \pi (r_{(h)})^3 - (m_{Balloon} + m_{payload})}{M_{mole}} \quad (4-15)$$

This will allow the balloon to travel at constant ‘pressure’ altitude (pressure altitude and real altitude are not always the same). Given that the wind data is also mapped to pressure attitude axes, this complication will not be a problem.

Gas must be added or removed in order to reach a desired velocity. The governing equation (eq 4-6) can be rearranged to give moles, n as a function of goal velocity, at a goal altitude. It is important to note that ρ changes with height whilst r changes with both height and the previous

n_{moles} (as per the Mooney-Rivlin elastic model).

$$F_L = F_D$$

$$\begin{aligned} \left(\rho_{(h)} \frac{4}{3} \pi r^3 - (n_{moles} M_{mole} + m_{Balloon} + m_{payload}) \right) g &= \frac{1}{2} \rho_{(h)} v^2 C_D \pi (r_{(h)})^2 \\ (n_{moles} M_{mole} + m_{Balloon} + m_{payload}) &= \rho_{(h)} \frac{4}{3} \pi r^3 - \frac{1}{2g} \rho_{(h)} v^2 C_D \pi (r_{(h)})^2 \\ n_{moles} &= \frac{\rho_{(h)} \frac{4}{3} \pi (r_{(h)})^3 - \frac{1}{2g} \rho_{(h)} v^2 C_D \pi (r_{(h)})^2 - (m_{Balloon} + m_{payload})}{M_{mole}} \end{aligned} \quad (4-16)$$

Eq 4-15 was the special case of this equation, when goal velocity was zero. 4-16 gives the number of moles required to have velocity, v , at an altitude of h . This requires calculation of internal density and radius at the goal altitude, both of which are a function of n_{moles} . This equation therefore has an indirect circular reference; it can only be solved iteratively.

4.3 ATMOSPHERIC MODEL

The International Standard Atmosphere model is used to describe pressure, temperature and density at each altitude. Real forecast weather data is used where possible to fine tune these values. This forecast data is derived from NOMADS servers, just like the wind data that forms the basis of the wind model.

4.4 WIND MODEL

A weather balloon is typically a purely passive craft. Reliable wind data is required to accurately predict its trajectory. It is assumed that the balloon moves the same speed as the wind.

Ideally, wind data should describe the cross-sectional wind vector fields at a large range of altitudes. To effectively analyse the predictability of the trajectory, both forecast and real wind data must be known over a large time period.

A very large amount of data is required. Wind speeds vary significantly at all levels of the atmosphere. Speed and direction also vary from season to season. The figure below indicates how the magnitude of the wind vectors change with altitude. Several important zones are evident, at approximately 10km where wind is at a local maximum, and 20km where it is at a minimum.

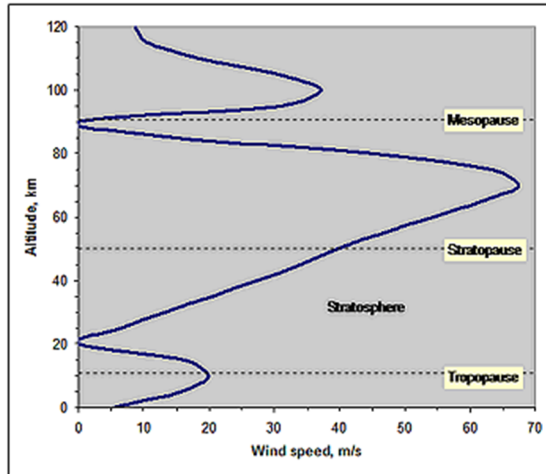


Figure 4-3 : Average wind speeds at Altitude, values vary with season and location (Struzak, 2003)

To understand how these winds vary with time, geography, and weather, it is important to understand the basic wind mechanics.

4.4.1 Turbulent momentum flux

Air within the atmosphere is under the influence of four forces:

1. Weight due to gravity
2. Pressure gradient force
3. Coriolis force
4. Molecular friction between particles

Gravity is independent of the flow whilst Coriolis force is a function of the fluid's speed. Air is a Newtonian fluid; friction is proportional to the velocity gradient. Given these relations, conservation of momentum means that the dynamic flow can be derived by equating the forces exerted on the fluid particles to the rate of change of momentum. This method gives the famous atmospheric Navier-Stokes equation (Matthias & Focken, 2005).

$$\rho(\delta_t \vec{u} + (\vec{u} \cdot \nabla) \vec{u}) = -\nabla p + 2\rho(\vec{u} \times \vec{\Omega}) + \eta \nabla^2 \vec{u} - f_g \quad (4-18)$$

Eq 4-18 allows the modelling of most forms of wind flow – even thermal effects and chaotic behaviour can be described with the left-hand function. Solving this equation is difficult as the atmosphere is very turbulent with parameters constantly fluctuating. To account for this difficulty, Matthias & Focken (2005) suggest that focus is shifted to the dominating mean-flow effects, removing the details of finer fluctuations. This leads to a Reynolds-averaged equation:

$$\rho(\delta_t \vec{U} + (\vec{U} \cdot \nabla) \vec{U}) = -\nabla p + 2\rho(\vec{U} \times \vec{\omega}) + \nu \nabla^2 \vec{U} - f_g - \nabla \tau_t \quad (4-19)$$

This equation is similar to the Navier-Stokes (eq 4-18) except has been re-written to describe the mean variables instead of instantaneous values. Notably, this equation still describes the effects of turbulent motion by the introduction of an additional force on the right-hand side, $\nabla \tau_t$, the turbulent momentum flux.

4.4.2 Neutral logarithmic wind-shear profile

The turbulent momentum flux term, $\nabla \tau_t$, (shown in eq 4-19) is the basis of the logarithmic wind-shear profile.

$$-\nabla \tau_t \quad (4-21)$$

$$\tau_{tij} = \rho \bar{u}_i \bar{u}_j \quad (4-20)$$

By running a Taylor expansion on the velocity profile the equation is re-arranged as follows:

$$\tau_{tij} = -\rho l^2 (\delta_z U)^2 \quad (4-22)$$

$$\tau_{tij} = -\rho (KZ)^2 (\delta_z U)^2 \quad (4-23)$$

$$\delta_z U = \sqrt{-\frac{\tau_{tij}}{\rho}} \cdot \frac{1}{KZ} \quad \rho = \frac{u_*}{KZ} \quad (4-24)$$

This is integrated to get the logarithmic wind-shear profile. The constant, z_0 , is the roughness length, a function of the surface roughness of the terrain.

$$U(z) = \frac{u_*}{K} \ln \left(\frac{z}{z_0} \right) \quad (4-25)$$

4.4.3 Thermal Stratification

The windshear profile (eq 4-25) does not consider any thermal effects. In reality these play an important role in real atmospheric winds. These are of obviously of particular interest in the analysis of bushfires.

To account for these effects, a dimensionless thermal modification function is introduced into the wind-shear profile. This function depends on heat flux H , friction velocity u_* , and the altitude z .

$$\delta_z U = \frac{u_*}{KZ} \Phi_m(H, u_*, z) \quad (4-26)$$

As air-parcels rise, they expand due to the decreasing atmospheric pressure. The work of this expansion absorbs energy, causing a decrease in temperature. This convection process continues until the temperature of the air-parcel corresponds to that of the new, higher environment. To represent this vanishing temperature gradient, both a potential temperature $T(z)$, and a cooling term is introduced. This cooling term is known as the dry adiabatic temperature gradient due to the expansion of an air parcel $\Gamma(z)$.

$$\mathcal{H}(z) = T(z) + \Gamma(z) \quad (4-27)$$

The sign of this gradient function allows the characterisation of vertical air movements; are they damped or enhanced? This damping factor is used to determine the current level of atmospheric stability. This term is used to calculate the Monin-Obukhov length. If L is positive, the cooling process is stable. If negative, stratification cooling is unstable.

$$L = \frac{u^3 \mathcal{H} c_p \rho}{kgH} \quad (4-28)$$

Using this knowledge, the thermal modification function is redefined in terms of Monin-Obukhov length:

$$\Phi_m(H, u_*, z) = \Phi_m\left(\frac{z}{L}\right) \quad (4-29)$$

The initial logarithmic wind-speed profile is then modified depending on sign of the Monin-Obukhov length (eq 4-28). This gives two equations for the modification function:

$$if: \quad \left(\frac{z}{L} > 0, stable \right)$$

$$\Phi_m \left(\frac{z}{L} \right) = -5 \frac{z}{L} \quad (4-30)$$

$$if: \quad \left(\frac{z}{L} < 0, unstable \right)$$

$$\Phi_m \left(\frac{z}{L} \right) = 2 \ln \left(\frac{1+x}{2} \right) + \ln \left(\frac{1+x^2}{2} \right) - 2 \tan^{-1}(x) + \frac{\pi}{2} \quad (4-31)$$

$$where: x = \left(1 - 16 \frac{z}{L} \right)^{\frac{1}{4}}$$

These are fed into the wind-speed profile:

$$U(z) = \frac{u_*}{K} \left(\ln \left(\frac{z}{z_0} \right) - \Phi_m \left(\frac{z}{L} \right) \right) \quad (4-32)$$

Ideally, this wind-speed profile (eq 4-32) would be directly modified to include the thermal effects of the bushfire. This modification would require detailed knowledge of the fire's fuel load and burn rate in order to calculate the atmospheric heat flux (as inputted into eq 4-26). Unfortunately, this data is not publically available – although it is likely that rural fire services have access to it, as it forms the basis of existing fire path prediction software. If this were available, the heat flux data could be used to determine how the bushfire effects local wind fields and convection currents.

Importantly, these thermal stratification effects only reach to the end of the troposphere (10 to 15km altitude), as this is the limit of the earth's 'Convective Boundary Layer' (CBL). Above this boundary layer, the effect of the fire can be assumed to be zero – upper atmospheric wind will not change (Obserson, 2010). The balloon trajectory will be primarily modelled above the CBL as all trajectory looping will be between 10km and 25km altitude. The balloon will briefly pass through the lower altitude to reach these heights but this will happen before the balloon is above the fire-front. For this reason, the thermal effects of the bushfire have been excluded from the simulation as they would result in unnecessary complications with only a minor increase in trajectory accuracy.

4.4.4 Wind Data

The National Centers for Environmental Prediction (NCEP) is the world leader in environmental modelling data. NCEP is a branch of the United States National Oceanic and Atmospheric Administration (NOAA), providing a variety of free forecast data covering a range of geographic regions. This data is made available through the 'NOAA Operational Model Archive and Distribution System' (NOMADS).

NOMADS data is typically compressed into a file format known as NetCDF (*.nc, *.nc4, *.ncd). This format is designed to represent complex multi-dimensional arrays or matrix-orientated scientific data. This allows the storage of a variety of 2D vector fields that vary with both position and time.

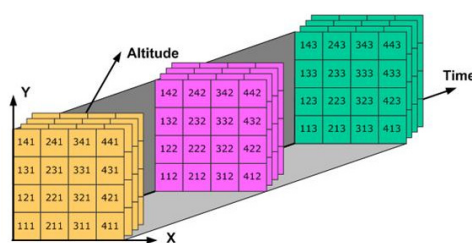


Figure 4-4: Breakdown of a single multi-dimensional netCDF variable (Chungwook, 2007)

The data resolution (in all 3 axes) is of importance when selecting the vector wind data. High resolution is required to interpolate and form a continuous wind model in all directions, x, y and z. Research suggests the interpolation between these points should be done with a cubic spline method (Sim, 2007).

NOMADS offers high resolution data (0.05 degrees lat/lon increments) across Continental United States (CONUS) and lower resolution data globally (0.5 degrees). The latter model, known as the GFS (Global Forecast System) provides 7.5 days, or 180 hours of forecast data and runs 4 times per day. (NOMADS NCEP, 2014)

OPeNDAP/DODS Data URL: http://nomads.ncep.noaa.gov:9090/dods/gfs_hd/gfs_hd20140309/gfs_hd_00z	
Description:	GFS half degree (0.5x0.5) fcst starting from 00Z09mar2014, downloaded Mar 09 04:27 UTC
Documentation:	(none provided)
Longitude:	0.0000000000°E to 359.5000000000°E (720 points, avg. res. 0.5°)
Latitude:	-90.0000000000°N to 90.0000000000°N (361 points, avg. res. 0.5°)
Altitude:	1000.0000000000 to 1.00000000000 (47 points, avg. res. 21.717)
Time:	00Z09MAR2014 to 00Z17MAR2014 (65 points, avg. res. 0.125 days)
Variables:	(total of 227)

Figure 4-5: Details of GFS data resolution and variables (Nomads NCEP, 2014)

5 SIMULATION METHODOLOGY

The balloon's trajectory simulation was conducted within Matlab. There were three different systems that made up this simulation:

1. Physical Model – This described the balloon's internal and external mechanics. How does the stress-strain relationship work? How do external effects change the movement of the balloon?
2. External Model – This described the various atmospheric effects. How does air density and pressure vary with altitude and temperature? What are the atmospheric wind conditions?
3. Control System – This determined how the balloon would complete the trajectory loop. What are the most efficient and reliable winds to use in the loop? How much hydrogen gas should be added or removed from the balloon to reach the required altitude?

5.1 AREA OF INTEREST

The NCEP GFS model provides 0.5 degree forecast data across the whole globe while higher resolution 0.05 degree data can be found for smaller geographic domains. Initial tests suggested that the lower resolution GFS data was too inaccurate to serve as the basis for the simulation:

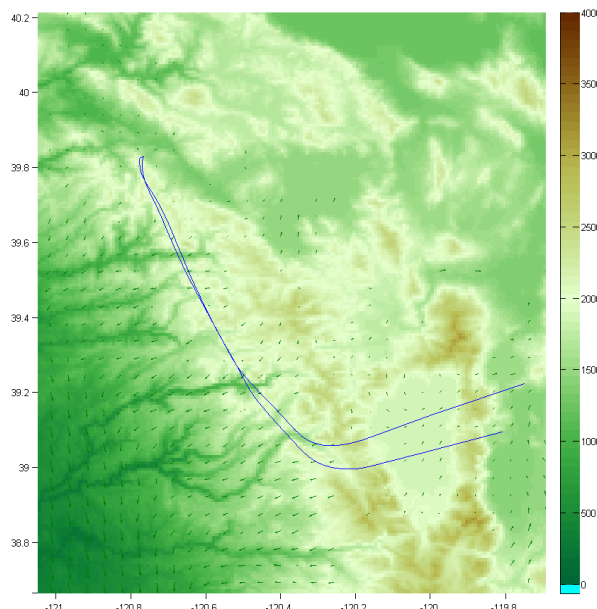


Figure 5-1: Demonstration of two basic trajectories, one modelled with 0.5 deg GFS data, the other with 0.05 deg NAM CONUS data.

For this reason, the simulation area was specified as a point within continental United States. This selection made use of the high resolution NAM CONUS data that is made available free of charge by NOMADS. Similar Australian data can be obtained by the Australian Bureau of Meteorology at cost (Bureau of Meteorology, 2014). Given the early stages of this analysis, this cost could not be justified.

The simulation point was selected to be in the Angora Lakes region just south of Lake Tahoe, California:

$$\text{Latitude} = 38.85^\circ \text{ North}$$

$$\text{Longitude} = 120.05^\circ \text{ West}$$

This was the site of a damaging wildfire between 24/June/2007 and 10/July/2007. A total of 12.5 km² of forest was burned, leading to the destruction of 242 houses and a further 67 commercial structures. \$11.7 million was spent by the Californian government to fight this fire which ultimately caused \$141 million in damages with a further \$1 billion in losses to the local tourist-driven economy (Stockwell, 2007).

Although this fire caused significant damage and destruction – its size is far from comparable to Australian bushfires which typically burn faster (due to eucalyptus oil) and over a much larger area. For example (as shown in Table 1-1), during the 2002-2003 season, 150,000 km² of bushland was destroyed in the Australian Northern Territory alone. Large fires such as the Victorian Black Saturday fires burn around 5,000 km² (Romsey Australia, 2012).

In order to more closely represent an Australian bushfire, the simulated fire was chosen to be 1,000 km². This meant a square width as follows:

$$1,000 = w^2$$

$$\text{Width} \approx 31.6 \text{ km}$$

This simple size and position data was used to create a simple square observation area. This allowed various trajectories to be compared by the period of time they stayed above the observation area.

It should be noted that this area of interest is static, unlike a transient fire. Additionally, any simulation of an Australian size bushfire with American wind data is inherently biased – nonetheless this should not cause an issue given the early stages of the feasibility analysis.

5.2 DATA ACQUISITION

Meteorological forecast data was downloaded directly from the American NOMADS NCEP servers. This archive contains approximately the last 30 days of forecast data with four forecast packages each day. These data packages provided a map of all important meteorological variables at 0.046° latitude intervals and 0.047° longitudinal intervals across all of continental United States (CONUS). This data is spread across a 2.625 day temporal forecast grid with a resolution of 3 hours. This standard is known as the North American Model (NAM) – for this reason we get the abbreviation, NAM CONUS.

OPeNDAP/DODS Data URL: http://nomads.ncep.noaa.gov:9090/dods/nam/nam20140419/nam_conusnest_18z		
Description:	NAM CONUS Nest every 3 hours starting from 18Z19apr2014, download Apr 19 20:46 UTC	
Documentation:	(none provided)	
Longitude:	-152.85299700000°E to -49.40219446122°E	(2191 points, avg. res. 0.047°)
Latitude:	12.19000000000°N to 61.27160909091°N	(1064 points, avg. res. 0.046°)
Altitude:	1000.00000000000 to 10.00000000000	(42 points, avg. res. 24.146)
Time:	18Z19APR2014 to 06Z22APR2014	(21 points, avg. res. 0.125 days)
Variables:	(total of 302)	

Figure 5-2: Details of NAM CONUS data resolution, there are 302 variables across this grid (Nomads NCEP, 2014)

Many important variables are distributed amongst an additional 42 point non-standard altitude grid ranging from 1000 to 10 millibars (approx. 100m to 25km altitude). Notably, this includes the 3 most important wind vector variables required for balloon analysis:

- ugrdprs: Zonal (x direction) component of wind (m/s)
- vgrdprs: Meridional (y direction) component of wind (m/s)
- dzdptrs: Vertical (z direction) component of wind (m/s)

Throughout this simulation it is assumed that the 0h forecast data is the real wind data. This is partially true; 0h forecasts assimilate satellite data with real-time wind, temperature and pressure measurements made by weather stations. It therefore represents the most accurate wind data possible without physically measuring wind on each atmospheric layer.

In addition to wind-data, NOAA also provides high quality topographic map information that is accessible via their ERDDAP server. The ‘usgsCeSrtm30v1’ model outlines a global topographic

map with 30 arc second resolution. This was connected to the Matlab code via a simple API, allowing specified geographic regions to be downloaded automatically (NOAA ERDDAP, 2014).

5.3 DATA REMAPPING AND INTERPOLATION

All wind and topographical data was remapped to the terrains' longitude (deg), latitude (deg) and altitude (m) axes. Importantly, the pressure mapped wind vectors were converted to the altitude grid with the following formula:

$$h_{alt} = \left(1 - \left(\frac{P_{sta}}{1013.25} \right)^{0.190284} \right) \times 145,366.45 \quad (5-1)$$

Pressure (kPa) to Altitude (m) conversion (NOAA, 2012)

An observation area was defined as ± 3 degrees around the fire: ($38.85^\circ N, 120.05^\circ W$). This led to a raw wind data matrix of $42 \times 130 \times 127$ data points. These points were interpolated in three dimensions with a spline method in order to produce a much higher quality $301 \times 601 \times 601$ resolution dataset. The effects of this method can be seen in the figure below wherein the average wind magnitude for the area on the 16/04/2014 is plotted.

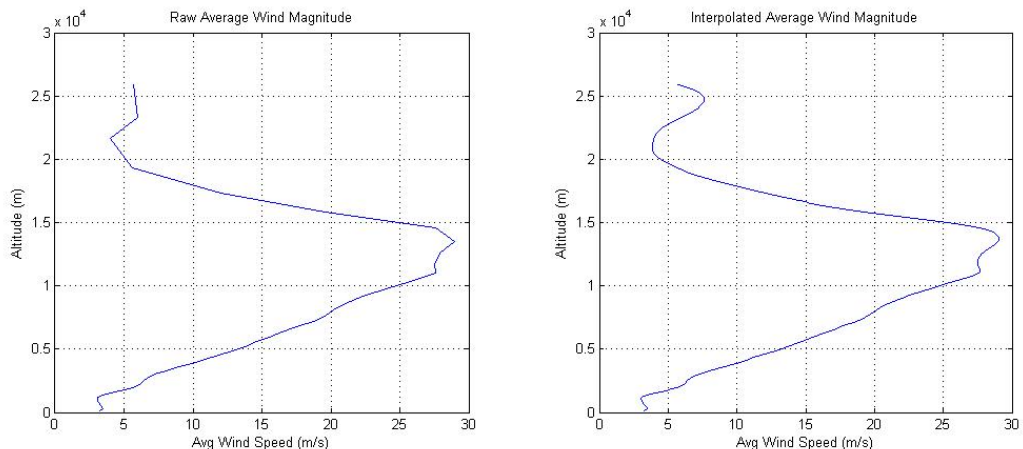


*Figure 5-3: Comparison between raw wind data (left) and spline interpolated data (right)
This spline interpolated data has questionable accuracy at high altitudes.*

Conversion between polar position (lat, long, alt) and Cartesian (x, y, z) was achieved with the haversine formula:

$$d = 2r \arcsin \sqrt{\sin^2\left(\frac{\phi_2 - \phi_1}{2}\right) + \cos(\phi_1) \cos \phi_2 \sin^2\left(\frac{\lambda_2 - \lambda_1}{2}\right)} \quad (5-2)$$

5.4 SYSTEM ALGORITHMS

A number of algorithms were designed to accurately and efficiently implement the simulation. A basic explanation of these algorithms is included in the following subsections. For further details, please refer to the code in the Appendix.

5.4.1 Physical balloon Model (PBM)

The complex physical behaviour of the balloon was modelled with a Runge-Kutta iterative method. This allowed the multi-order integral and inter-related circular referenced equations to be solved numerically. The accuracy of this method was largely a result of the chosen time step – calculated as follows:

$$\frac{u_{max} \Delta T}{\Delta L} < 0.5 \quad (5-3)$$

Using a ΔT increment of 1 second gives a worst case ΔL of 80m when there is a maximum wind speed of 40m/s. Draxler (1995) suggests time steps ranging from 60 seconds to 60 mins are suitable for long duration balloon trajectories; 1 second should be more than adequate for this short distance trajectory.

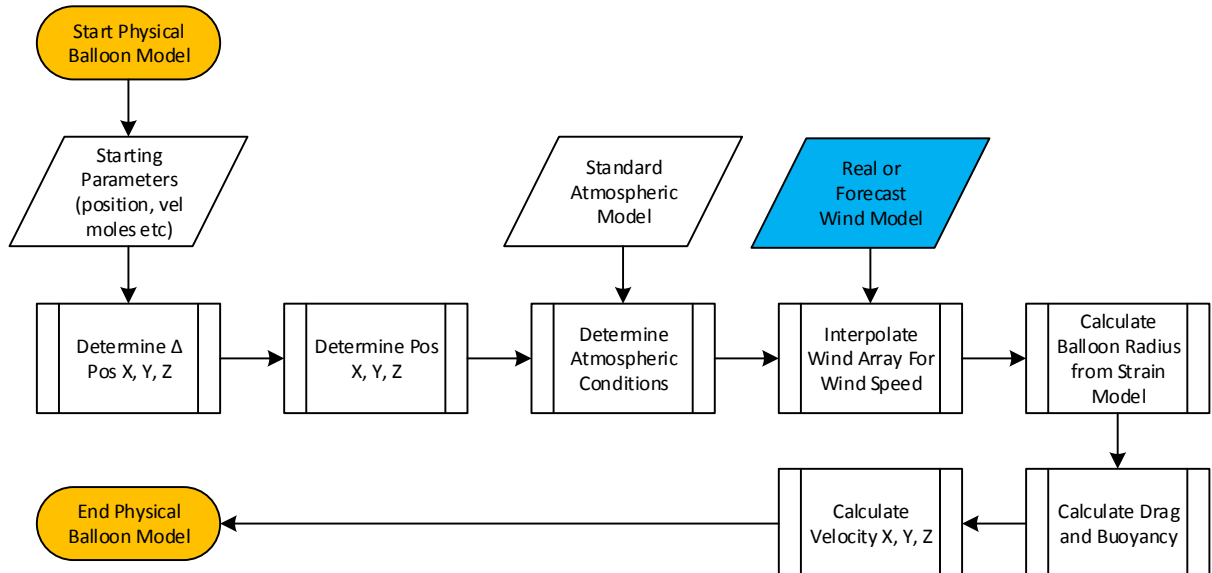


Figure 5-4: Flow chart showing how a single iteration (1 second) of the integration routine works. This process includes the calculation of governing internal and external equations featured in section 4.1 and 4.2. Note that no accelerations are included in this model, instead it is assumed that the balloon travels at terminal velocity. Calculating the radius requires solving the complicated Mooney-Rivlin stress-strain model.

This algorithm required significant development in order to maximise accuracy whilst minimising computational time. For example, many of the parameters such as Radius, Atmospheric Conditions and even Terminal Velocity were pre-calculated. Large matrices were created to represent these parameters as a function of altitude and number of moles. These values were extracted from their combination matrix with a 2D linear interpolation method. Without this method it would have been impossible to run the Monte-Carlo simulation on a consumer grade computer.

Similarly, the speed of interpolating the wind array improved 50 fold by predefining the high definition spline interpolated array and using a subsequent tri-linear interpolation method. Comparisons suggest that this method was just as accurate as the initial three-dimensional spline interpolation method.

5.4.2 Lifting Gas Control System (LGCS)

A simple gas control system was implemented by following the equations shown in section 4.2.5. The number of moles required for neutral buoyancy was calculated for each altitude and saved into a predefined array. These values were interpolated to find the exact number of moles required. A perfectly efficient system would fill the balloon to this number. This was not a feasible method as it meant a very slow transfer speed between layers. The goal altitude behaved as though it were an asymptote.

To speed up the transfer speed, the control system either over or under filled the balloon by 10% depending on the goal direction. This led to a great improvement in layer transfer time but led to wasted lifting gas. This is demonstrated below:

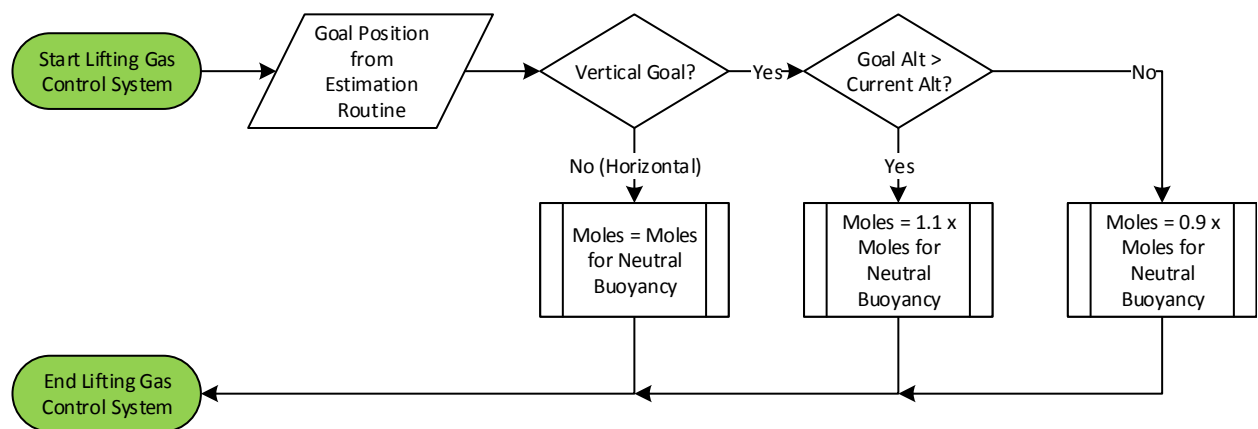


Figure 5-5: Flow chart depicting the operation of the very simple lifting gas control system.

Importantly, the LGCS relied on the assumption that the number of moles in the balloon is known with certainty, and the number of moles added could be controlled precisely. The reality of these assumptions is unclear. The LGCS may be able to incorporate a feedback loop that provides this information; a pressure sensor could potentially determine the number of moles in the system.

5.4.3 Goal Estimation Routine (GER)

An ideal loop would require two wind currents that are exactly opposite in direction. Such atmospheric conditions are very rare. Instead, looping can be achieved with three different wind layers, referred to as the triangular 'looping trajectory'.

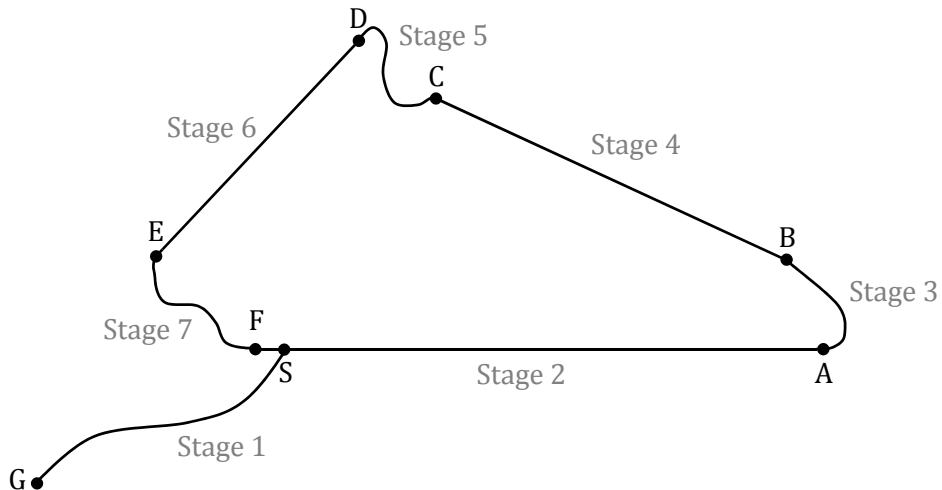


Figure 5-6: Top view of the triangular looping trajectory. Curved lines represent altitude changes (varying wind direction), straight line are areas of constant altitude (near constant wind direction). Stage 2-7 repeat to create the loop.

Stage #	Range	Description	Unknowns	Knowns
Stage 1	G → S	Transfer from ground to main observation alt	Alt_{SA}	Alt_G
Stage 2	S → A	Main observation path, length of fire zone		T_{SA}, Alt_{SA}
Stage 3	A → B	Transfer 1 to return path 1	Alt_{BC}	Alt_{SA} ,
Stage 4	B → C	Return path 1	T_{BC}	Alt_{BC}
Stage 5	C → D	Transfer 2 to return path 2	Alt_{DE}	Alt_{BC} ,
Stage 6	D → E	Return path 2	T_{DE}	Alt_{DE} ,
Stage 7	E → F	Transfer 3 to initial observation alt		Alt_{DE}, Alt_{SA}
Goal	F → S	Minimise difference between start and finish	N/A	Alt_{SA}

Two parameters, Altitude and Time, were required to describe each stage of this trajectory. From these, estimates for position and lift gas consumption could be determined from the

physical balloon model and knowledge of the wind field. In total, there were 5 different descriptive trajectory parameters that were to be determined from the estimation routine:

$$\text{Descriptive Parameters} = Alt_{SA}, Alt_{BC}, Alt_{DE}, T_{BC}, T_{DE}$$

Calculation of these parameters was achieved analytically via a computationally intensive ‘dumb’ iterative estimation routine. These parameters were varied one-by-one in order to create a complex, multi-dimensional ‘possible pathways matrix’. This matrix effectively described all the possible trajectories that could be obtained by varying the balloon’s altitude to one of 16 different pre-defined levels (the 16 levels were spread evenly between 10km and 25km altitude). Importantly, this routine ran as a nested ‘for’ loop, meaning computation time quickly increased as the parameter range was extended. For example, adding just two extra altitude layers would mean a $18^3/16^3 - 1 = 42\%$ increase in computation time. Sixteen layers provided reasonable performance whilst completing in under 5 seconds on a high end consumer level desktop computer.

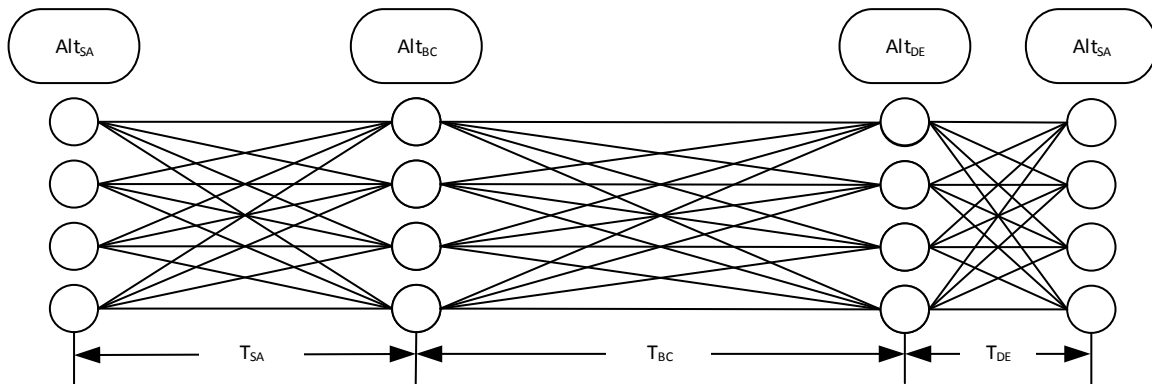


Figure 5-7: Diagram showing some of the many possibilities when varying Alt_{SA} , Alt_{BC} and Alt_{DE} between just 4 different altitude levels. The actual estimation routine varies them between 16 levels and also varies T_{BC} and T_{DE} between a further 50 time periods. This explains why over 10 million trajectories are included in the possible pathways matrix ($16^3 \times 50^2 = 10,240,000$ trajectory combinations).

Each one of these 10 million trajectories included 3 different altitude changes (Stage 3, 5, 7) causing significant computational difficulty. Typically, computing the trajectory from one altitude to another required the use of both the iterative Runge-Kutta Physical Balloon Model and the Lifting Gas Control System. To simplify this process, the average layer transfer trajectory was calculated and saved into a 16×16 matrix. When required, the ΔX , ΔY and ΔZ values were read directly from this predefined matrix and saved into the possible pathways matrix.

Calculation of the constant altitude section trajectories (Stage 2, 4, 6) was also simplified to reach the desired computation speed. The average wind speed and angle was computed for each layer – this value was multiplied by the time T_{BC} and T_{DE} . This assumption erroneously assumed that wind speed and angle is constant across an altitude level and therefore that the balloon will follow a perfectly straight path.

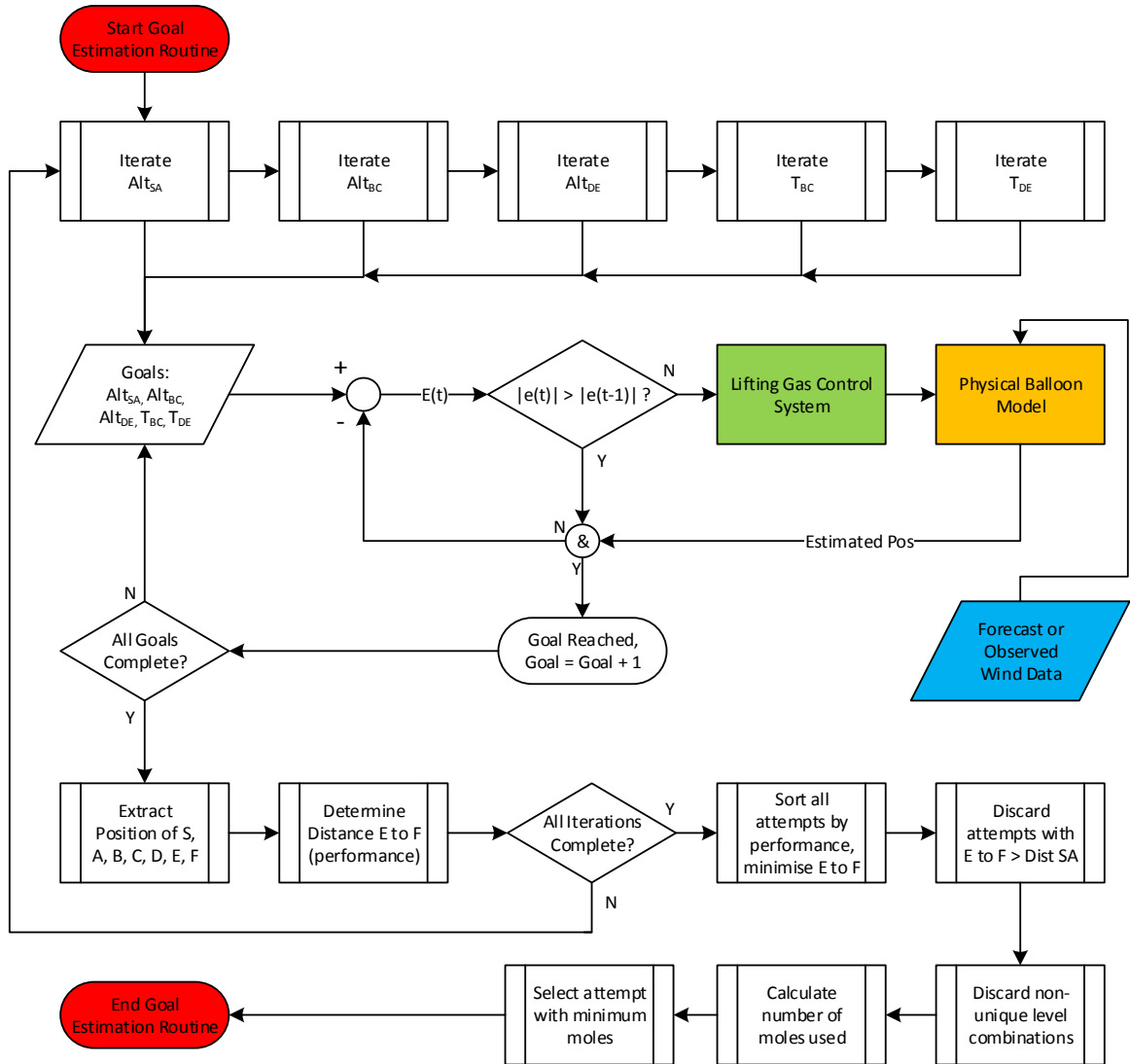


Figure 5-8: Flow chart demonstrating the iterative goal optimisation algorithm. This extended version shows the use of the 'Physical Balloon Model' and 'Lifting Gas Control System' algorithms. In reality, this section is predefined to speed up the calculation. This runs as a nested 'FOR' loop meaning approximately 10 million combinations are tested and compared.

5.4.4 Observed Wind Array Update Routine (OWAUR)

Any forecast wind data is going to have some innate bias or error. Initial analysis made it clear that some form of wind-sensor (GPS and/or inertial) must be included to observe the real wind conditions mid-flight. This observed data would be used to update the forecast wind array, replacing forecast data with observed where possible. Trends in observed data could be used to adjust the forecast data for non-observed altitudes. This could then be used to determine when there has been an extreme weather event that means all forecast data is incorrect. This update routine was key to the accuracy of the ‘smart’ trajectory algorithm.

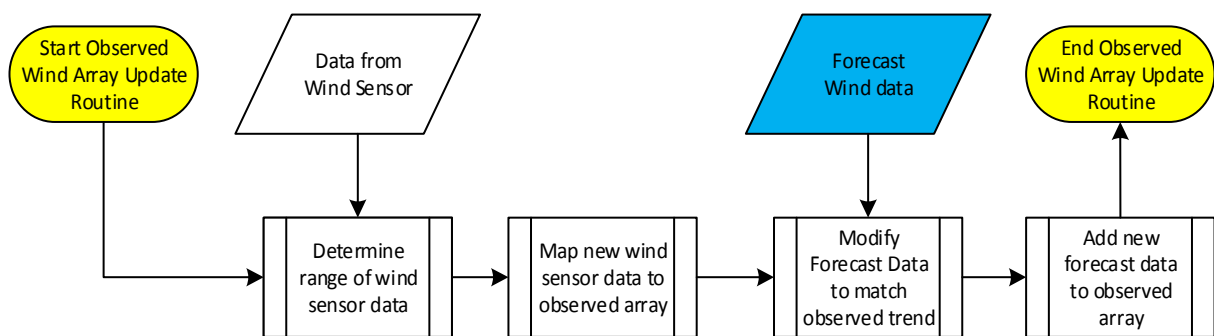


Figure 5-9: Flow chart depicting the operation of the wind update routine.

5.5 SIMULATION ALGORITHM

Using these sub-systems, two different versions of the simulation were designed:

1. Pre-Launch Simulation: This simulation used forecast wind data to determine if the balloon should be launched. A Monte-Carlo method was used to determine the robustness of the proposed trajectory; was it likely to successfully complete trajectory loops? If the balloon failed to meet these pre-launch requirements the balloon would not be launched.
2. Real Launch Simulation: This simulation used real, 0h assimilated wind data to observe how well the balloon would have really performed. The control system was analysed to see how well it could adjust to forecast error. GPS and inertial sensors were simulated to provide a feedback loop. This provided the basis of the ‘smart’ control system which would modify the proposed trajectory loop in real-time as sensors observed new wind conditions.

These two simulations were primarily made up of the ‘Initial Trajectory Estimate’ and the ‘Main Model’ respectively. The other steps relate to the ‘Monte Carlo Robustness Test’ which was used to determine if the balloon should be launched and where the most robust launch site was.

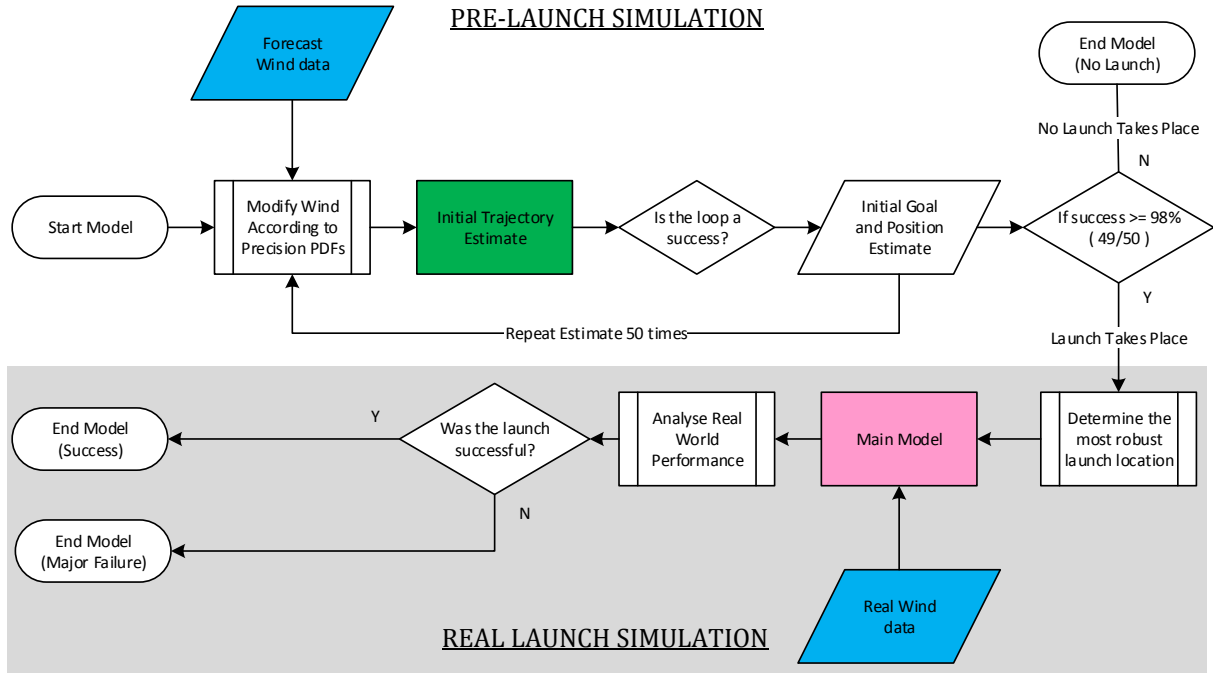


Figure 5-10: Full System Algorithm demonstrating how data from the initial estimate is fed into the main model. The requirements of the Monte-Carlo Robustness Test are also shown.

5.5.1 Initial Trajectory Estimate (ITE)

The ITE algorithm was designed to provide an initial prediction of launch position and the 5 descriptive trajectory parameters. This optimal trajectory was selected by the Goal Estimation Routine. This was the trajectory which successfully looped, consumed minimal filling gas and maximised imaging time above the bushfire zone. Importantly, this solution was based on 6hr forecast data meaning both the PBM and GER algorithms provided nothing more than a best estimate.

The ITE reveals occasions where there is not enough wind variation for a loop to succeed. In these cases, the balloon would not be launched. The likelihood of success is determined by iteratively solving this ITE as part of the Monte Carlo Robustness Test. If success is deemed likely, the balloon launch crew have six hours to drive out to the designated launch site and prepare the balloon for launch.

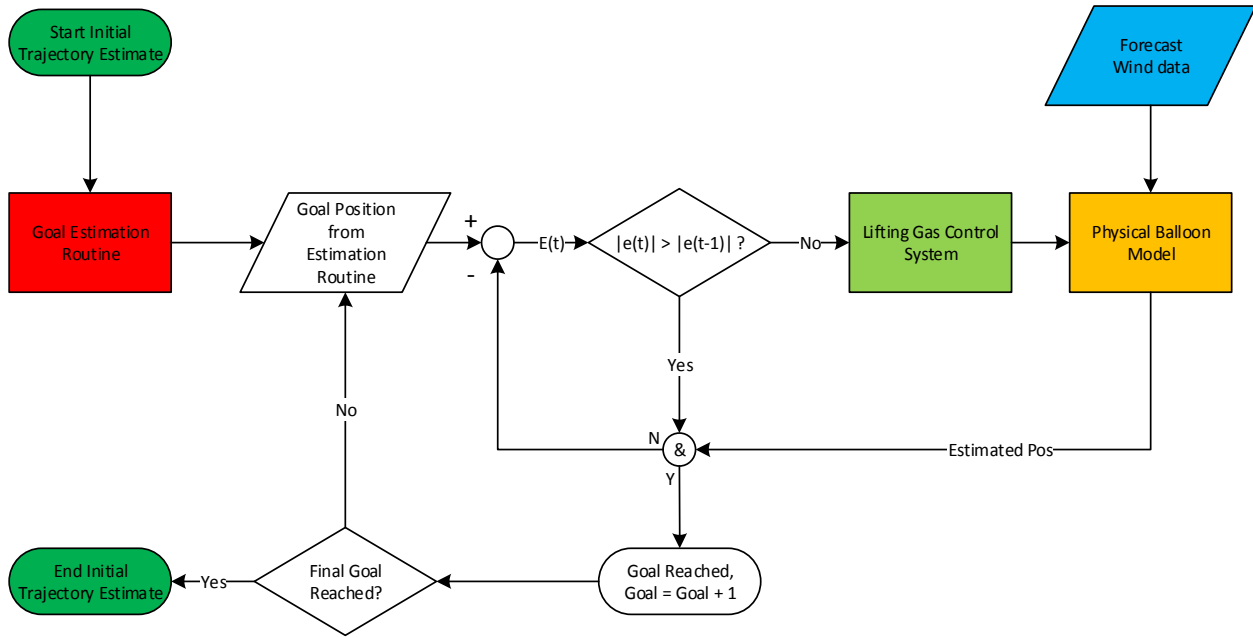


Figure 5-11: Flow chart portraying the Initial Trajectory Estimate algorithm based on forecast wind data. When the balloon begins to move away from the goal position ($|e(t)| > |e(t-1)|$) the system moves on to the next stage. This control process requires knowledge of current position, i.e. a GPS sensor. This does not demonstrate the selection of launch position or Monte-Carlo Robustness Test. These require iteratively solving this Trajectory Estimation function.

5.5.2 Monte-Carlo Robustness Test (MCRT)

Some altitudes are risky to implement in a looping trajectory because they are either prone to large change over a 6 hour period or exhibit a larger than average forecast precision error.

Typically, the altitudes to avoid are those outside of the 7km-20km zone, as will be demonstrated in figure 6-13. If the balloon's trajectory requires winds outside of this zone, it faces a larger risk of failure as the forecast data is more likely to be incorrect.

To account for this risk, a Monte-Carlo analysis was conducted to compare the robustness of each potential trajectory suggested by the ITE. This Monte-Carlo analysis required the 'Forecast Wind' Array to be varied according to the 'Forecast Precision' probability density functions (examples of these PDFs are demonstrated in Figure 6-15 and 6-16). Each atmospheric layer has its own unique PDF, as described in figure 6-13 and 6-14.

The Monte-Carlo process was roughly as follows:

1. A range of possible solutions were determined using the ‘Goal Estimation Routine’ under ‘Forecast Wind’ conditions. These possible solutions were ones that were able to complete a trajectory loop to within 20% of the initial position whilst minimising gas consumption.
2. The ‘Forecast Wind’ Array was modified according to the ‘Forecast Precision’ PDFs to produce a ‘Simulated Real Wind’ Array.
3. The balloon trajectory performance for each one of the initial possible solutions (from step 1) was determined under the ‘Simulated Real Wind’ conditions.
4. Step 2 and Step 3 were repeated 50 times (this was limited by computation power – the Monte-Carlo analysis would be easily improved by increasing this number).

The most robust solution (from step 1) was the one that had the best average performance over the 50 simulations (as conducted in step 4). This robust solution was selected as the optimal looping trajectory as it was most likely to succeed under real wind conditions.

These steps were previously demonstrated in figure 5-10.

5.5.3 Main Model

The ‘Main Model’ algorithm was created to simulate the real-world mechanics of the balloon launched from the position determined MCRT. This model simulated both the balloon (under the effects of real assimilated wind data) and the balloon’s trajectory control system (which assumed 6h forecast data as the best estimate of wind fields).

As the balloon travelled along its trajectory, wind speed readings were simulated from an inertial and GPS sensor with error terms. From this data, the balloon’s control system would update its Observed Wind Array (using the OWAUR) to provide the best estimate of current atmospheric conditions. This observed wind data was progressively fed into the Goal Estimation Routine in order to re-calculate the descriptive looping parameters.

When the OWAUR observed real wind conditions that were different to the forecast data, the GER would be re-run. The GER would then use the current position and wind information to re-determine the most efficient trajectory. Often this meant a trajectory was changed mid-flight as changes in wind conditions meant the previous trajectory was no longer possible.

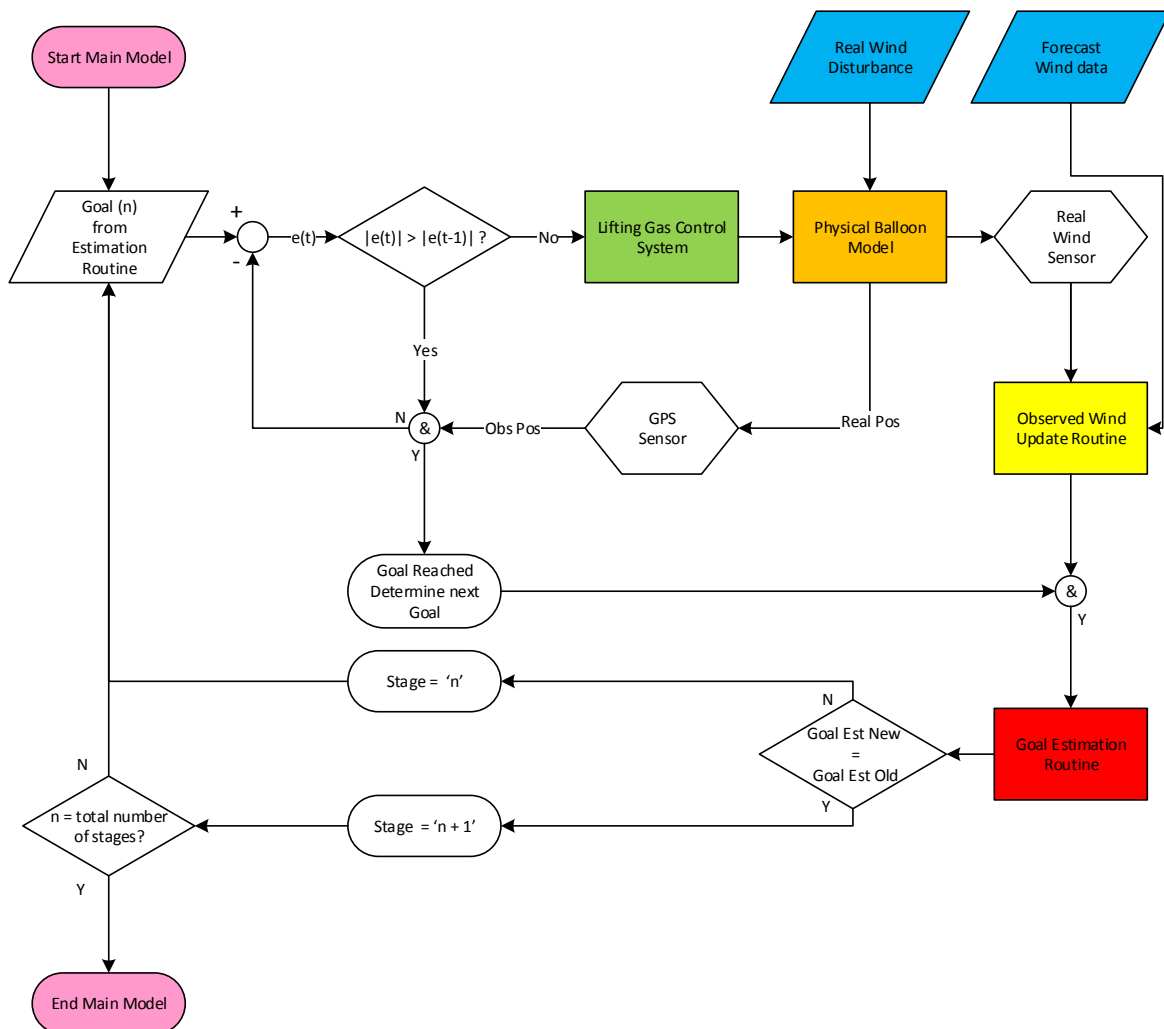


Figure 5-12: Flow chart demonstrating how the 'Main Model' simulation works. This includes error terms in both the GPS sensor and Real Wind Sensor. The 'Real Wind Disturbance' is based on 00h assimilated forecast data. This model was run 144 times (4 times a day for 36 days) to see how successful it was over a variety of wind conditions.

6 RESULTS AND DISCUSSION

6.1 WINDS ANALYSIS

Significant analysis of one month's wind data was completed in order to understand how wind vectors vary with position and time. This analysis provided key insight, describing the plausibility of a variety simulation assumptions including the initial viability of the looping trajectory.

NOMADS wind data is effectively a 5 dimensional matrix of x-y-z vectors that vary with latitude, longitude, altitude, forecast package and forecast period. To deal with this complexity, the matrix is broken down and analysed a few dimensions at a time.

The following analysis was based on the Lake Tahoe observation area, latitude 36 to 42, longitude -123 to -117. There were 4 forecast packages each day from 27/March/2014 to 1/May/2014. Each forecast package contained 11 forecast points ranging from 0h to 60h with 6h intervals.

It should be noted that the whiskers of the following box plots are drawn to $\pm 2.7 \sigma$ to cover 99.3% of data points. Outliers are indicated with a 'red plus'.

6.1.1 Layer Consistency

Step 1 was to determine how the wind parameters change with latitude or longitude. To do this, the atmosphere was sliced horizontally, statistically analysis was performed on each slice.

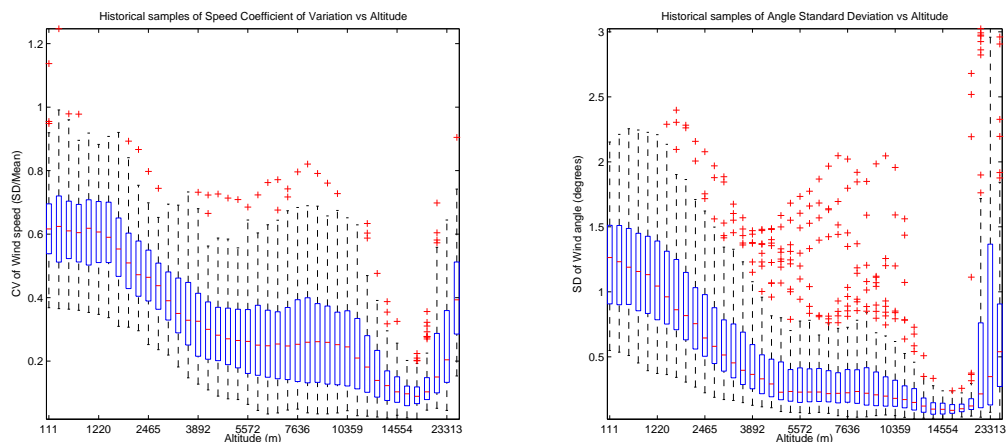


Figure 6-1: Coefficient of Variation / Standard Deviation at each horizontal atmospheric slice.

This first box plot demonstrates wind speed's standard Coefficient of Variation for each atmospheric layer. The CV is highest at the 100m and gradually falls until around 17km altitude. This result is consistent with the basic atmospheric boundary layer theory; planar wind vectors should vary more at low altitude. In this region winds are greatly affected by surface drag due to terrain such as mountains and valleys.

After approximately 17km, the layer CV quickly reduces; wind speed is almost identical across the entire section. This zone roughly corresponds to the end of the troposphere, the area affected by the atmosphere's convective boundary layer. From this point onwards the variation quickly rises again as the average wind speed falls.

This coefficient of variation is typically quite large – around 0.4. This explains why the assumption that wind-speed magnitude is near constant has caused inaccuracies in the basic control system simulations. By adding a GPS sensor to the system, inaccurate knowledge about wind speed can be corrected.

The second plot demonstrates the historical changes in the Standard Deviation of the wind angle. This follows a similar pattern to the wind speed, highest at 100m and falling steadily until around 17km. There is a significant spike around the 20km zone wherein the average size of the quartiles, whiskers and outliers jumps hugely. The reason for this jump cannot be identified in existing literature. Nonetheless, the Standard Deviation in all these cases is low enough not to cause any issues with the simulation – no more than a couple of degrees.

Layer inconsistency will not cause significant inaccuracy in a properly controlled trajectory. Inaccuracies in wind speed can easily be accounted for so long as the control system has a GPS sensor. Variation in wind angle is a larger problem, although the results show that this effect is minor. Importantly, these results say nothing about altitude layer correlation. If there is a higher than average variation on one layer, will the trend continue on the following layers? This is a question deserves further research.

6.1.2 Changes with Altitude

Next, the atmosphere is examined vertically to determine how winds vary with altitude. The average wind speed and angle shown is plotted at each altitude level using historical 0h forecast data. This gives the average atmospheric conditions for the observation period (27/March/2014 to 1/May/2014):

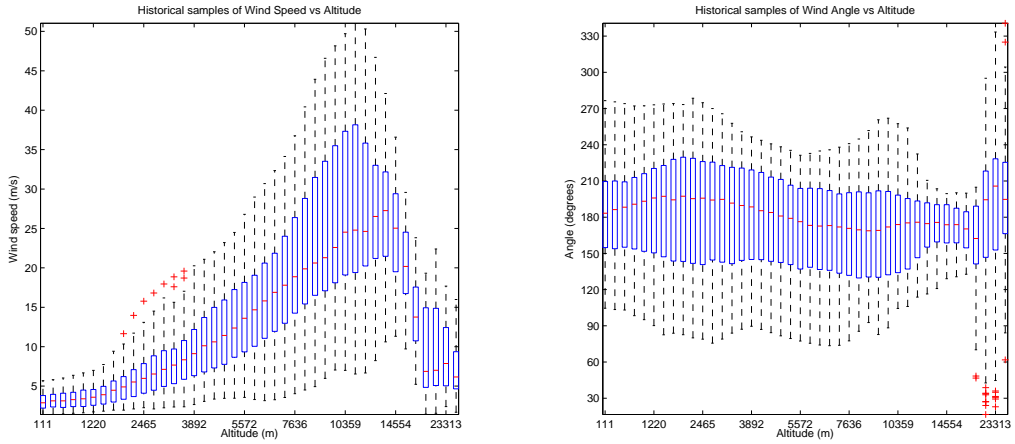


Figure 6-2: Standard wind parameters for the average vertical atmospheric column.

This first plot demonstrates the variation in average wind speed at each altitude. The shape of this curve is roughly what one would expect, rising in magnitude until the tropopause and falling after this point. The second plot shows that the angle of the wind is reasonably constant across all altitudes. This size of the whiskers indicates that that the standard deviation varies significantly across these altitudes.

Plotting the coefficient of variation and standard deviation of the wind speed/angle gives a better indication of how these parameters vary with altitude.

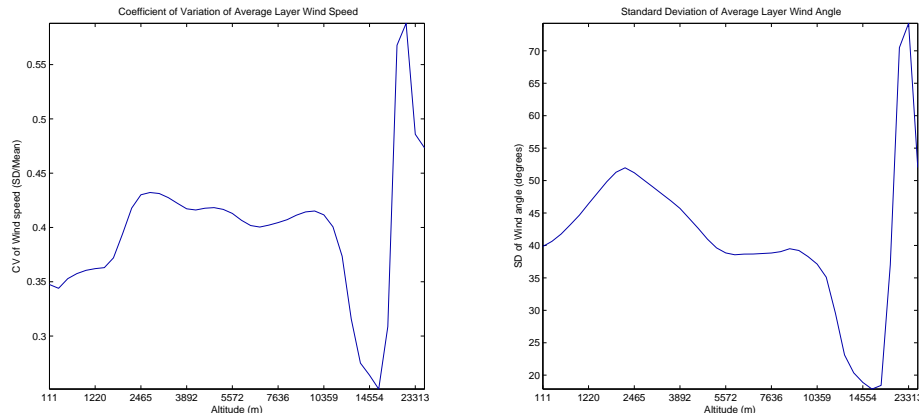


Figure 6-3: CV and SD of average wind speed and angle at each altitude across the time range.

Both the CV of the wind speed and the SD of the wind angle follow a similar trend, staying relatively constant and then falling drastically at the tropopause where winds are much more reliable. After this point, both suddenly rise, only to peak at around 20km, the point of lowest wind magnitude. This 20km point experiences extreme speed and angle standard deviations

meaning it will be pivotal in the looping procedure. It will however be risky to implement in a trajectory as it may be more prone to change.

6.1.3 Changes with Time

Time variation of a wind field presents significant problems for any the balloon system. To determine the extent of this problem a variety of figures were created to demonstrate how quickly wind speed and direction change with time and altitude.

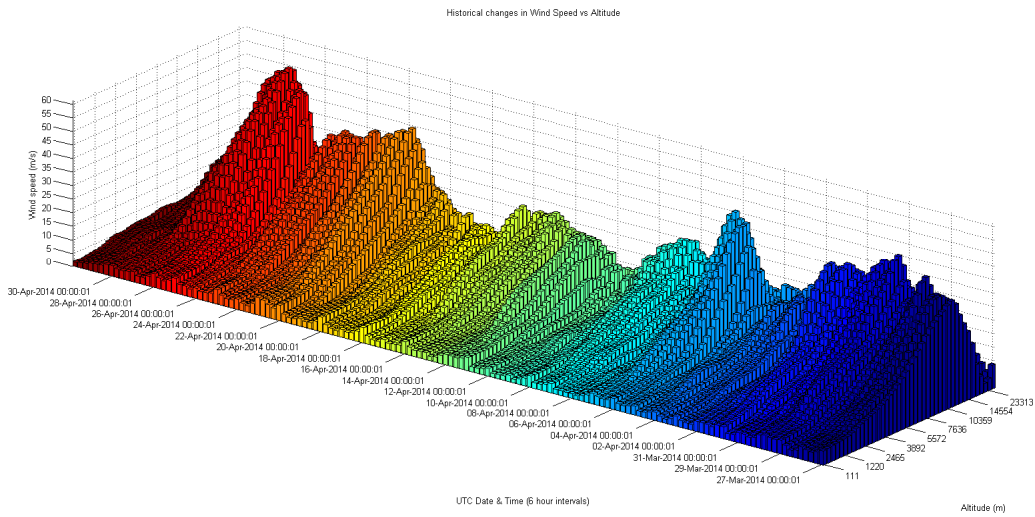


Figure 6-4: Wind speed at each altitude versus time.

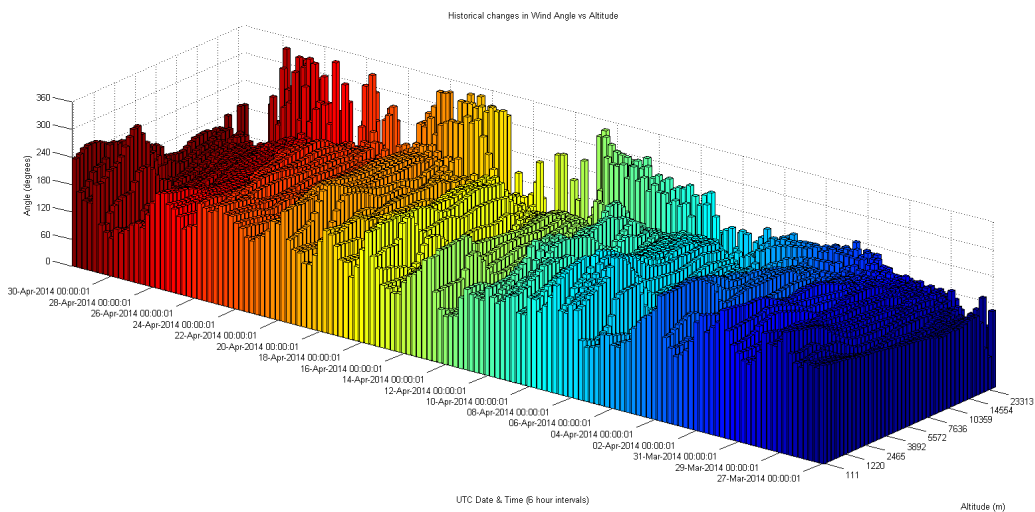


Figure 6-5: Wind angle at each altitude versus time.

Both figure 6-4 and 6-5 effectively demonstrate the transient nature of wind speed and angle. A cross-section through a constant altitude level reveals a wave like shape; there is a high correlation between future and historic winds. Although there are significant variations in layer

wind speed (as shown in Figure 6-2), these parameters move gradually rather than randomly. Forecast wind data can therefore be used to interpolate wind conditions at any time.

Figure 6-5 also indicates the high standard deviations in the upper atmosphere; this is also shown in figure 6-3. Through this zone of approx. 20-25km altitude, wind angle and speed appears to fluctuate wildly with little relation to previous strength or direction. This figure also demonstrates that there is only minor angle variation during the end of March – this may make looping impossible. Successful looping requires a large variation in angle across different altitudes.

Additional statistical analysis of this phenomenon was conducted to determine how these parameters vary over a 6 hour period.

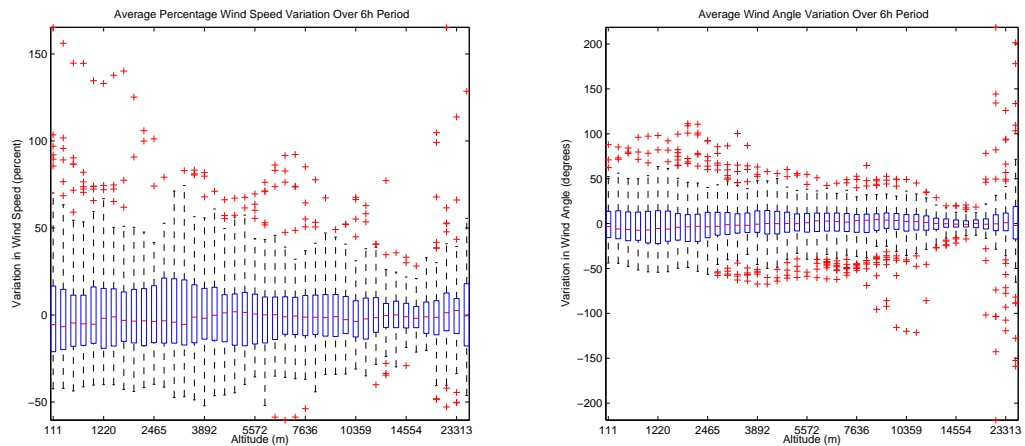


Figure 6-6: Variation of wind speed and angle over a 6 hour period.

Figure 6-6 demonstrates that over a 6h period, wind speed and angle can vary significantly. Wind speed is unlikely to vary by more $\pm 50\%$ whereas wind angle typically varies by less than ± 40 degrees. Again, we notice that at around 20-25km both speed and angle vary wildly. There are multiple occasions in which the 25 km winds completely reverse direction in just 6 hours.

This form of high altitude variation is of significant concern for balloon trajectories which aim to make use of favourable high altitude winds. There is a reasonable chance of these winds fluctuating wildly over a 6 hour period. Accurate forecast data will therefore be key to predicting the transient nature of winds. If forecasts are correct, wind conditions at any point in time can be determined from a spline interpolation method.

6.1.4 Forecast Variation

The NAM CONUS forecast dataset contains 2.5 days of forecast data broken into 6 hour forecast intervals. In order to determine the accuracy of these forecasts, plots were produced to outline how older forecasts compared to the +0h assimilated data. For reference, +0h refers to now, whereas a +60h forecast refers to data released 60 hours ago for a period 60 hours in the future, also now.

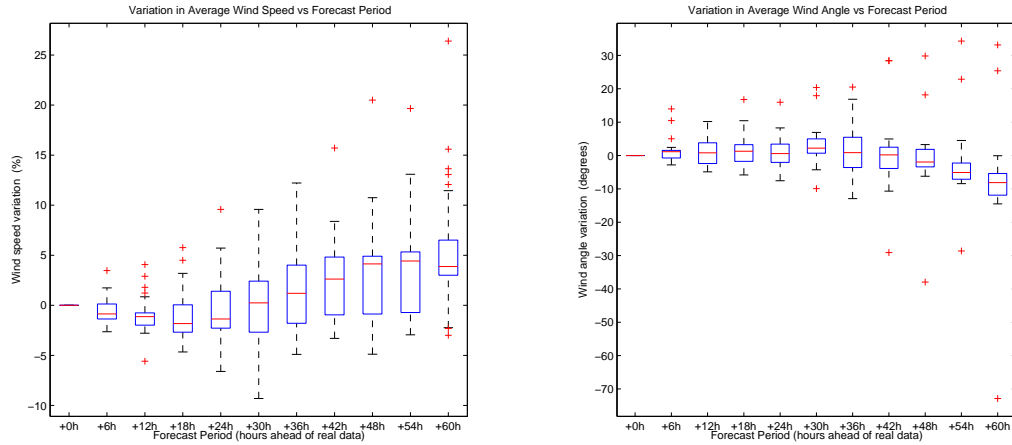


Figure 6-7: Variation in wind speed and angle at each forecast period

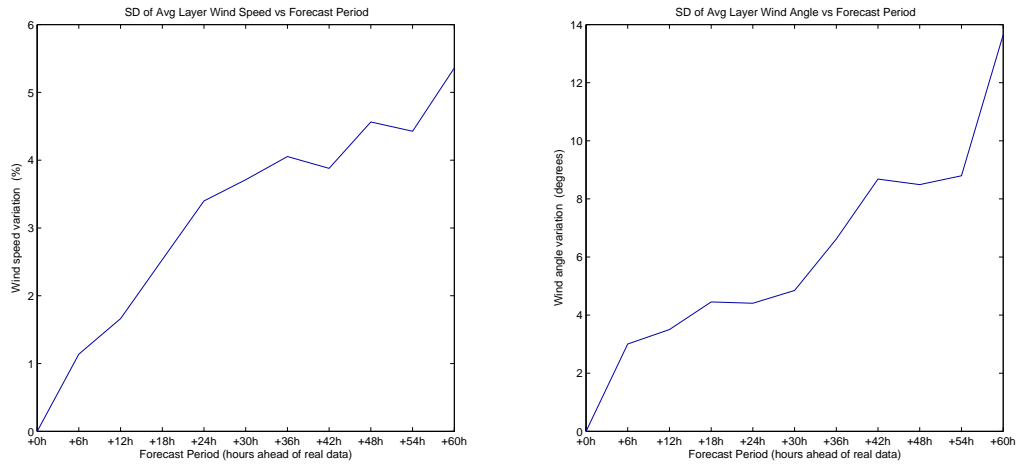


Figure 6-8: Standard deviation of wind speed and wind angle vs. forecast period.

Both figure 6-7 and 6-8 show that the certainty of wind speed and angle decreases almost linearly with time. By using a +12h forecast instead of a +6h forecast the results will be twice as inaccurate. It is important to note that these plots are produced by using the averages over the 36 day period – the variation in the box plot is due to variation at different altitude levels.

Additional figures were produced in order to study how these parameters varied with altitude:

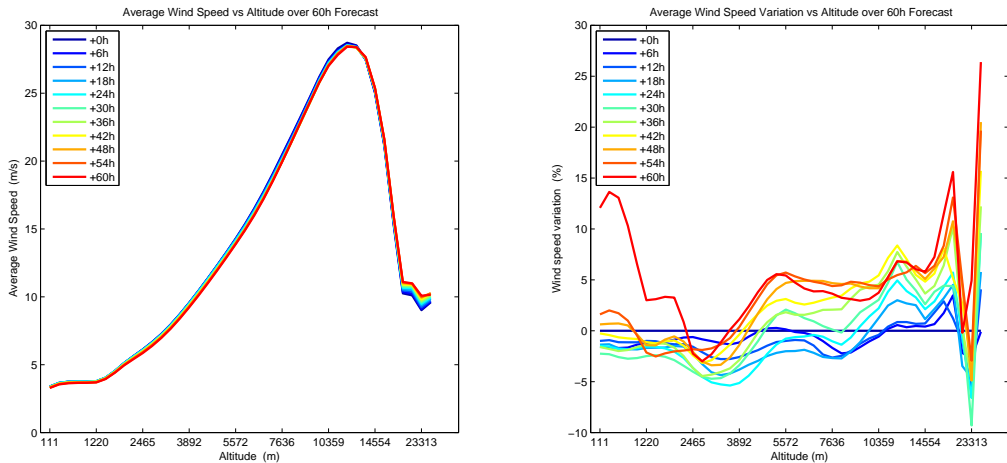


Figure 6-9: Average wind speed for each forecast period versus altitude.

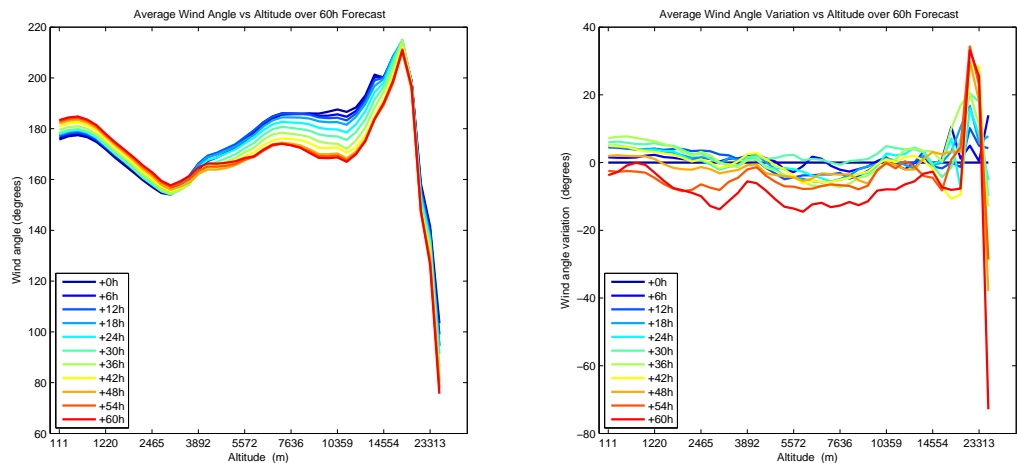


Figure 6-10: Average wind angle for each forecast period versus altitude.

Both figure 6-9 and 6-10 show that error increases drastically in the higher altitudes. This is due to the innate randomness of these upper winds – as also shown in figure 6-2 and 6-3. As expected, the +6h forecast significantly outperforms other forecasts across all altitudes and parameters.

At lower altitudes, the average 6 hour forecast variation is close to the real parameters – varying by no more than a 2 percent. At the higher altitudes, wind speed is typically out by as much as 5% whereas wind angle can be out by 20 degrees. This large error means more than just forecast data will be needed in order to accurately complete a trajectory loop. Wind sensors will certainly be needed if balloon ventures into these high altitudes.

6.1.5 Forecast Precision

Precise and accurate forecast data is key to successfully completing a looping trajectory. The error in the forecast data must therefore be fully understood. To demonstrate this, the difference between +6h forecast and +0h assimilated data was plotted across a range of altitude layers.

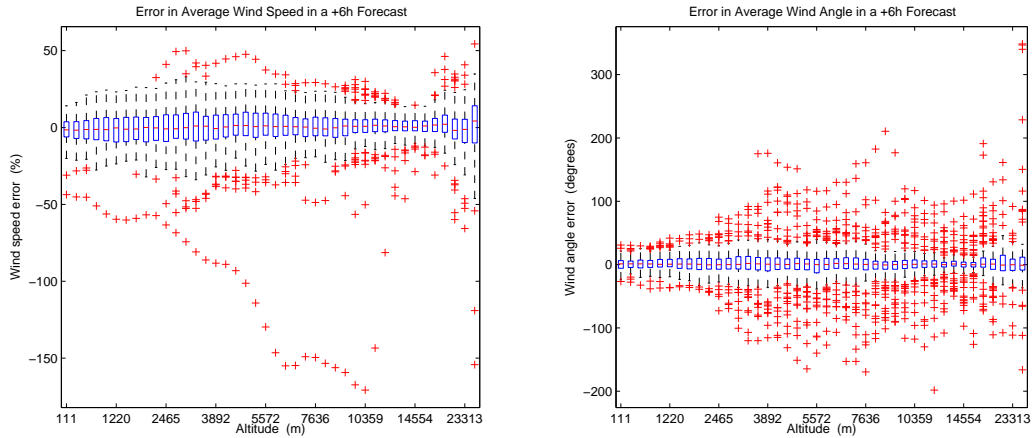


Figure 6-11: Difference between +0h and +6h wind speed and angle data.

Figure 6-11 demonstrates that the mean error is typically very close to zero. 6 hour wind speed error is rarely more than a 10 percent while wind angle is normally accurate to within 10 degrees. Importantly, there are significant outliers in both wind speed and wind angle. These outliers are the result of unpredictable, extreme weather events.

To better understand this error, a histogram was plotted for the final altitude level, 25km. A standard normal distribution was fitted to this data in figure 6-12 below.

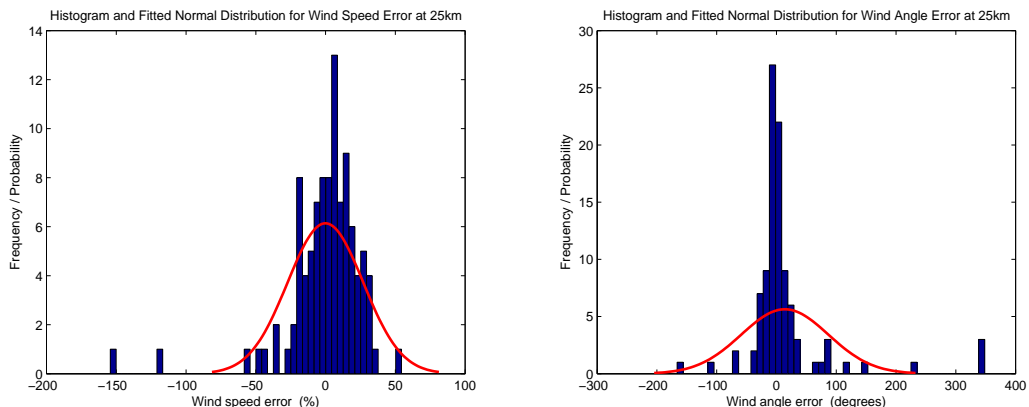


Figure 6-12: Histogram and fitted normal PDF outlining wind errors between +0h and +6h data at 25km altitude.

Figure 6-12 immediately demonstrates the significant failings of a standard normal distribution to map the extreme weather events that cause errors in forecast data. To fix this, log likelihood functions were calculated for a range of common probability density functions including: Exponential, Student-T, Gamma, Log Normal, Weibull, Pareto, Burr, Generalized Extreme Value, Double Exponential and Generalised Normal.

Analysis using the ‘Akaike Information Criterion’ suggested that a three parameter Generalised Normal Distribution $GND(\mu, \alpha, \beta)$ provided the best fit for both wind magnitude and angle data:

The PDF and CDF of the Generalised Normal Distribution can be seen below.

$$f_X(x) = \frac{\beta}{2\alpha\Gamma\left(\frac{1}{\beta}\right)} e^{-\left(\frac{|x-\mu|}{\alpha}\right)^\beta} \quad (6-1)$$

$$F_X(x) = \frac{1}{2} + sgn(x - \mu) \frac{\gamma\left[1/\beta, \left(\frac{|x-\mu|}{\alpha}\right)^\beta\right]}{2\Gamma\left(\frac{1}{\beta}\right)} \quad (6-2)$$

Note that Γ and γ represent the typical ‘gamma’ and ‘incomplete gamma’ functions:

$$\Gamma(t) = \int_0^{\infty} x^{t-1} e^{-x} dx \quad (6-3)$$

$$\gamma(t, s) = \int_0^s x^{t-1} e^{-x} dx \quad (6-4)$$

Existing literature fails to mention the use of the GND for forecast wind variation. Nonetheless, the Generalised Normal Distribution out-performs all other PDFs tested, including the 2 parameter Weibull which has historically been used for raw wind magnitude measurements (WindPower Program, 2014).

Figure 6-13 and 6-14 demonstrate how the Generalised Normal Distribution’s μ, α and β parameters vary with altitude. These figures also outline how well the Akaike Information Criterion fits the data.

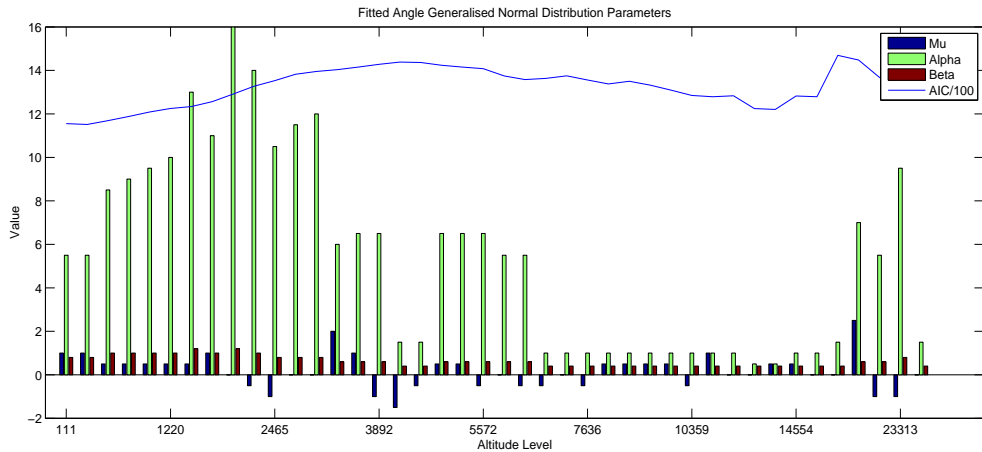


Figure 6-13: GND(μ, α, β) Parameters and Akaike Information Index for Δ Wind Angle between +6hr and +0hr forecast

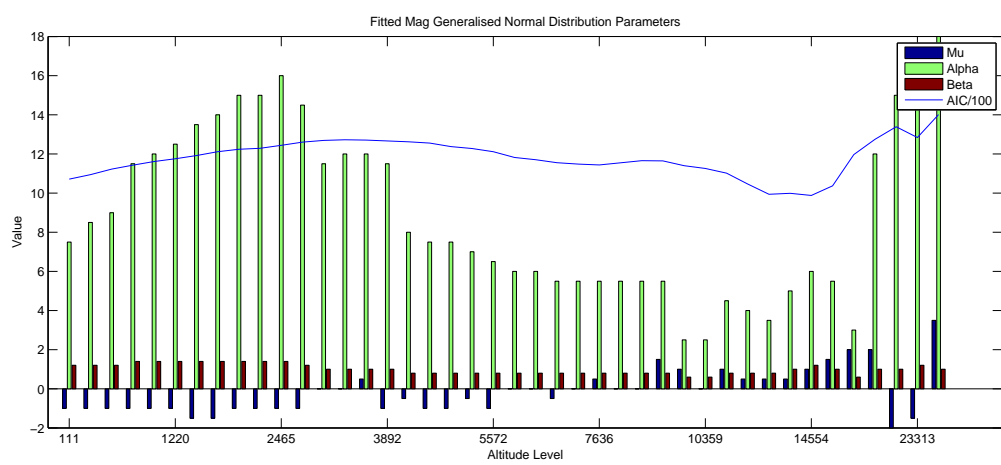


Figure 6-14: GND(μ, α, β) Parameters and Akaike Information Index for Δ Wind Speed between +6hr and +0hr forecast

These parameters vary significantly across the different altitudes. α ranges from 2 to 18 while μ and β stay reasonably constant. This α parameter represents the GND's scale – how spread out the distribution is. A larger α corresponds to a larger standard deviation. For this reason, a lower α is preferable as it means the wind is subject to smaller forecast error. Importantly, the largest alphas are in the lower altitudes (below 6km) which will only effect the balloon during its quick transfer into the higher altitudes.

The alpha's for wind angle in these middle layers (7km to 20km) are much lower than for magnitude. This is welcome news given that the balloon's control system can easily correct for wind magnitude errors but cannot easily correct for angle errors. After about 20km, the alphas for both angle and speed begin to rise. These layers are more prone to forecast error and are therefore more risky to implement as part of a trajectory loop.

These figures also outline the Akaike Information Criterion. This was approximately 1,100-1,400 for both delta angle and delta speed. This relatively consistent value suggests the Generalised Normal Distribution is a good fit for both wind angle and speed across all altitudes. To more fully understand this fit, several cross-sectional examples are plotted:

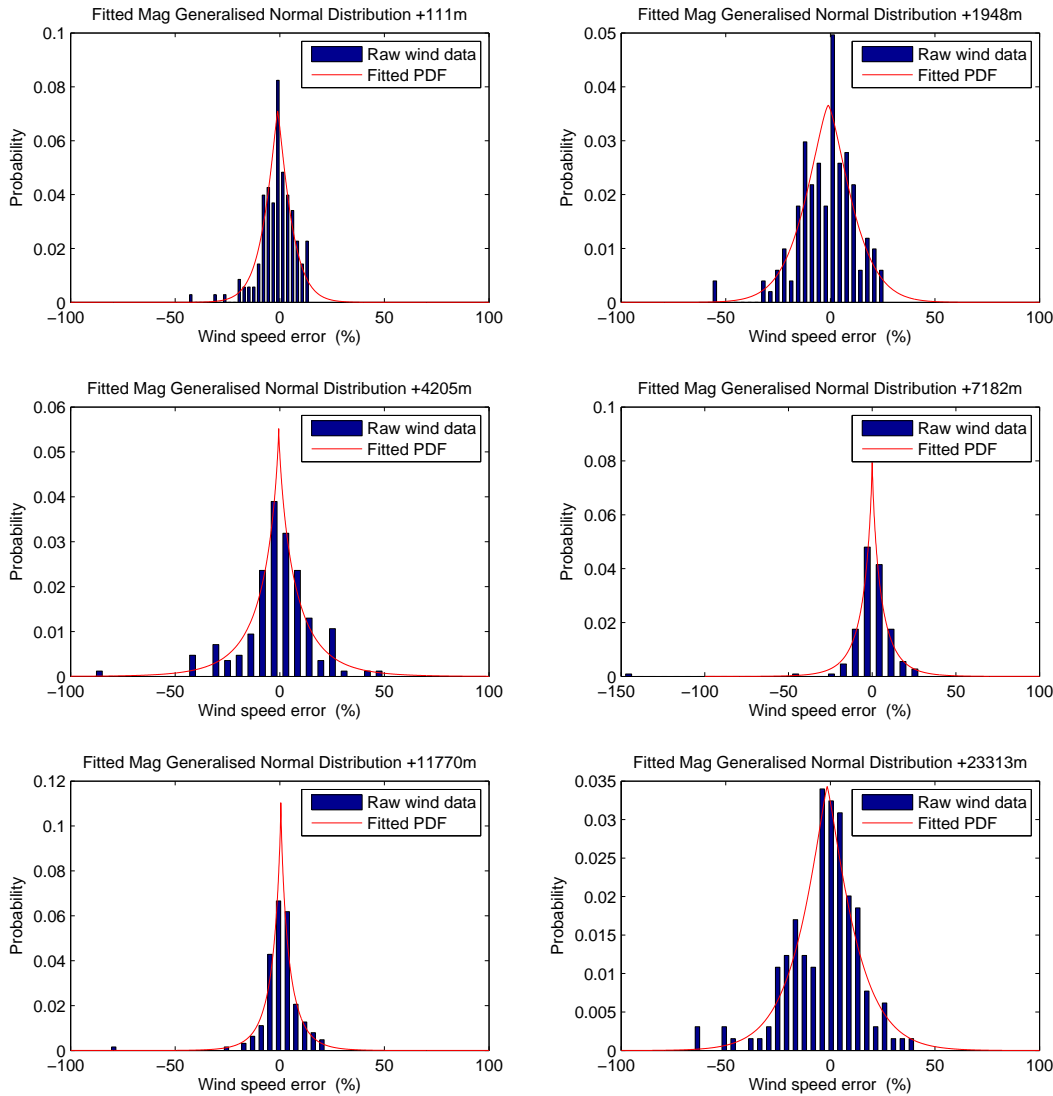


Figure 6-15: Histogram and fitted GND(μ, α, β) distributions for wind speed error at 6 of 42 levels

Figure 6-15 and 6-16 demonstrate the fitted Generalised Normal Distribution relative to the raw data histogram. These plots were constructed using just 36 days of data, 144 forecasts. This sample size is too small to expect an exact fitting distribution. Nonetheless, it is clear that the GND(μ, α, β) provides a very good approximation of 6hr forecast wind error.

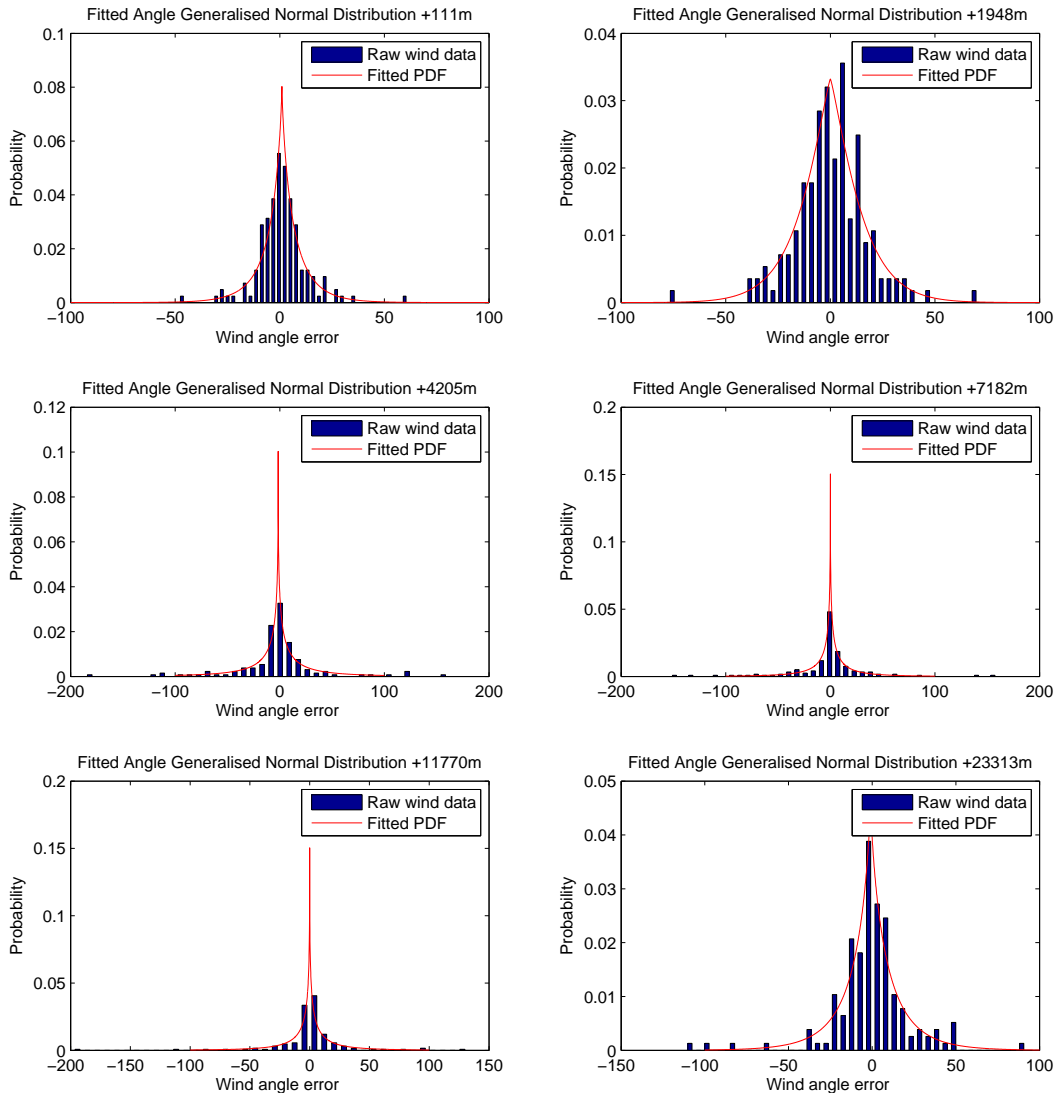


Figure 6-16: Histogram and fitted GND(μ, α, β) distributions for wind angle error at 6 of 42 levels

It can be assumed that the error between +6hr forecasts and +0hr assimilated data follows these PDFs perfectly. This means the GND parameters can be used to simulate possible ‘real wind conditions’ at each altitude level. This technique formed the basis of the Monte-Carlo Robustness Test (MCRT) which was used to determine when the balloon should be launched.

These PDFs could be improved with more data or further statistical analysis. It would be helpful to understand how error one layer’s error correlates to error on other layers. One must also determine how generic the GND parameters are; how do they relate to geographic and climate regressors? Finally, how do these outliers correlate to storms and rain (which will have a strong negative correlation to bushfires)? This information could be used to significantly improve the accuracy of both the MCRT and the Observed Wind Array Update Routine (OWAUR).

6.2 LOOPING EXAMPLE

In order to demonstrate what one of these triangular trajectory loops looks like, 12 pm on the 19th of April 2014 was chosen as an example period. The optimal trajectory for this period will be described in the following section.

6.2.1 Forecast Trajectory with Forecast Winds

Under forecast wind conditions, the most robust, optimal looping trajectory is determined using the Monte Carlo Robustness Test and the Initial Trajectory Estimate.

Using this information, the optimal forecast looping trajectory can be simulated under forecast wind conditions:

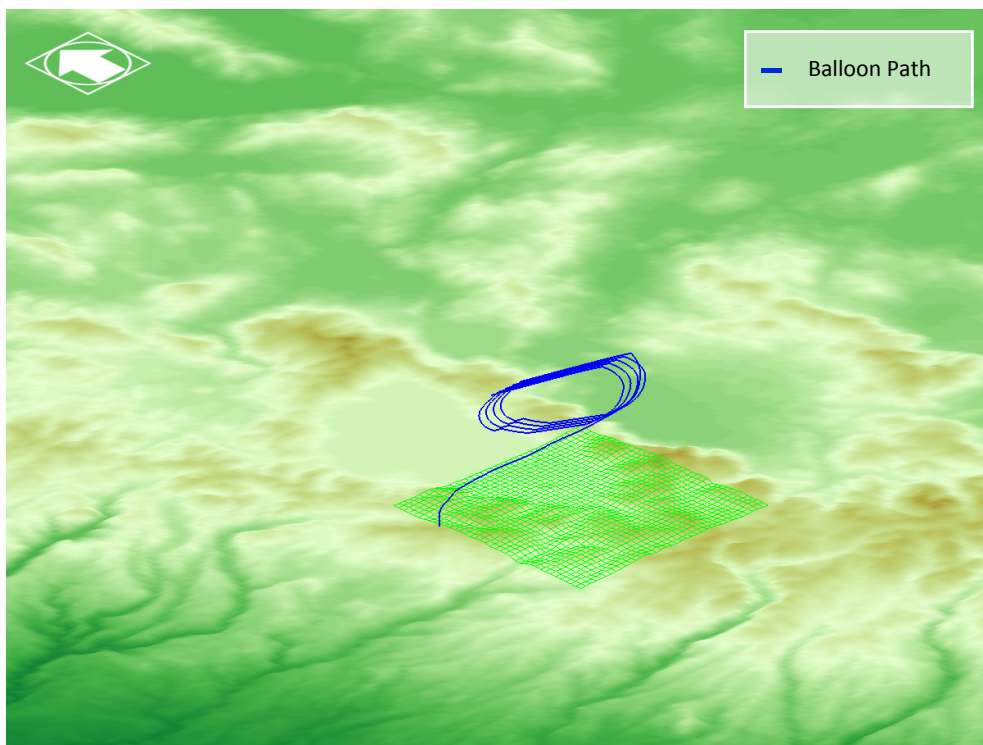


Figure 6-17: Example of optimal looping trajectory under forecast wind conditions (19/Apr/2014 - 12pm). The green gridded area below the trajectory is the approx. 34km x 34km fire observation region

This figure demonstrates the path of the balloon as it completes 3 trajectory loops. This is a good example of a successful loop, each loop is almost perfectly overlapping the previous loop. The balloon spends all its time over the observation zone, 12.19 hours of remote sensing.

This balloon could continue to loop above the goal zone for as long as it has lifting gas to spare. In this example, each loop consumes 23.2mol of hydrogen gas, this is 46.77 grams. Hence, 140.31 grams of hydrogen gas would be required to replicate the above trajectory.

6.2.2 Forecast Trajectory with Real Winds

The Monte-Carlo analysis allowed the most robust solution to be selected. Nonetheless, this is still prone to error. If the optimal looping trajectory (under forecast winds) is attempted under real wind conditions, forecast error will cause the trajectory loop to differ greatly or fail:

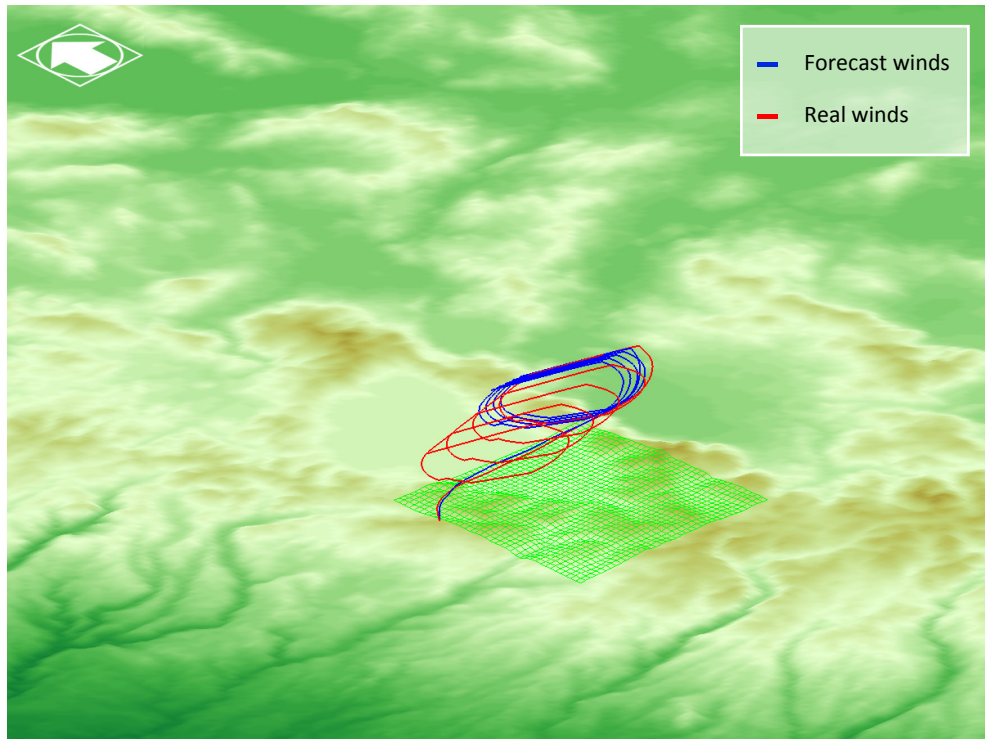


Figure 6-18: Example of the optimal forecast looping trajectory under both forecast and real wind conditions (19/Apr/2014 - 12pm). The control system in both cases is identical.

The path shown in red is the result of following the optimal forecast trajectory under real wind conditions. The performance of this path is far worse than for the forecast path (shown in blue), drifting quickly to the South East.

By the 3rd loop the balloon is no longer above the observation area meaning no more useful data can be collected. This path only results in 9.31 hours of imaging whereas the forecast trajectory could have provided hundreds of hours (fuel permitting). Clearly, following looping parameters outlined under forecast wind conditions does not meet the performance requirements

6.2.3 Real Trajectory with Real Winds

The ‘Main Model’ algorithm outlined in section 5.5.2 was designed to provide a ‘smart trajectory’ control system that is able to update mid-flight when wind conditions vary from the forecast expectation. This system relies on real-time wind estimates produced by GPS and Inertial sensors on board the craft. This observed wind data is used to update the forecast wind array to provide a much better indication of real wind conditions. This process is contained within the ‘Observed Wind Update Routine’

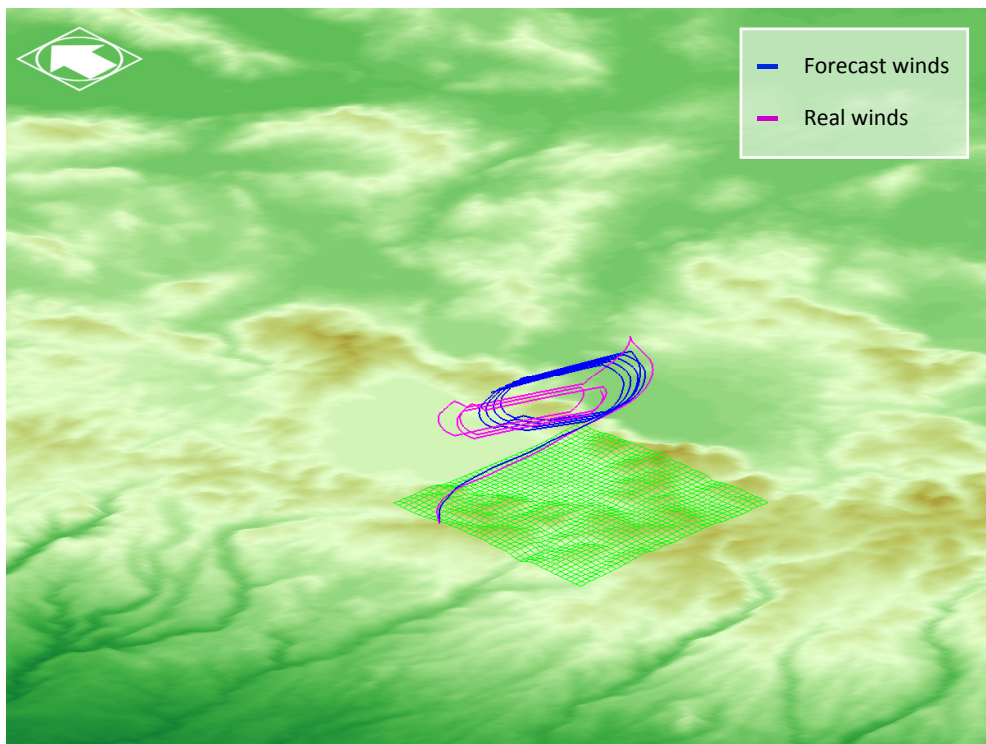


Figure 6-19: Comparison between 3 loops of optimal trajectory under forecast wind conditions and the smart trajectory under real wind conditions (19/Apr/2014 - 12pm)

Figure 6-19, above, demonstrates three loops of the ‘smart trajectory’, shown as the magenta path. The performance of these loops is comparable to the optimal trajectory under forecast conditions (in blue), each loop almost perfectly overlaps the previous loop. This is a significant improvement over the optimal trajectory under real wind conditions (as demonstrated in figure 6-18).

It is important to note that, although the robust initial solution (as determined from the Monte-Carlo analysis) fails to out-perform the ‘smart trajectory’ (under real wind conditions), this was nonetheless a crucial step to determine the launch location.

The ‘smart trajectory’ control system is able to correct the drifting that was apparent in the initial optimal trajectory under real winds. This trajectory spends almost all its time (97%) over the observation zone, almost identical to the optimal trajectory under forecast conditions. This is evident in figure 6-20 below.

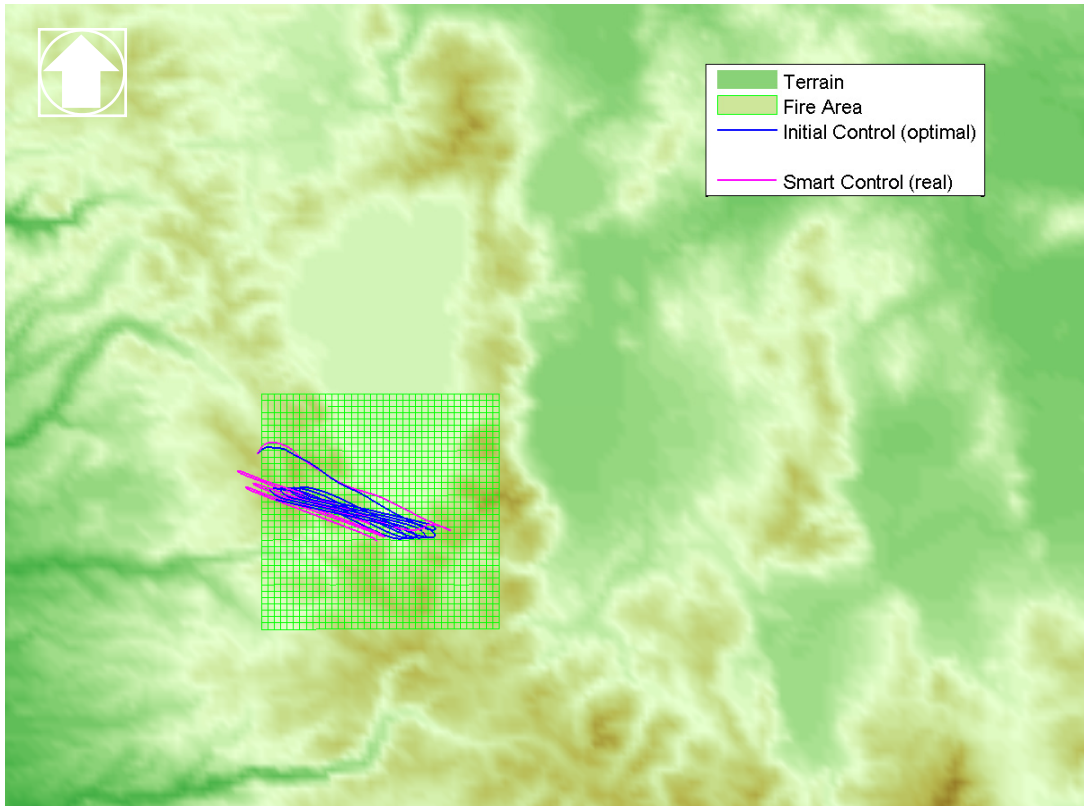


Figure 6-20: Top view of both 3 loops of optimal trajectory (under forecast winds) and smart trajectory (under real winds). This is for 19/Apr/2014 - 12pm

Each loop consumes an average of 31.7mol, equivalent to 63.91 grams hydrogen gas. This is 36.6% more than was expected under the initial optimal trajectory. This extra gas usage naturally results from this smart algorithm as it “tests the water”, probing the skies above it to determine what the real wind conditions are.

In this case, the system expects to use winds at roughly 21km altitude for its initial S-A observation leg (refer to figure 5-6 for the stage abbreviations) but the real winds at this altitude (as observed by the on-board sensors) make this impossible. Instead the balloon dips down to 17km for the S-A observation leg and performs a completely different trajectory loop. This is where the extra filling gas is wasted, the hydrogen bottle must therefore have some spare gas to account for this behaviour.

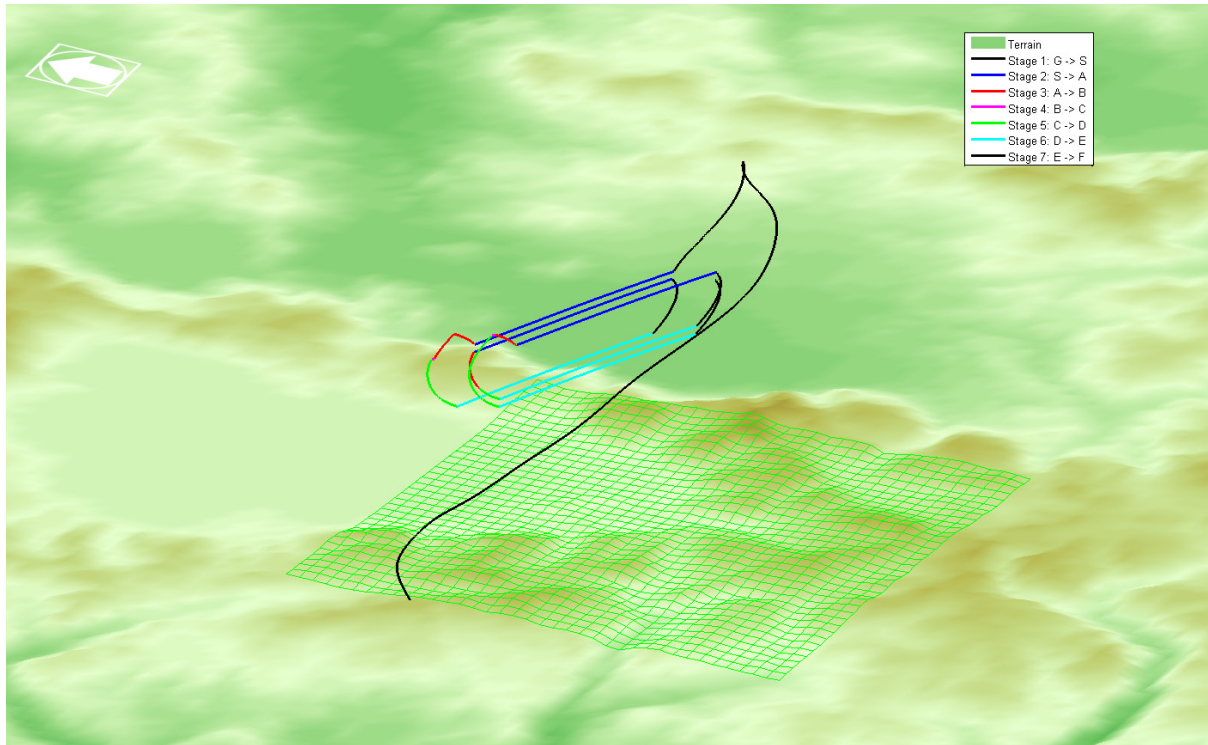


Figure 6-21: Detailed view of the path of the balloon under real winds, using the smart trajectory (19/Apr/2014 - 12pm). Each stage of the balloon's trajectory is shown in a different colour. 3 loops are completed.

In this example, stage 4 (Return path 1: B-C) is not required as the wind vectors used in stage 2 (Observation: S-A) and stage 6 (Return path: D-E) are close to 180 degrees from one another. This simplifies the trajectory, explaining why there is no magenta colour shown in figure 6-21. Minor differences in Stage 3 (A-B) and Stage 5 (C-D) can also be seen in this figure, these paths differ in each loop as the system re-adjusts to observed winds.

These re-adjustments would be much more extreme if the transient nature of wind was included in this model. Ultimately, the smart algorithm will nonetheless converge to a solution that works. The amount of gas required to reach this solution depends on the accuracy of the initial forecast data.

The number of moles required to complete an optimal forecast loop follows a regular pattern. For example, stage 1 in loop 1 uses the same as stage 1 in loop 2. This is not the case for the 'smart trajectory' where no pattern exists. Time and geographic differences mean that the 'observed wind array' will change at every point of the loop. At any time the control system may designate a completely different trajectory loop to follow. This behaviour is clearly shown in 6-22.

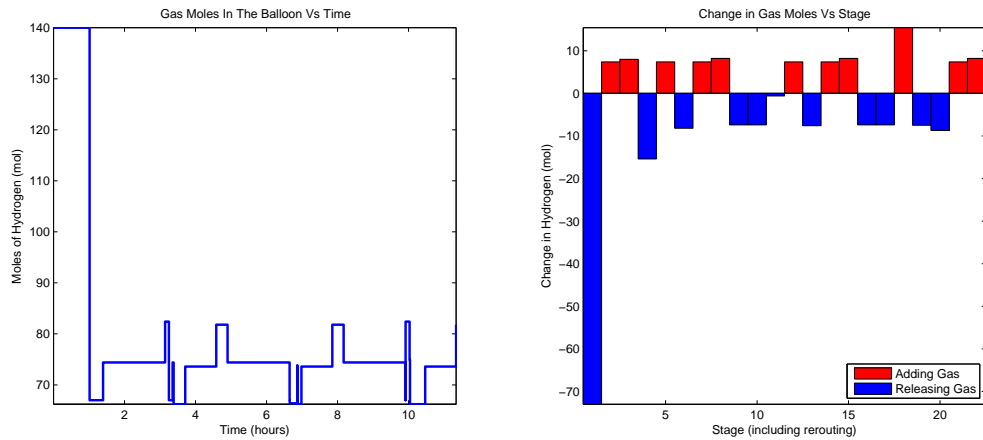


Figure 6-22: Number of moles in the balloon at each point in time (left). Number of moles of H₂ gas added or removed from the balloon at each stage of the loop (right).

This figure also demonstrates the amount of time required by each stage of the loop. The first path, from the ground to 21km altitude takes around 1 hour. This transfer period is relatively fast because the balloon is initially over filled with 140 mol of gas. Subsequent stages take between 10 minutes to 2 hours. It has been assumed that the control forces are added instantly. This assumption adequate if hydrogen is being used to apply the control force. If the sky-anchor method is used (requiring air to be pumped), it may not be possible to apply the control force within the 10 minute period.

At stage 1 (when the balloon reaches the 21km observation altitude) the balloon expels 70 mol of gas. This corresponds to an 80cm decrease in the balloon's diameter. It is important to understand how this large change affects the balloon's size and elastic material. Does the material fatigue or reach a plastic deformation point? The cyclical changes in radius and vertical velocity are demonstrated in the figure below:

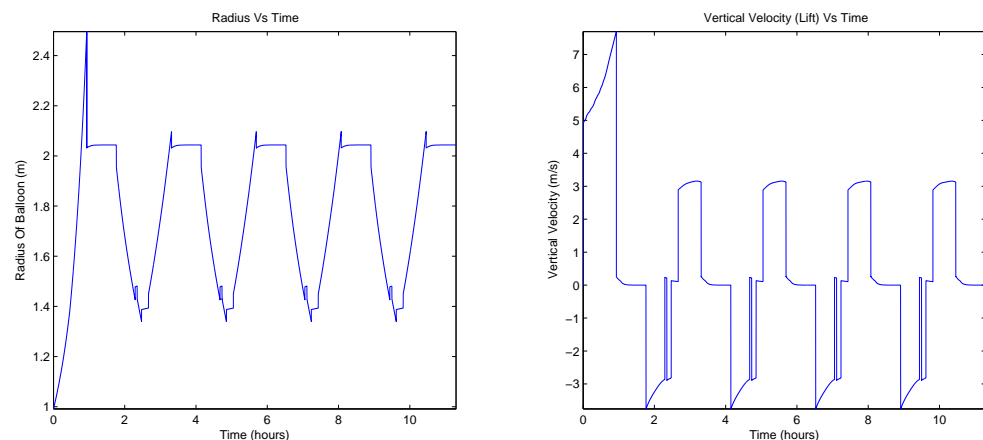


Figure 6-22B: Variation of the Balloon's Radius and Vertical Velocity with time.

6.3 LOOPING VIABILITY

The previous section made it clear that performing a trajectory loop is possible at 12 pm on the 19th of April 2014. To better understand the viability of the triangular trajectory loop, the analysis was extended across a period from 27/March/2014 to 1/May/2014.

The Initial Trajectory Estimate (ITE) algorithm was run for each of the 4 daily forecasts in this 36 day range, a total of 144 data points. This ITE algorithm determined if a trajectory loop could be completed under the forecast wind conditions. This gave an initial launch probability of:

$$P_{\text{launch}} = \frac{46}{144} = 31.94\%$$

68.06% of the time, there was not enough atmospheric wind angle variation to complete a loop. Launch would only be considered on 31.94% of the days analysed

The Monte-Carlo Robustness Test (MCRT) was then run for each of the 46 period where looping was considered possible. Each one of these periods were simulated a further 50 times, creating the ‘Simulated Real Wind’ conditions from the ‘Forecast Precision’ PDFs. For the solution to be robust enough to warrant a real launch, a 98% chance of success of was required.

If more than one of the 50 simulated scenarios failed ($2 / 50 < 0.98$), the solution was considered inadequate (not robust enough) and launch would be postponed. Out of the 46 data points tested, 4 had a probability of failure greater than 2 percent. This led to a revised launch probability of:

$$P_{\text{launch}} = \frac{42}{144} = 29.17\%$$

In summary, 70.83% of the time, atmospheric winds were considered inadequate to warrant launching the balloon as the chance of success for these attempts would be less than 98%. Only 42 of 144 days would the balloon be likely to complete a successful trajectory loop.

This 29.17% value is much lower than one would hope for. It is important to note that this probability is heavily dependent on the selected geographic region and time period (in this case, Lake Tahoe 27 Mar – 1 May). It is very possible that other regions exhibit much more atmospheric wind angle variation, and are therefore much more likely to succeed.

6.3.1 Chance of Success

On 42 of these 144 days, the chance of successfully looping was over 98% (as determined from the ITE and MCRT) meaning the balloon would actually be launched. This launch was simulated using the ‘Main Model’ algorithm to see how well the trajectory performed under real wind conditions. This success is outlined in the following figure:

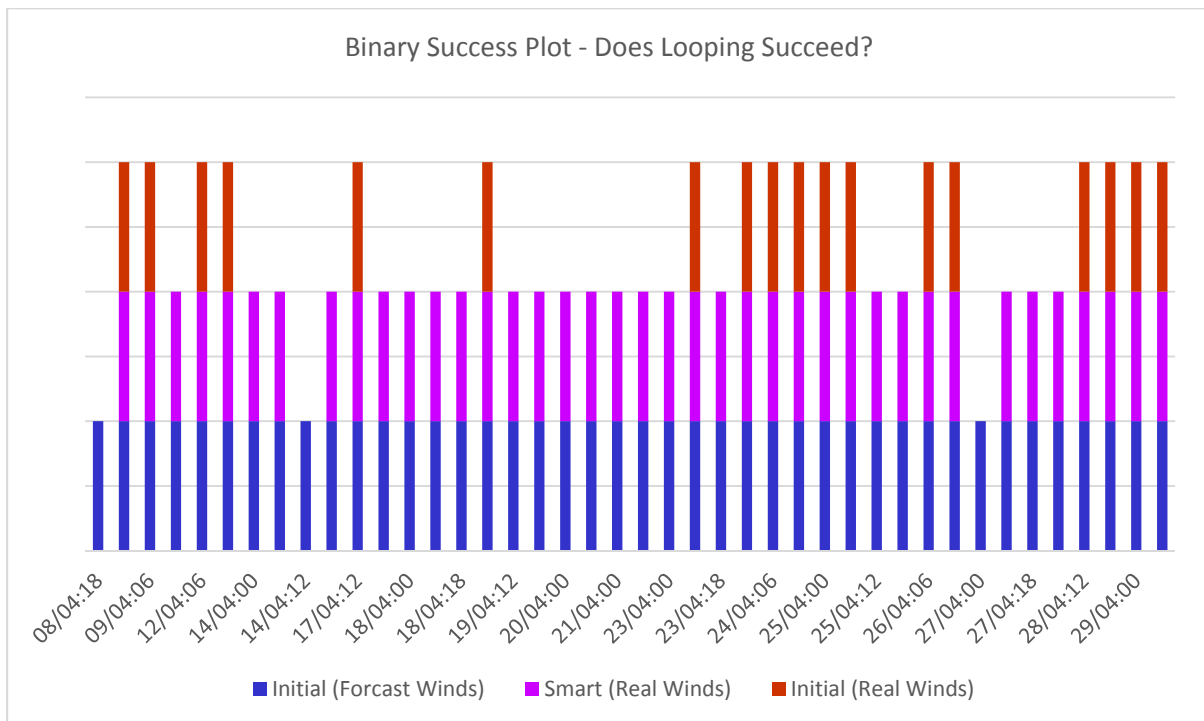


Figure 6-23: Binary demonstration of looping success (coloured bar) or failure (no coloured bar) for each scenario.

As expected, the initial optimal solution under forecast conditions (blue) succeeded every time as this was the initial requirement for launch to proceed. This same control system under real wind conditions (red) succeeded only 42.86% of the time (18 / 42). The ‘Smart’ control system under real wind conditions (magenta) succeeded 92.86% of the time (39/42).

When the ITE and MCRT suggest launching the balloon, that balloon will have a 92.86% chance of successfully completing trajectory loops. The difference between this, and the 98% specified within the MCRT is a result of either, inaccurate probability density functions or, more likely, not enough simulations being run within the MCRT (only 50 were used). By increasing the simulations run within the MCRT to over 1000, extreme weather events would be better accounted for. This would subsequently suggest that launching on the periods, 08/4/2014:18, 14/4/2014:12 and 27/4/2013:18 would all be too risky and prone to failure.

6.3.2 Further Examples

Several different scenarios were evident across the observation period. A few examples of these different trajectories are shown in the following figures.

Most commonly, the initial control system (forecast winds) out-performed the smart control system (real winds). The initial control system (real winds) almost always failed to perform a loop. An example of this is shown figure 6-24 below.

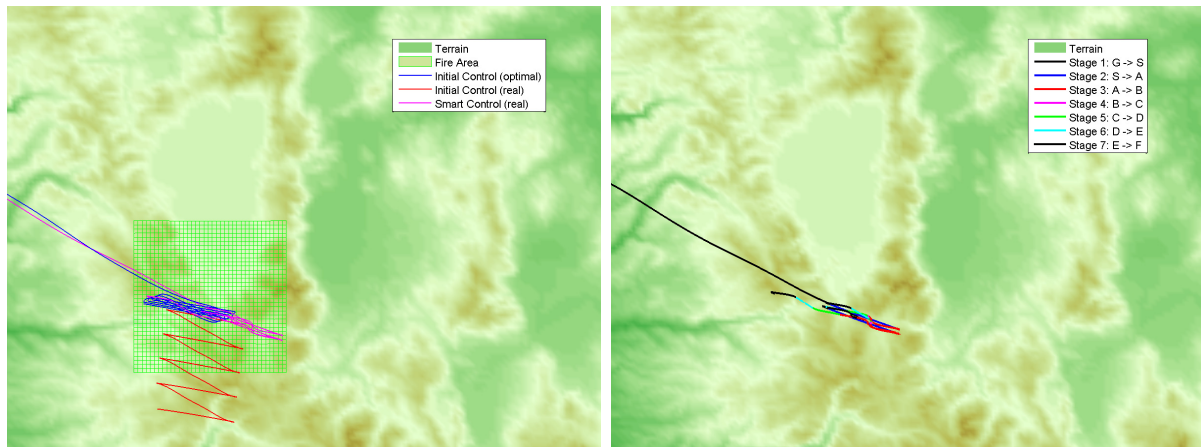


Figure 6-24: Top view of trajectory 27/Apr/2014:18h

Typically it was possible to perform the entire loop over the bushfire area as this maximised observation time. Nonetheless, there were occasions where wind conditions demanded a longer, more complicated trajectory. On such occasions, the balloon inevitably had to leave the bushfire zone, wasting valuable observation time. An example of this is shown in figure 6-25.

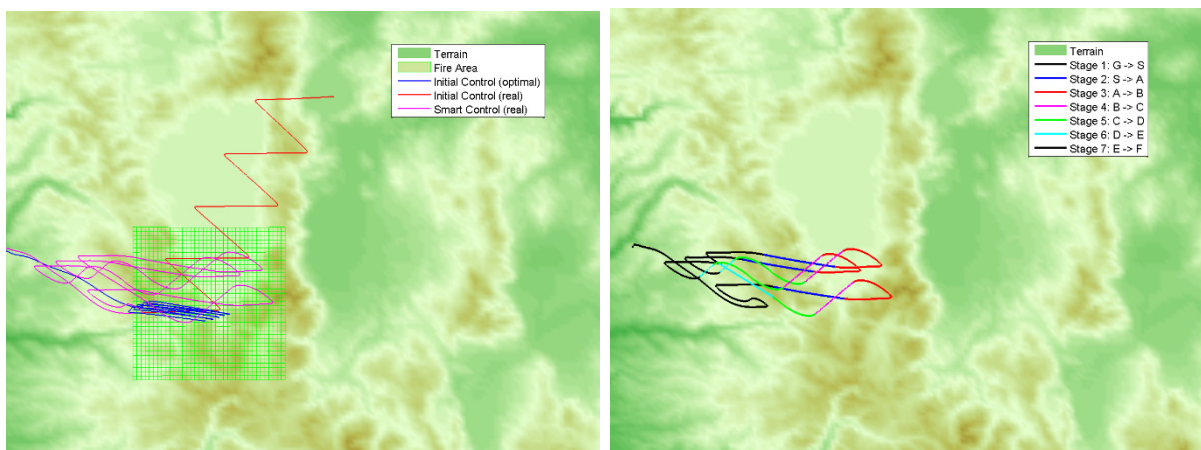


Figure 6-25: Top view of trajectory 20/Apr/2014:06h

There were also occasions where the real wind conditions were better suited to looping than the forecast conditions. During such times, the smart control system was able to outperform the initial control system.

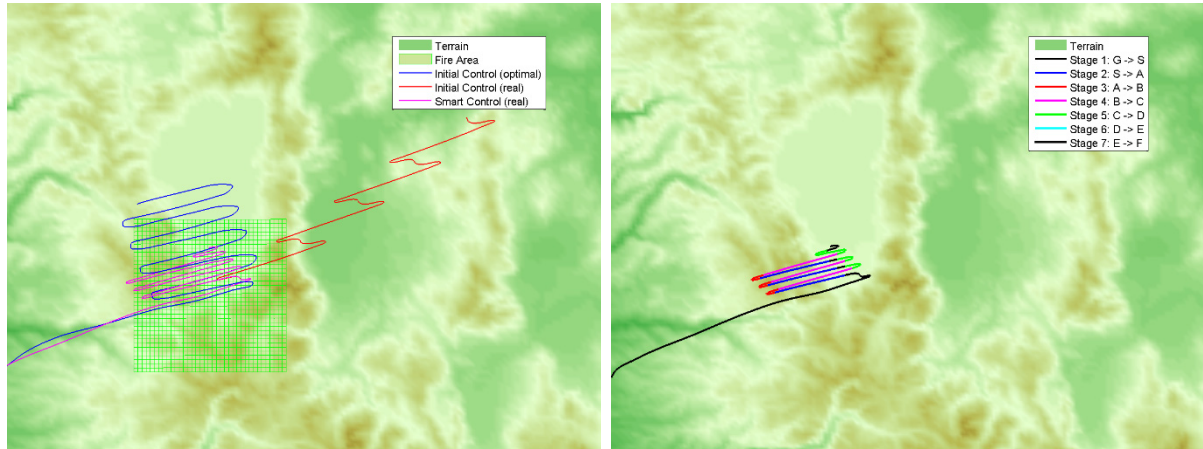


Figure 6-26: Top view of trajectory 25/Apr/2014:00h

Finally, there were several occasions where there was a large error between the forecast and real wind conditions. This made it impossible for the smart control system to find a working trajectory loop. These conditions were only possible when the Monte-Carlo Robustness Test failed to identify the occasions that were at high risk of failure. An example of one of these occasions is demonstrated below in figure 6-27.

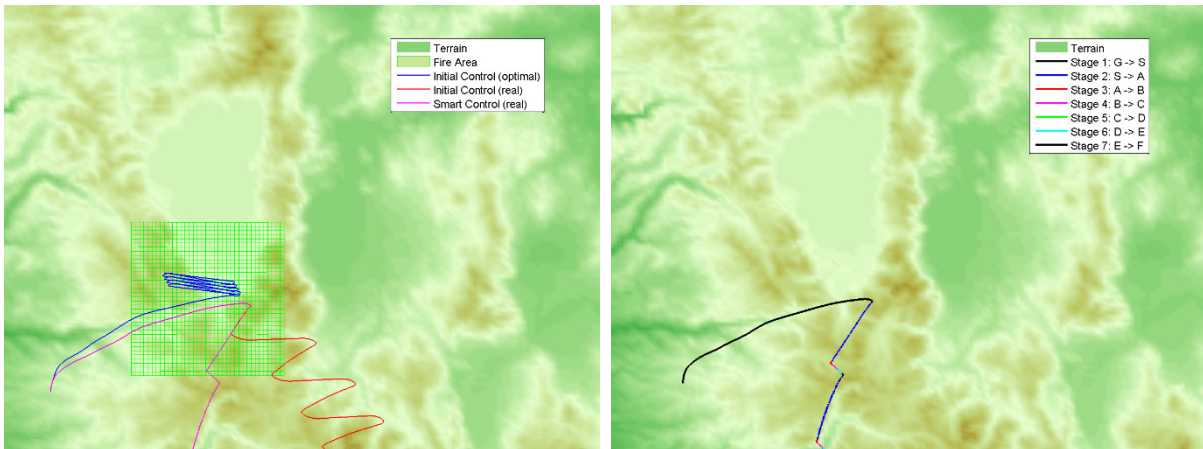


Figure 6-27: Top view of trajectory 8/Apr/2014:18h

Here, the ‘smart’ algorithm determines looping is impossible. It can instead be seen drifting south. On such occasions, the balloon should continue to rescan the upper atmospheric layers, hoping that winds change in a way that would allow it to traverse back into the bushfire zone.

6.3.3 Average Moles Required For a Loop

The number of moles of hydrogen gas required to perform each loop under forecast conditions was initially determined with the ITE algorithm. This is shown below:

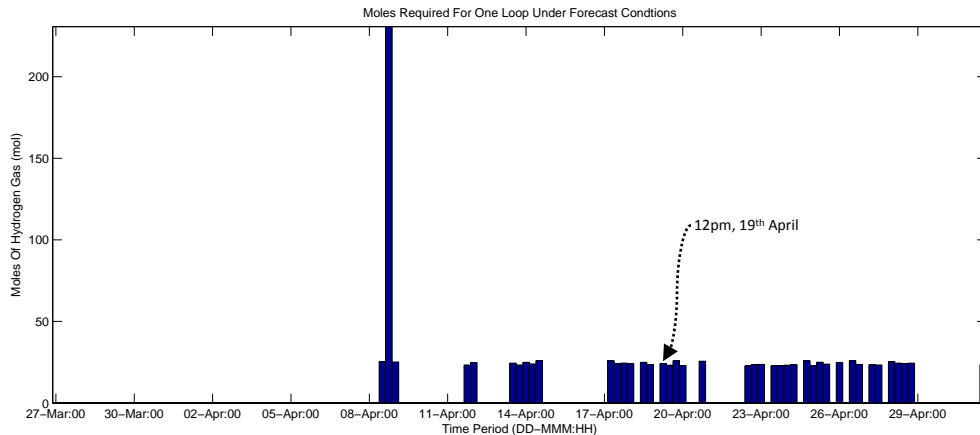


Figure 6-28: Moles of Hydrogen gas required to complete one loop under forecast wind conditions. The areas with no value shown are times where it was deemed impossible or unlikely that the balloon would successfully complete a loop (so no launch was simulated). There is one bar for each forecast period with 4 forecasts per day, 144 data points.

Excluding the outlier on the 9th of April, the average amount of hydrogen gas required to complete a trajectory loop under forecast circumstances was:

$$\overline{n_{forc}} = 24.14 \text{ mol} \quad \overline{m_{forc}} = 48.67 \text{ grams}$$

As mentioned in section 6.2.3, the ‘smart’ trajectory naturally requires more gas than the forecast trajectory because it must adjust to the real wind conditions. The Figure below demonstrates the amount of hydrogen gas required for an average ‘smart’ loop:

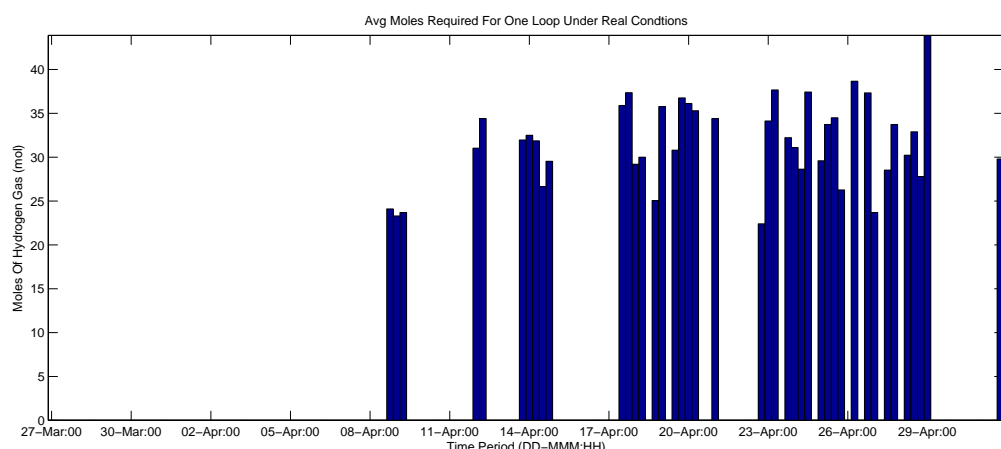


Figure 6-29: Average moles of hydrogen gas required to complete one ‘smart’ loop under real wind conditions.

Averaging these values, the amount of hydrogen gas required for a standard ‘smart’ loop was:

$$\overline{n_{real}} = 31.21 \text{ mol} \quad \overline{m_{real}} = 62.92 \text{ grams}$$

On average, 29.28% more gas (by mass) was used by the ‘smart’ system than by the initial trajectory estimate. The 29th April 0h had the worst performance in the observation period, using 78.12% more gas (by mass) than expected.

Although this does not seem like a lot of gas, difficulty storing hydrogen means that it is actually quite significant. Importantly, an efficient Lifting Gas Control System could reduce this value significantly. The number of moles required for the system to maintain neutral buoyancy is described in figure 6-30 below.

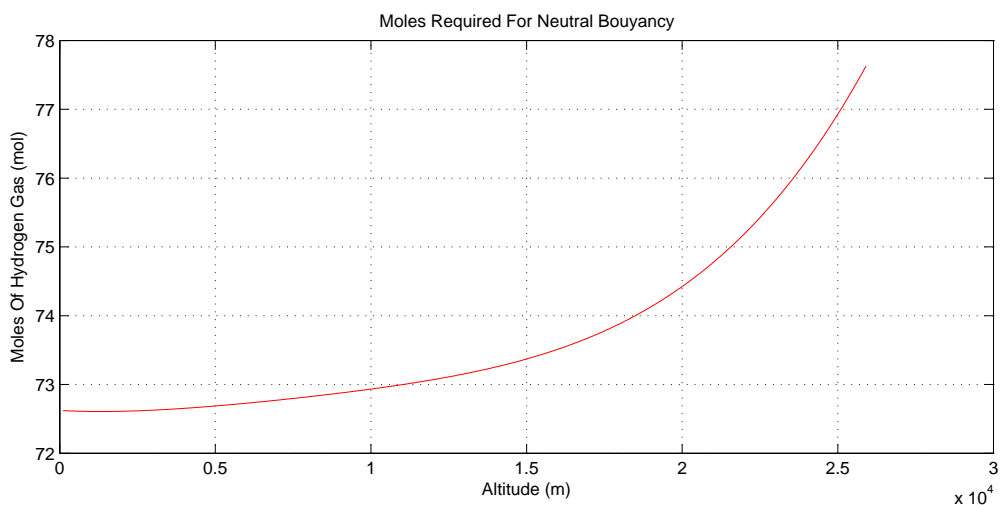


Figure 6-30: Moles required for the weather balloon to maintain neutral buoyancy at each altitude.

This figure demonstrates that no more than 3.5 mol of hydrogen gas is required to transfer from 15km to 25km (this is close to the maximum transfer required by the control system). A perfectly efficient LGCS would therefore need no more around 5 mol of gas. This is 85% less than was demonstrated by the ‘smart’ algorithm.

The current LGCS over or under fills the balloon by 10%. Given that the balloon typically has 75 mol of H₂, even the most minor control force would waste 7.5 mol of gas. This over/under filling was used to speed up the transfer time between different altitude layers. Over/under filling will still be required by the system, but this overfill percentage could change dynamically with the requirements of the trajectory.

Trajectories that are completed across larger areas can have much slower transfer times, potentially reducing the mole requirement to under 10 mol per loop. Any trajectory loop with a straight section is innately inefficient. An efficient trajectory loop should always be curved because it is always gradually changing altitude.

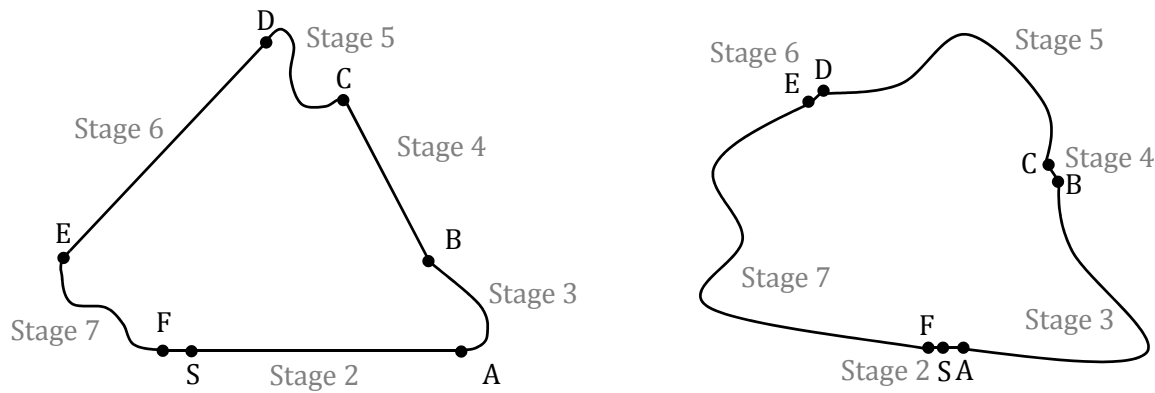


Figure 6-31: Two looping trajectories, view from above. The first is H₂ inefficient (left) as it changes layer too fast. The second is H₂ efficient (right) as it spends almost all the time gradually drifting through different altitude layers.

6.3.4 Average Time Required For a Loop

The time taken to complete three trajectory loops was determined by running the 'Main Model' algorithm for each of the 42 launch days:

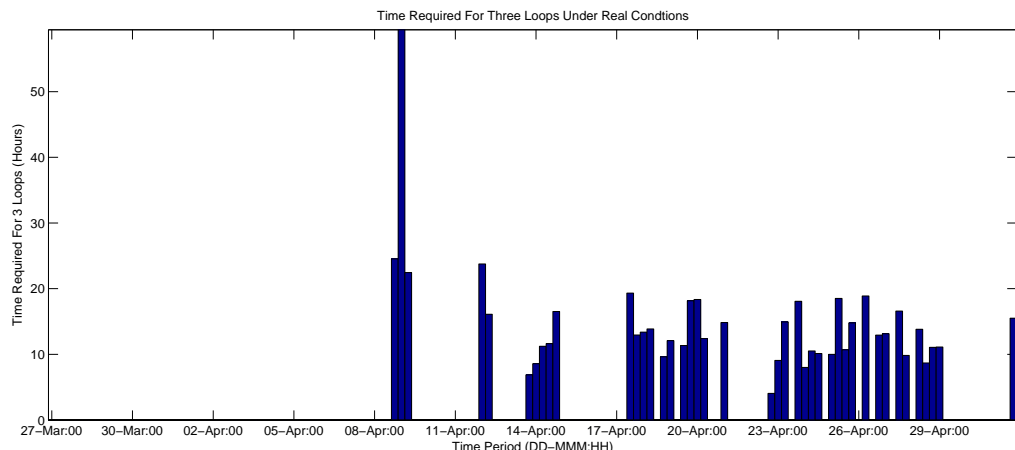


Figure 6-32: Time taken to complete 3 'smart' trajectory loops under real wind conditions.

Across all 42 launch days, the average time taken to complete these three loops was $\bar{t}_{3l} = 15.09$ hours. In short, with 188.76 grams of hydrogen gas the balloon should be able to stay aloft above the bushfire zone for 15.09 hours. If the efficiency of the LGCS was improved it may be possible to reduce this consumption down to 60 grams for 15.09 hours.

7 FUTURE CONSIDERATION AND CONCLUSIONS

7.1 CONCLUSIONS

This thesis investigated the feasibility of an altitude controlled, bushfire sensing balloon. The analysis focused on the balloon's innovative station-keeping method; the triangular looping trajectory. It aimed to determine if this trajectory could be accurately predicted from wind forecast data and if the trajectory loop could reliably be performed.

An initial statistical analysis was conducted for 36 days of wind forecast data ($4 \times 36 = 144$ sample points). This revealed that each horizontal slice of the atmosphere had a highly regular wind angle, typically varying by no more than 1 degree. The wind speed on each layer was much more irregular, exhibiting an average coefficient of variation of 40%. This variation suggested that a GPS sensor would be required by the balloon's control system as position cannot be accurately determined from time and wind speed forecasts alone.

Further analysis demonstrated how wind speed and angle varied with altitude. Wind angle was relatively constant across all altitudes, typically varying by no more than 60 degrees. There were only a few days in the observation period where two layers of wind were 180 degrees from one another. Only about a third of the time were there 3 wind vectors that added up to 180 degrees, as required by a triangular trajectory. This lack of atmospheric wind variation suggested it may be impossible to complete a successful looping trajectory across much of the observation period.

Next, a statistical analysis was conducted to determine how winds varied with time. This showed that over a 6 hour period, winds changed quite gradually, wind angle typically varying by no more than 25 degrees in either direction. To account for this variation, wind forecasts for 6 hours in the future would be required. A spline interpolation method could be accurately used to interpolate any future wind conditions. This transient wind variation was therefore removed from the simulation as it would add unnecessary computational complexity without providing any further information about viability.

Finally, the precision of the 6h forecast wind data was analysed by comparing it to 0h 'real' assimilated data. This demonstrated that forecast wind speed was normally accurate to within a few percent, forecast wind angle was normally accurate to within 10 degrees. Nonetheless,

there were many outliers for both of these parameters, revealing that wind forecasts were easily affected by unexpected, extreme weather events. Because of this result, it is clear that wind sensors must be included on the balloon to observe real wind conditions and update the wind forecast data accordingly. This was achieved by adding both GPS and inertial sensors to the simulation. This forecast precision data also demonstrated that certain atmospheric layers were more prone to forecast errors than others. To show this, the parameters for a series of generalised normal probability density functions were estimated for each altitude layer.

The viability of the looping trajectory was determined by examining simulation results across the 36 day period. This analysis suggested that launching the balloon would only be considered 31.94% of the time. A Monte-Carlo Robustness Test was then used to exclude days where a slight wind variation would lead to failure. This test was based on the forecast precision generalised normal PDFs. Ultimately, this revealed that the balloon would have only been launched 29.17% of the time (42 of 144 data points).

For the 42 occasions where success was deemed likely, the launch was simulated with real wind data. This simulation required the balloon to adapt to the real wind conditions by observing them with simulated GPS and inertial sensors. Of the occasions where the balloon was launched, successful trajectory loops were completed 92.86% of the time.

The initial pre-launch simulation (based on forecast wind data) suggested each trajectory loop required 48.67 grams of hydrogen gas to complete. When the simulation was extended to use real wind data, an average of 62.92 grams of H₂ was required, 29.28% more than the initial estimate. This meant that a balloon completing 3 trajectory loops over a bushfire would require an average of 188.76 grams of H₂, allowing for an average flight time of 15.09 hours above the bushfire zone. Importantly, it is expected that this high gas consumption could be reduced by up to 85% by introducing a better Lifting Gas Control system that does not over/under fill by 10%.

In summary, the triangular looping trajectory can, with the help of on-board wind sensors, be accurately and reliably performed. Nonetheless, it is still too early to say if an altitude controlled bushfire sensing balloon is likely to be practical. There are two main questions that must still be answered:

1. Do other areas (such as Australia) exhibit robust launch rates much higher than 29.17%?
2. Is it possible to provide control forces equivalent to 188.76 grams of hydrogen gas? To what extent can this be reduced by if modifications are made to the Lifting Gas Control System?

7.2 FUTURE CONSIDERATIONS

7.2.1 Improvements to simulation accuracy

There are a number of improvements that could be made to increase the accuracy of the trajectory simulation. In order of importance, these are:

- Include a more detailed thermal model outlining how radiative and convective heating / cooling affects the hydrogen gas. These temperature fluctuations can have a significant effect on the neutral buoyancy position of an elastic weather balloon. Both gas density and balloon size can vary greatly with temperature.

The NASA-SINBAD model outlines a full range of global atmospheric thermodynamic parameters (XSimbard, 2014). This includes real-time and forecast parameters for both infrared radiation and albedo. Alternatively, the elastic balloon could instead be replaced with a super-pressure balloon as these are less influenced by thermal effects.

- Include the transient nature of the wind. This was excluded from this simulation to reduce computation time. In reality, wind direction could change by as much as 25 degrees in the time taken to complete one loop.

Winds at any location and time can be easily be determined by spline interpolating the forecast wind data. This would cause a large increase to simulation accuracy but would require increased computation time. It is important to note that adding these effects to the simulation would not greatly affect the previous viability calculations.

- Throughout this simulation, 0h assimilated forecast data was assumed to be identical to the real wind data. It may be possible to obtain seasonal RMS errors from NOAA in order to describe the true accuracy of the 0h forecast data. By integrating this error into the simulation, a range of likely positions could be determined. This would be critical to understanding the true accuracy of the trajectory simulation.
- The Lifting Gas Control System was designed to over or under-fill the balloon by 10% in order to reduce the altitude transfer time. This 10% value was arbitrarily selected and led to a significant waste of hydrogen gas. A variable system could be designed that reduces this waste when a slower transfer speed is suitable. For example, the 31.21mol required to complete an average loop couple be reduced to as little as 5mol. It is expected that as much as an 85% reduction could be achieved over large trajectories.

7.2.2 Other Considerations

There are a range of other issues that should be considered to better determine the project feasibility:

- A widespread geographical analysis should be conducted to determine which areas exhibit high levels of wind angle variation, as required for a successful looping trajectory. It is expected that some places will have stratospheric winds that are reliability different in direction to tropospheric winds. In such locations, the chance of successfully completing a trajectory loop would be much higher, close to 100 percent. The seasonality of these winds should also be analysed.
Are there places, prone to bushfires, which exhibit ideal atmospheric wind conditions during bushfire season? If the answer to this is no, there is little future to altitude controlled balloons in the realm of bushfire remote sensing.
- A more detailed analysis should be conducted, comparing the efficiency of different control force methods. Importantly, do current hydrogen storage techniques exceed the current system mass limitations? Is the risk of explosion too high? How viable are other systems such as pumping air into a ballonet or fixed volume container?
- Additional analysis should also be conducted to determine how a feedback loop could be added to the LGCS. Is it possible to accurately determine the amount of gas in the balloon? Is it possible to accurately determine how much gas is being added / vented?
- The current algorithm outputs the position of the balloon's ideal launch site. Often the specified location is on top of a mountain, far from roads or in the middle of a forest. The algorithm could be modified to avoid these difficult launch sites and instead recommend a location which is easier to reach. It would be important to determine how well the balloon could perform when it is not launched from the ideal location.
- Basic regulatory requirements should also be considered. What sorts of payload and trajectory limitations are imposed by the Civil Aviation Safety Authority (CASA)? Can the balloon fly through altitudes commonly used by commercial aircraft?
- A wide range of statistically correlations should also be researched. It became clear that extreme weather events were a major cause of failure. It is expected that these extreme weather events are related to unpredictable rains and storms. Rain obviously has a strong negative correlation to bushfires so knowing these correlations could vastly improve the viability of an altitude controlled bushfire sensing balloon.

8 WORKS CITED

Aaron, K., Heun, K. & Nock, K., 2001. *A METHOD FOR BALLOON TRAJECTORY CONTROL*, Altadena: GLOBAL AEROSPACE CORPORATION.

Appleby, J., Wang, C. & Little, F., 2003. *High Power Alkaline Fuel Cell with Intrinsic Energy Storage*. Orlando, The Electrochemical Society, Inc..

Arora, A., 2005. *PATH PREDICTION FOR AN EARTH BASED DEMONSTRATION FLIGHT*. [Online] Available at:

<http://www.cds.caltech.edu/~marsden/wiki/uploads/jplcdsmeetings/resources/AnujAroraSurf.pdf>

[Accessed 07 03 2014].

Australian Bureau of Statistics, 2006. *Bushfires*. [Online]

Available at:

<http://www.abs.gov.au/ausstats/abs@.nsf/0/ccb3f2e90ba779d3ca256dea00053977?OpenDocument>

[Accessed 1 12 2013].

Barrado, C., Meseguer, R., López, J. & Pastor, E., 2010. *Wildfire Monitoring Using a Mixed Air-Ground Mobile Network*, Catalonia: IEEE CS.

Beemer, J., 1975. *The Analysis and Design of a High Altitude Airship*, s.l.: Raven Industries.

Blackwell, D. et al., 2006. *BalloonSat: Design, Implementation, and Application of a low-cost tethered weather balloon remote sensing station*, Calpoly: s.n.

Blamont, J., Heinsheimer, T. & Pommereau, 1974. New Method of Studying the Dynamics of the Stratosphere, Principle and Initial Results. *Science Physiques*, 278(7), pp. 249-254.

Bourke, E., 1969. *A unique approach to balloon station keeping*. 1 ed. s.l.:Raytheon Co.

Brand, R., 2014. *High Altitude Balloon Rates / Fees*. [Online]

Available at: <http://wotzup.com/balloon-rates/>

[Accessed 17 05 2014].

- Bureau of Meteorology, 2014. *ACCESS NWP Data*. [Online]
Available at: <http://www.bom.gov.au/nwp/doc/access/NWPData.shtml>
[Accessed 25 04 2014].
- Bushnell, S. & Cottrell, A., 2007. Increasing community resilience to bushfire — implications from a north. *The Australian Journal of Emergency Management Queensland community case study*, 22(2), pp. 3-9.
- Carten, A., 1974. *An Investigation of the Applicability of High Altitude, Lighter-than-Air (LTA) Vehicles to the Tactical Communications Relay Problem*, s.l.: United States Air Force.
- Chungwook, S., 2007. *Estimating the Optimal Location of a New Wind Farm based on Geospatial Information System Data*, Austin: University of Texas at Austin.
- Clapeyron, E., 1834. Mémoire sur la puissance motrice de la chaleur. *Journal de l'École Polytechnique*, pp. 153-190.
- Draxler, R., 1995. *Trajectory Optimization for Balloon Flight Planning*. [Online]
Available at: <http://www.arl.noaa.gov/documents/reports/balloon.pdf>
[Accessed 17 4 2014].
- Emergency Management Australia, 2006. *Eyre Peninsula Bushfire*. [Online]
Available at: <http://www.royalcommission.vic.gov.au/getdoc/bd8ab811-d8bf-4492-a7b6-29813bd242a4/RSCH.030.001.0327.pdf>
[Accessed 01 12 2013].
- Flynn, S., 2009. *Firefighting needs investment, not inquiries*. [Online]
Available at: <http://www.smh.com.au/national/firefighting-needs-investment-not-inquiries-20090212-85z1.html>
[Accessed 31 05 2014].
- Forghani, A. et al., 2007. *Applying fire spread simulation over two study sites in California*.
Barcelona, Geoscience and Remote Sensing Symposium.
- Geoscience Australia, 2014. *About SENTINEL*. [Online]
Available at: <http://sentinel2.ga.gov.au/acres/sentinel/about.shtml>
[Accessed 16 05 2014].

Graml, R. & Wigley, G., 2007. *Bushfire Hotspot Detection Through Uninhabited Aerial Vehicles and Reconfigurable Computing*, Adelaide: Reconfigurable Computing Laboratory.

HYDROGEN "COMPONENTS", INC, 2014. *SOLID-H™ METAL HYDRIDES*. [Online]
Available at: <http://www.hydrogencomponents.com/BL-220.htm>
[Accessed 29 05 2014].

L3, 2013. *16-Megapixel Infrared Sensor Engine*. [Online]
Available at: http://www.cinele.com/images/Documents/Datasheets/ir2013/4k_x_4k.pdf
[Accessed 15 05 2014].

Matthias, L. & Focken, U., 2005. *Physical Approach to Short-Term Wind Power Prediction*. 1 ed.
Berlin: Springer.

Merino, L., Caballero, F., Martínez-de Dios, J. & Ollero, A., 2005. *Cooperative Fire Detection using Unmanned Aerial Vehicles*. Seville, Robotics, Computer Vision and Intelligent Control Group, University of Seville.

Müller, I. & Strehlow, P., 2004. *Rubber and Rubber Balloons: Paradigms of Thermodynamics*. 2004 ed. Berlin: Springer.

NOAA ERDDAP, 2014. *List of griddap Datasets*. [Online]
Available at: <http://coastwatch.pfeg.noaa.gov/erddap/griddap>
[Accessed 21 04 2014].

NOAA, 2012. *Pressure Altitude*. [Online]
Available at: <http://www.srh.noaa.gov/images/epz/wxcalc/pressureAltitude.pdf>
[Accessed 21 04 2014].

NOMADS NCEP, 2014. *GFS half degree documentation*. [Online]
Available at: http://nomads.ncep.noaa.gov/txt_descriptions/GFS_half_degree_doc.shtml
[Accessed 06 04 2014].

Nomads NCEP, 2014. *GrADS Data Server*. [Online]
Available at: <http://nomads.ncep.noaa.gov:9090/dods/nam>
[Accessed 21 04 2014].

NovaLynx, 2014. <http://novalynx.com/products/upper-air/400-82xx-weather-balloons/>. [Online] Available at: <http://novalynx.com/products/upper-air/400-82xx-weather-balloons/> [Accessed 20 03 2014].

Obserson, J., 2010. *The Convective Boundary Layer*. [Online] Available at: <http://www.soaringmeteo.ch/CBL.pdf> [Accessed 16 05 2014].

Onda, M. et al., 1999. *A Stratospheric LTA Stationary Platform for Telecommunication and Environmental Protection*. Morioka, SICE.

Perry, W., 1998. *Sounder: High Altitude Solar Powered Airship*, s.l.: Jet Propulsion.

Romsey Australia, 2012. *Summary of Major Bush Fires in Australia Since 1851*. [Online] Available at: <http://home.iprimus.com.au/fo07/firesum.html> [Accessed 1 12 2013].

Sim, C., 2007. *Estimating the Optimal Location of a New Wind Farm based on Geospatial Information System Data*. [Online] Available at: <http://www.crwr.utexas.edu/gis/gishydro08/Introduction/TermProjects/Sim.htm> [Accessed 14 03 2014].

Sowman, K., Greig, A. & Richman, D., 2010. *CUSF Landing Predictor 2.5*. [Online] Available at: <http://predict.habhub.org/> [Accessed 22 04 2014].

Stockwell, K., 2007. *U.S. Forest Service: Illegal Campfire Sparked Angora Fire*. [Online] Available at: <http://www.ktvn.com/Global/story.asp?S=6729050> [Accessed 25 04 2014].

Struzak, R., 2003. *Mobile telecommunications via stratosphere*. [Online] Available at: <http://www.intercomms.net/AUG03/content/struzak1.php> [Accessed 06 03 2014].

University of Wyoming, 2014. *Balloon Trajectory Forecasts*. [Online] Available at: [http://weather.uwyo.edu/polar/balloon traj.html](http://weather.uwyo.edu/polar/balloon_traj.html) [Accessed 19 04 2014].

Wetzel, M., Borys, R., Lowenthal, D. & Brown, S., 1995. Meteorological support to the Earthwinds transglobal balloon project. *Bull. Amer. Meteor. Soc*, Volume 76, pp. 477-487.

WindPower Program, 2014. *Wind statistics and the Weibull distribution*. [Online]
Available at: http://www.wind-power-program.com/wind_statistics.htm
[Accessed 12 05 2014].

XSimbad, 2014. *SIMBAD Astronomical Database*. [Online]
Available at: <http://simbad.u-strasbg.fr/simbad/>
[Accessed 22 04 2014].

Yadaiah, N., 2011. *Fuzzy Kalman Filter based trajectory estimation*. Melacca, Hybrid Intelligent Systems (HIS).

8.1 OPEN SOURCE MATLAB FUNCTIONS

Chapman, M., 'Weather Balloon Physics', *zmatt beta*. [Online]
Description: Basic altitude based elastic balloon mechanics with stress strain relationship.
Available at: <http://www.zmatt.net/files/balloon-0.1.zip>

D'Errico, J., 'inpaint_nans', *Matlab File Exchange*. [Online]
Description: Interpolates and extrapolates NaN elements in a 2d array.
Available at: <http://www.mathworks.com.au/matlabcentral/fileexchange/4551-inpaint-nans>

Schlining, V., 'nctoolbox', *GitHub*. [Online]
Description: Reads NetCDF files, provides additional functions for weather analysis.
Available at: <https://github.com/nctoolbox/nctoolbox>

Wyser, K., 'NetCDF / GRIB reader', *Matlab File Exchange*. [Online]
Description: Reads NetCDF and GRIB files, converts them to Matlab format.
Available at: <http://www.mathworks.com.au/matlabcentral/fileexchange/21579-netcdfgrb-reader>

9 APPENDIX

9.1 MATLAB CODE

More than 2,000 lines of original Matlab code was created for this simulation. This code can be accessed online. Please download the folder as zip and follow the included instructions:

Dropbox URL:

https://www.dropbox.com/sh/ez0frs7y8z4v213/AACXyP_5XodL21srWNGcqghla

Shortened URL:

bit.ly/1kZWUqO

1861 forecast periods were analysed to perform the statistical analysis. This equated to 12.2GB or raw wind data (well over 1TB when interpolated and expanded).

A sample of this data has been included in the online code package.

If more data is required, the included Matlab functions can be used to download more.

9.2 INITIAL PARAMETERS

```
%% ===== PARAMETERS =====
% -----BALLOON PARAMETERS-----
R_Uninf=0.54;           % uninflated radius (m)
R_Init=0.95;            % initial radius (m)
R_Burst=3.4;             % burst radius (m)

M_gas=2;                 % molecular mass of gas (2 x Hydrogen)
M_Ball=0.8;              % balloon mass (kg)

Rubberrho=1100;          % density of rubber (kgm-3)
Thick0=M_Ball/(4*pi*R_Uninf2*Rubberrho);    % uninflated thickness
StretchMax=(R_Burst/R_Uninf)*1.08;               % theoretical max stretch
% (1.08 fudge factor over burst point, need to compare to experiment)
Jm=2*StretchMax2+StretchMax-4-3;           % Gent parameter

% -----PAYLOAD PARAMETERS-----
M_Pay=1.15;              % payload mass (kg)
M_Tot=M_Ball + M_Pay;    % total mass including balloon(kg)
FOV_Angle = 9.366;        % angle of the camera

% -----FIRE PARAMETERS-----

Lat_fire = 38.85; Lon_fire = -120.05;   % Latitude and Longitude of Centre
Rad_fire1 = 5000; Rad_fire2 = 10000;     % Radius of Fire Zone 1 and 2

% -----AREA PARAMETERS-----
lon_range=[Lon_fire-3 Lon_fire+3];       % Longitude of the Area of Interest
lat_range=[Lat_fire-3 Lat_fire+3];         % Latitude of the Area of Interest
```